TECHNICAL MEMORANDUM
X-167

STATIC STABILITY CHARACTERISTICS OF A SERIES OF

HYPERSONIC BOOST-GLIDE CONFIGURATIONS AT

MACH NUMBERS OF 1.41 AND 2.01

By Gerald V. Foster

Langley Research Center
Langley Field, Va.

NATIONAL AERONAUTICS AND SPACE ADMINISTRATION

WASHINGTON

November 1959
Declassified October 16, 1961
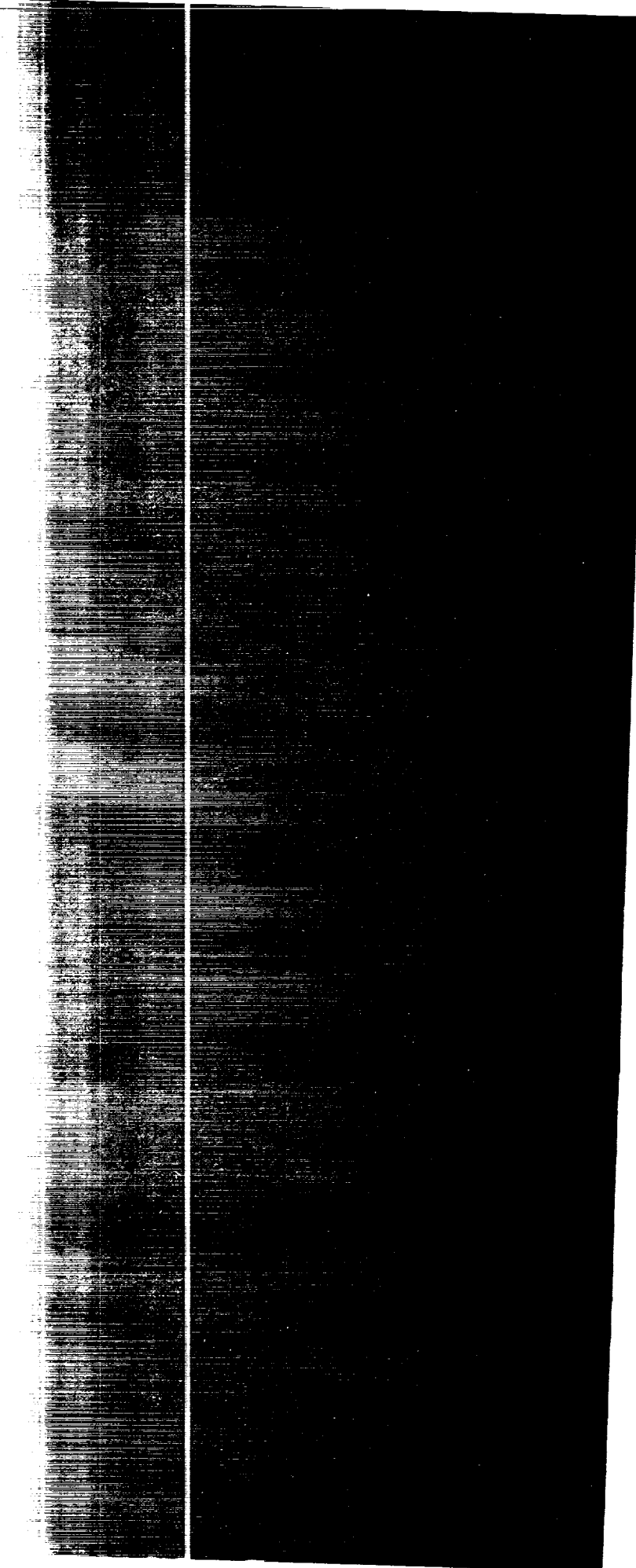
NATIONAL AERONAUTICS AND SPACE ADMINISTRATION

_____

TECHNICAL MEMORANDUM X-167

_____

STATIC STABILITY CHARACTERISTICS OF A SERIES OF

HYPERSONIC BOOST-GLIDE CONFIGURATIONS AT

MACH NUMBERS OF 1.41 AND 2.01

By Gerald V. Foster

SUMMARY

An investigation of the static stability characteristics of several hypersonic boost-glide configurations has been conducted in the Langley 4- by 4-foot supersonic pressure tunnel at Mach numbers of 1.41 and 2.01 (with Reynolds numbers per foot of 2.90×10^6 and 2.41×10^6, respectively). This series of configurations consisted of a cone, with and without cruciform fins, a trihedron, two low-aspect-ratio delta wings that differed primarily in cross-sectional shape, and two wing-body configurations.

All configurations indicated reasonably linear pitching-, yawing-, and rolling-moment characteristics for angles of attack to at least 12°. The maximum lift-drag ratio for the zero-thrust condition (base drag included) was about 3 for the delta-wing configurations and about 4 for the wing-body configurations.

INTRODUCTION

Boost-glide and boost-skip vehicles have been seriously considered as a means of achieving manned flight at hypersonic speeds. Both types of vehicles would be boosted along a ballistic trajectory to a maximum speed and a predetermined altitude. The remainder of the flight would be unpowered, but the boost-glide vehicle would be maintained at a lift coefficient corresponding to maximum lift-drag ratio, whereas upon entering the atmosphere the boost-skip vehicle would be put into a pullup maneuver at maximum lift-drag ratio. This procedure would be continued throughout the descent until just prior to landing.

Some aspects of the design of hypersonic boost-glide vehicles are discussed in references 1 and 2. References 3 and 4 present the results of a study of the static-stability and control problems associated with hypersonic boost gliders.

This paper presents the results of an investigation of the static longitudinal and lateral stability and control characteristics of a series of boost-glide configurations for test Mach numbers of 1.41 and 2.01. This series of configurations included a cone, with and without fins, a trihedron, two low-aspect-ratio delta wings, and two wing-body configurations.

SYMBOLS

The results have been reduced to coefficients of forces and moments based on the geometric characteristics of the respective models. The aerodynamic characteristics are referred to the body-axis system except for the lift and drag coefficients, which are referred to the stability-axis system. (See fig. 1.) Unless otherwise specified the moment coefficients of all models are referred to a moment center located 66.6 percent of the theoretical body length rearward of model longitudinal station 0.

The symbols used herein are defined as follows:

C_L lift coefficient, F_L/qS

C_D' drag coefficient, F_D'/qS

C_m pitching-moment coefficient, M_Y'/qSx

C_N normal-force coefficient, F_N/qS

C_{N_α} rate of change of normal-force coefficient with angle of attack

C_A axial-force coefficient, F_A/qS

C_n yawing-moment coefficient, M_Z/qS_l

C_{n_δ} yawing-moment coefficient per degree of fin deflection

C_l rolling-moment coefficient, M_X/qSy

C_Y side-force coefficient, F_Y/qS

F_Y side force

F_L lift force

F_D' drag force

M_Y moment about Y-axis

F_N normal force

F_A axial force

M_Z moment about Z-axis

M_X moment about X-axis

q free-stream dynamic pressure

M Mach number

S reference area (table I)

x longitudinal reference length (table I)

y lateral reference length (table I)

$C_{D,B}$ base drag coefficient, $\dfrac{(p_{TS} - p_B)S_B}{qS}$

p_B static pressure at base

p_{TS} static pressure in test section

S_B area of model base

L/D lift-drag ratio

C_{n_β} directional-stability derivative

C_{l_β} rolling moment due to sideslip

C_{Y_β} side-force derivative

α angle of attack, deg

β angle of sideslip, deg

r radius

δ control deflection angle (positive when control trailing edge is deflected down or to the left)

δ_R deflection of right control, deg

δ_L deflection of left control, deg

δ_V deflection of vertical control, deg

MODEL AND APPARATUS

Pertinent dimensions and details of the seven models are given in figure 2 and table I. Photographs of the models are presented in figure 3.

In general the model configurations used in the present investigation consisted of (1) wingless bodies, (2) thick delta wings, and (3) wing-body combinations. The wingless body configurations included model 1, which was a 7.1° cone (fig. 2(a)), and model 2, which was a flat-bottom trihedron (fig. 2(b)). Model 3 consisted of a body similar to model 1 with the addition of cruciform fins. The horizontal fins extended from the apex to the base of the body and had approximately 82.8° sweepback of the leading edge. The vertical fins extended over approximately the rear 30 percent of the body and had 80° sweepback of the leading edge. (See fig. 2(c).)

The delta-wing configurations were represented by models 4 and 6. Model 4 had a sharp, highly sweptback leading edge with rhombic cross sections normal to the plane of symmetry along the forward part of the model (fig. 2(d)). The rear part of model 4 was composed of octagonal cross sections with a maximum thickness of 7.8 percent of the model length. Fixed vertical stabilizers were located on both the upper and lower surfaces adjacent to the base as well as at the wing tips. Details of stabilizers located at wing tips are shown in figure 2(e). Model 6 had rhombic cross sections normal to the plane of symmetry except for a region near the base (fig. 2(g)). The forward 20 percent

of model 6 was deflected up 5° from the model center line. Two sets of flaps were located rearward of the base; one set consisted of an extension of the wing lower surfaces, and a smaller set was mounted normal to the upper surfaces at the wing tips. Both sets of flaps could be deflected 10° from the flap-neutral position.

The wing-body combinations consisted of model 5 (fig. 2(f)), model 7 (fig. 2(h)), and model 8, which was model 5 in an inverted position. The wing of model 5 had a triangular plan form and was attached in a low-wing position to a conical body. Cone-shaped controls located at the wing tips could be deflected -8°, -18°, and -28° from the neutral position. Model 7 consisted of a flat-top wing-body combination. The wing incorporated a highly sweptback leading edge, wedge airfoil sections, and negative dihedral in the region of the tips. The rear part of the wing could be deflected 10° from the undeflected position. The angle of attack of model 7 was measured with respect to a line formed by the intersection of the wing upper surface and the plane of symmetry. Body coordinates of model 7 are presented in table II.

Force and moment characteristics of these models were obtained through the use of a six-component internal strain-gage balance attached to a rotary-type sting which permitted simultaneous variation of angle of attack and angle of sideslip. Four static-pressure tubes attached to the support sting were used to measure the pressure at the base of the models.

TESTS, CORRECTIONS, AND ACCURACIES

The tests were conducted in the Langley 4- by 4-foot supersonic pressure tunnel which is briefly described in reference 5. All models were tested at a Mach number of 1.41 through an angle-of-attack range from -1° to approximately 16° at zero sideslip angle and through a sideslip-angle range from -1° to approximately 15° at angles of attack of approximately 0°, 4°, 8°, and 12°. Similar tests were conducted at a Mach number of 2.01; however, at M = 2.01 it was possible to extend the range of angle of attack and sideslip angle to approximately 27°. Models 5, 6, and 7 were tested with controls deflected symmetrically to determine the longitudinal control characteristics and asymmetrically to determine the roll control characteristics.

The conditions of the tests were as follows:

Mach number 1.41   2.01
Stagnation pressure, lb/sq in. abs 10   10
Stagnation temperature, °F 110   110
Reynolds number per foot . . . . 2.90 × 10^6 2.41 × 10^6

The stagnation dewpoint was maintained sufficiently low (-25° F or less) to avoid significant condensation effects in the test section.

The angles of attack and sideslip were corrected for the deflection of the balance and sting under load. The drag characteristics presented herein include base pressure drag; however, the variation of the base drag coefficient of each model with angle of attack is presented in figure 4. The base drag was determined by utilizing the base pressure measured in the vicinity of the model support strut, and this measurement was applied to the total base area of each model.

Estimated probable errors in the force and moment data, based on the repeatability of the results, zero-shift calibration, and random error of instruments, are as follows:

M	F_N, lb	F_A, lb	M_Y, in-lb	M_Z, in-lb	M_X, in-lb	F_Y, lb
1.41	±3.6	±0.1	±2.1	±2.3	±0.9	±3.0
2.01	±1.7	± .1	±2.1	±2.1	± .9	±4.0

The angles of attack at zero sideslip and the sideslip angles at zero angle of attack are estimated to be correct to within ±0.1°. The combined angles of attack and sideslip are correct to within ±0.2°. Mach number is accurate within ±0.01.

PRESENTATION OF RESULTS

DISCUSSION

Longitudinal Characteristics

Body configuration.- The longitudinal aerodynamic characteristics of models 1, 2, and 3 presented in figure 5 are based on the geometric characteristics of model 1 and are resolved about both the stability and body axes.

In general, the pitching-moment characteristics presented in figure 5 indicate that the cone-shaped body (model 1) was neutrally stable through the angle-of-attack range at $M = 1.41$ and $M = 2.01$. The slope of the normal-force curve C_{N_α} near $\alpha = 0°$ increased from 0.025 at $M = 1.41$ to 0.035 at $M = 2.01$. For model 2 (flat-bottom trihedron) C_{N_α} was approximately twice as great as for model 1; however, the pitching-moment characteristics of model 2 are not significantly different from those of model 1 at either $M = 1.41$ or $M = 2.01$. A comparison of the C_N characteristics of models 1 and 3 indicates that the addition of the cruciform fins resulted in an increase in C_{N_α} from 0.025 to 0.12 for $M = 1.41$ and from 0.035 to 0.13 for $M = 2.01$. The pitching-moment characteristics of model 3 are essentially the same as those for models 1 and 2 at angles of attack up to 4°. At angles of attack greater than 4° the pitching-moment characteristics of model 3 indicate an increase in stability.

The lift-drag ratios of models 1, 2, and 3 are presented in figure 6 in a manner which indicates the effect of base drag. The results that include base drag are comparable to a condition of zero thrust, whereas the results corrected for base drag simulate a thrust condition at which the base static pressure for a given Mach number is equivalent to the free-stream static pressure.

Wing and wing-body configurations.- The longitudinal aerodynamic characteristics of wing configurations (models 4 and 6) and wing-body configurations (models 5, 7, and 8), referred to the stability-axis

system, are presented in figure 7 for M = 1.41 and M = 2.01. It should be recalled that the data obtained with each of these particular configurations was reduced to coefficient form by using the geometric characteristics of that particular configuration. Inasmuch as the geometric characteristics of models 4 and 6 are approximately the same, a comparison of the longitudinal stability characteristics of these models is presented in figure 8. The longitudinal stability characteristics of models 5, 7, and 8 are presented in figure 9. These results (figs. 8 and 9) indicate that changes in stability of models 4 to 8 through the range of angles of attack of this investigation were relatively small. The results presented in figure 8 indicate that the center of pressure of model 6 was located forward of the center of pressure of model 4. This is associated with the fact that model 6 has slightly more area forward of the center-of-moment location than model 4. Increase in Mach number from 1.41 to 2.01 had no significant effect on the longitudinal stability of models 4, 5, 6, and 8; however, in the case of model 7 increase in Mach number resulted in a negative trim change.

The L/D characteristics of the wing and wing-body configurations are presented in figure 10. These results were determined from drag characteristics both uncorrected and corrected for model base drag. The maximum L/D for the zero-thrust condition (base drag included) was approximately 2.7 and 3.0 for the wing configurations (models 4 and 6) at Mach numbers of 1.41 and 2.01, respectively. The maximum L/D (base drag included) of the wing-body configurations (models 5, 7, and 8) was approximately 4 for M = 1.41 and 2.01. Inverting model 5 resulted in the occurrence of the maximum L/D at a slightly lower angle of attack.

The results presented in figures 12 to 14 indicate that the longitudinal-control devices tested on models 5, 6, and 7 were effective throughout the angle-of-attack range.

Lateral Stability Characteristics

Body configurations.- The lateral stability characteristics of models 1, 2, and 3 (figs. 15 to 17) are summarized in figure 18. The results in figure 18 indicate that the directional stability of models 1 and 2 was zero through the angle-of-attack range at M = 1.41 and 2.01. A comparison of the directional-stability derivatives of models 1 and 3 indicates that the addition of cruciform fins to the cone configuration provided positive stability to moderately high angles of attack. At M = 2.01 the effect of fins deteriorated at high angles of attack, resulting in directional instability of model 3. The rolling moment due to sideslip C_{l_β} of models 1 and 2 was zero for a range of angles of attack up to approximately 12° for M = 1.41 and M = 2.01. At higher angles of attack, where data were obtained for M = 2.01 only, C_{l_β} for

model 2 became negative. The rolling moment due to sideslip for model 3 was negative throughout the angle-of-attack range of the investigation.

Wing and wing-body configurations.- The lateral stability charac-teristics of models 4 and 6 are presented in figures 19 to 21. A summary of the lateral stability characteristics, presented in figure 22, indicates that although both models 4 and 6 were directionally stable, C_{n_β} of model 4 decreased with angle of attack, whereas C_{n_β} of model 6 increased with angle of attack. Increase in Mach number resulted in a small decrease in the stability level. Both model 4 and model 6 exhib-ited positive effective dihedral.

The lateral stability characteristics of the wing-body configurations (models 5, 7, and 8) are shown in figures 23, 25, and 24, respectively. The summary in figure 26 indicates that, with the exception of model 7, these configurations were directionally unstable at both Mach numbers. Model 7 exhibited positive directional stability at $\alpha = 0^\circ$; however, with increase in angle of attack, C_{n_β} decreased for both Mach num-bers and became zero at about 3° to 4° angle of attack. At low angles of attack the rolling moment due to sideslip C_{l_β} was positive for models 5 and 7; however, with increase in angle of attack the rolling moment due to sideslip became negative for both these configurations. An increase in Mach number resulted in an increase in C_{l_β} of model 5 in the positive direction, whereas the increase in Mach number had an opposite effect on C_{l_β} of model 7.

The data presented in figures 27 to 36 show the effects of deflected yaw control on the aerodynamic characteristics of model 6 and the effects of deflected roll control on the aerodynamic characteristics of models 6 and 7. The results presented in figure 27 indicate that the vertical fins on model 6 provided directional control up to $\alpha \approx 8.5^\circ$, the effec-tiveness C_{n_δ} amounting to approximately -0.0004 at $M = 1.41$ and -0.0003 at $M = 2.01$. Deflecting the vertical fins of model 6 also produced a positive increment in rolling moment. Differentially deflec-ted horizontal flaps of model 6 were effective in providing roll control which varied linearly with α and β; however, differentially deflected flaps also produced a negative pitching moment and yawing moment. (See figs. 29 to 32.) Differentially deflected flaps of model 7 resulted in positive roll control accompanied by a positive increase in yawing moment.

CONCLUDING REMARKS

Results of an investigation at Mach numbers of 1.41 and 2.01 of the static stability characteristics of several hypersonic boost-glide con-figurations indicate that all configurations investigated possessed

reasonably linear pitch, yaw, and rolling-moment characteristics for angles of attack to at least 12°. The values of maximum lift-drag ratio for zero-thrust condition (base drag included) were about 3 for the delta-wing configuration and about 4 for the wing-body configurations.

Langley Research Center,
     National Aeronautics and Space Administration,
          Langley Field, Va., August 7, 1959.

REFERENCES

1. Seiff, Alvin, and Allen, H. Julian: Some Aspects of the Design of Hypersonic Boost-Glide Aircraft. NACA RM A55E26, 1955.

2. Eggers, A. J., Jr., and Syvertson, Clarence A.: Aircraft Configurations Developing High Lift-Drag Ratios at High Supersonic Speeds. NACA RM A55L05, 1956.

3. Rainey, Robert W.: Static Stability and Control of Hypersonic Gliders. NACA RM L58E12a, 1958.

4. Syvertson, Clarence A., Gloria, Hermilo R., and Sarabia, Michael F.: Aerodynamic Performance and Static Stability and Control of Flat-Top Hypersonic Gliders at Mach Numbers From 0.6 to 18. NACA RM A58G17, 1958.

5. Robinson, Ross B., and Driver, Cornelius: Aerodynamic Characteristics at Supersonic Speeds of a Series of Wing-Body Combinations Having Cambered Wings With An Aspect Ratio of 3.5 and a Taper Ratio of 0.2 - Effects of Sweep Angle and Thickness Ratio on the Aerodynamic Characteristics in Pitch at M = 1.60. NACA RM L51K16a, 1952.

TABLE I.- GEOMETRIC CHARACTERISTICS

Model 1:
   Length, ft 2.50
   Apex angle . . . . $7° 8'$
   Base diameter, ft 0.313
   Base area, sq ft 0.077
   Reference dimensions:
      x, y, ft 0.313
      S, sq ft 0.077

Model 2:
   Length, ft 2.50
   Base area, sq ft 0.082
   Reference dimensions:
      x, y, and S . . . . Parameters of model 1 used

Model 3:
   Length, ft 2.50
   Apex angle . . . . $7° 8'$
   Base diameter, ft 0.313
   Base area, sq ft 0.077
   Horizontal fin area (total), sq ft 0.36
   Vertical fin area 0.05
   Reference dimensions:
      x, y, and S . . . . Parameters of model 1 used

Model 4:
   Length, ft 2.50
   Base area, sq ft 0.14
   Reference dimensions:
      y (span), ft 0.79
      x, ft 1.67
      S, sq ft 1.19

Models 5 and 8:
   Length, ft 2.50
   Base area, sq ft 0.06
   Reference dimensions:
      y (span), ft 0.98
      x, ft 1.67
      S, sq ft 1.33

Model 6:
   Length, ft 2.50
   Base area, sq ft 0.13
   Reference dimensions:
      y (span), ft 0.83
      x, ft 1.67
      S, sq ft 1.34

Model 7:
   Length, ft 2.50
   Base area, sq ft 0.08
   Reference dimensions:
      y (span undeflected), ft 1.37
      x (mean geometric chord), ft 1.17
      S, sq ft 1.49

TABLE II.- BODY COORDINATES OF MODEL 7

Distance from nose, in.	r, in.
0.000	0.000
.529	.000
.767	.068
1.029	.118
1.529	.198
2.529	.337
3.529	.452
4.529	.561
8.529	.943
12.529	1.278
16.529	1.586
20.529	1.874
22.529	2.013
24.529	2.156
25.529	2.216
26.772	2.298
30.000	2.298
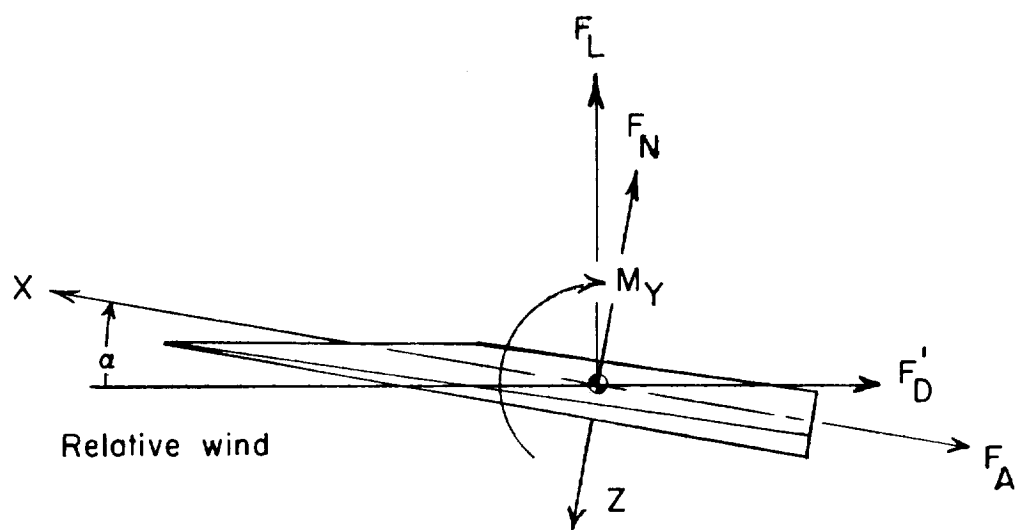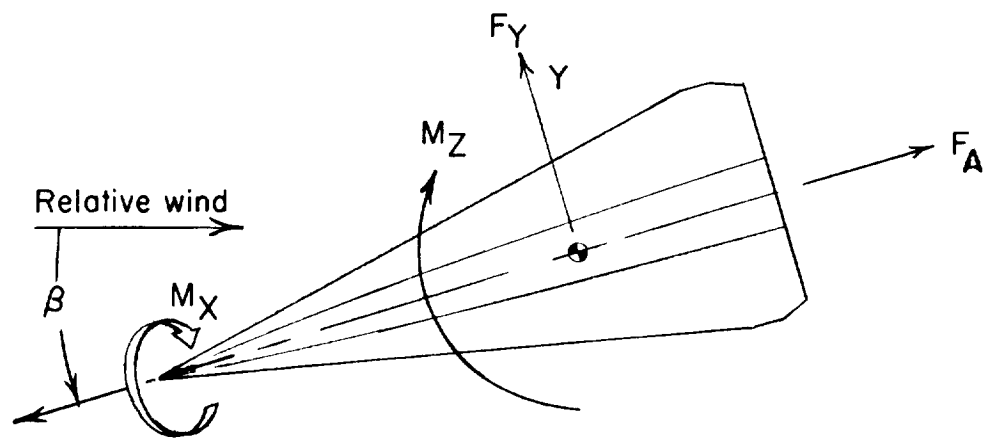
Figure 1.- Axis system. Arrows indicate positive directions.

16

(a) Model 1.

(b) Model 2.
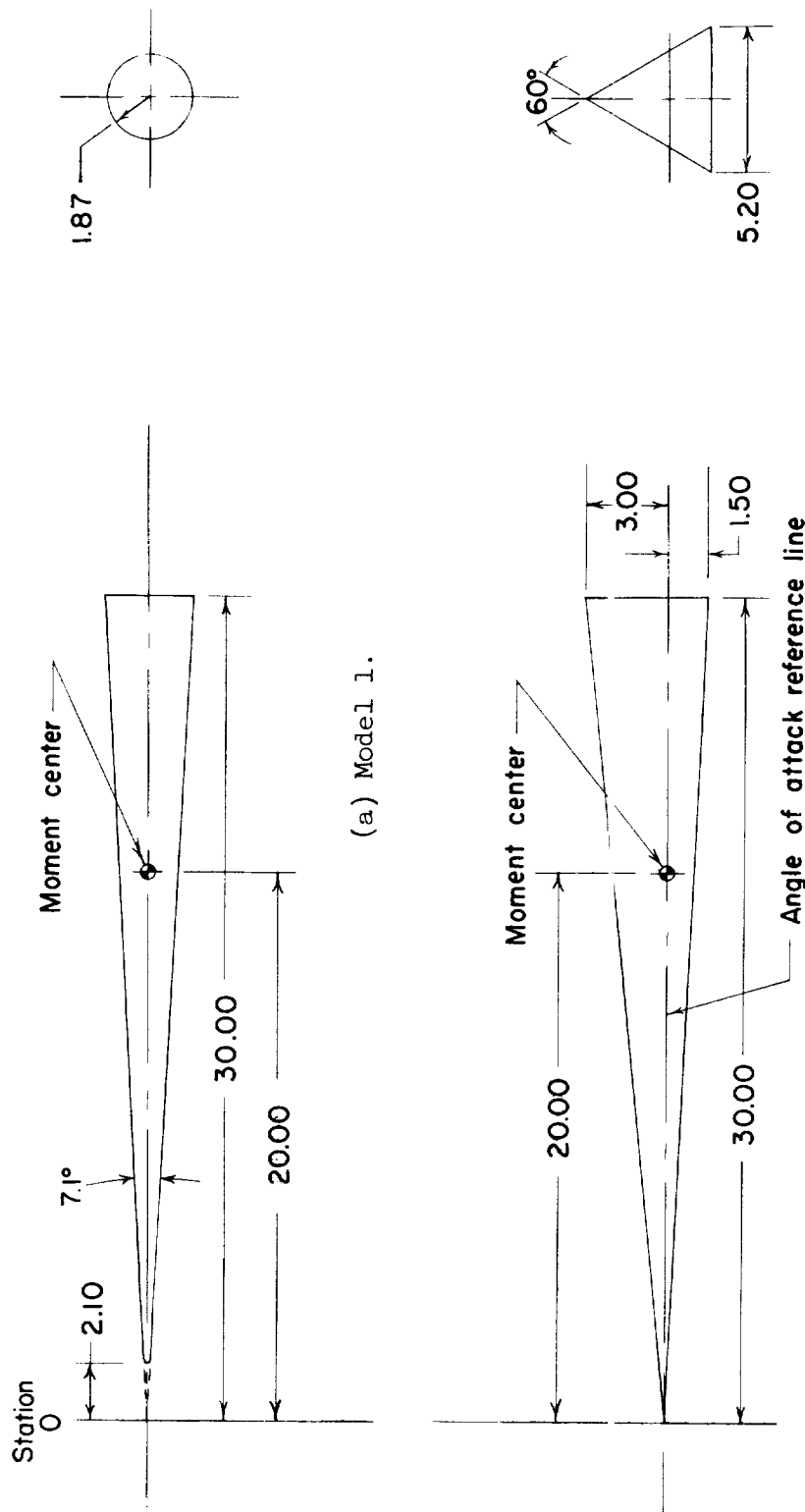
Figure 2.- Details of models. All dimensions are in inches unless otherwise noted.
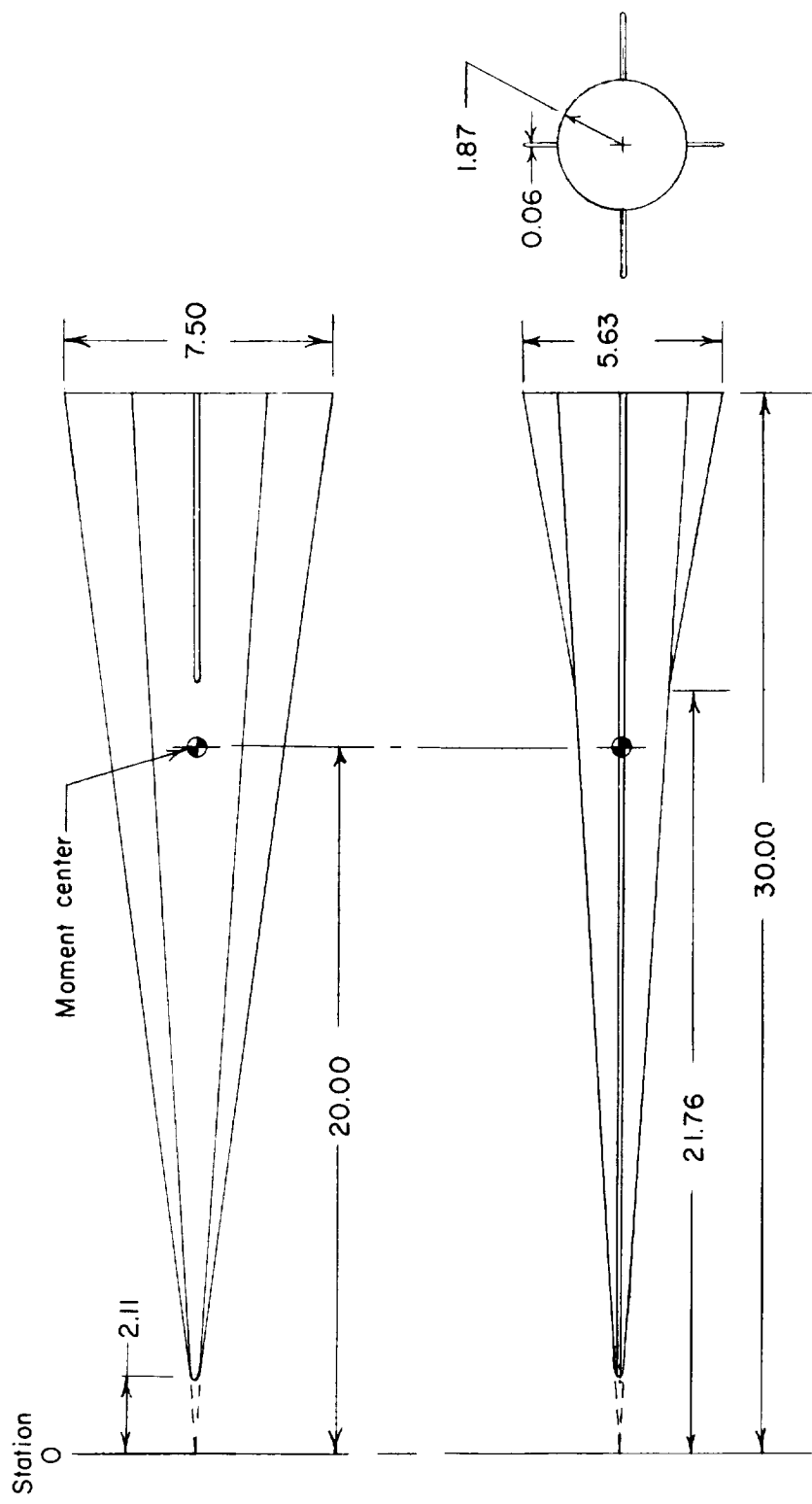
(c) Model 3.

Figure 2.- Continued.

18
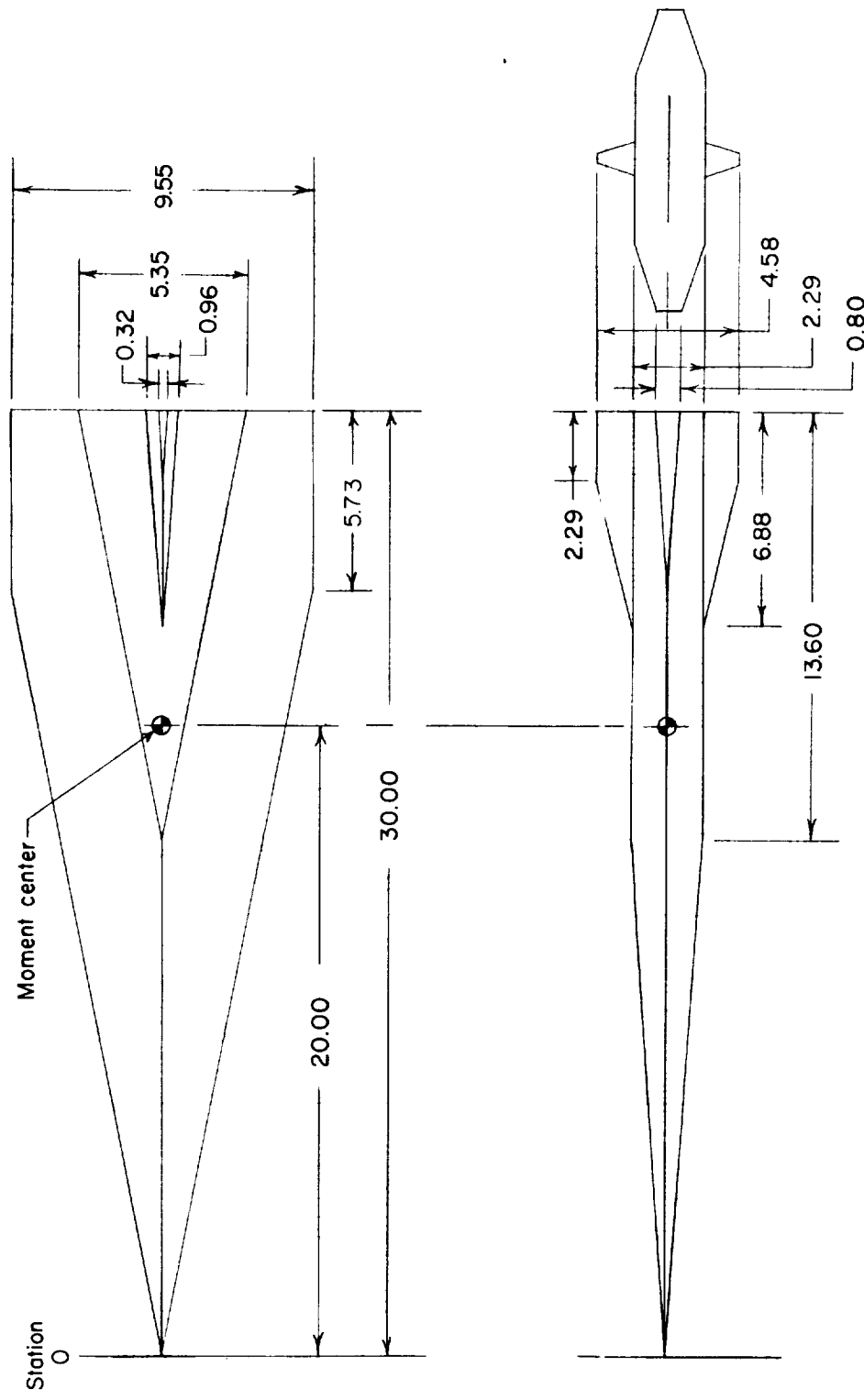
(d) Model 4.

Figure 2.- Continued.

5.73

0.80

1.5

1.70
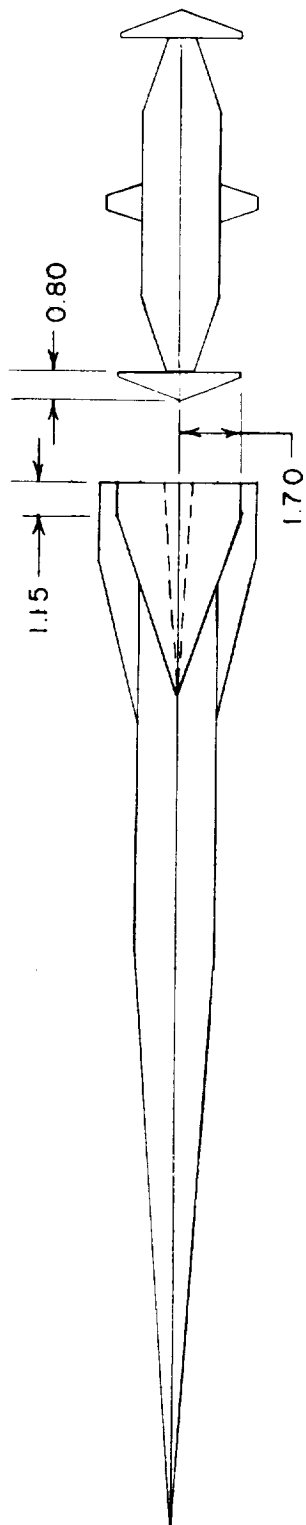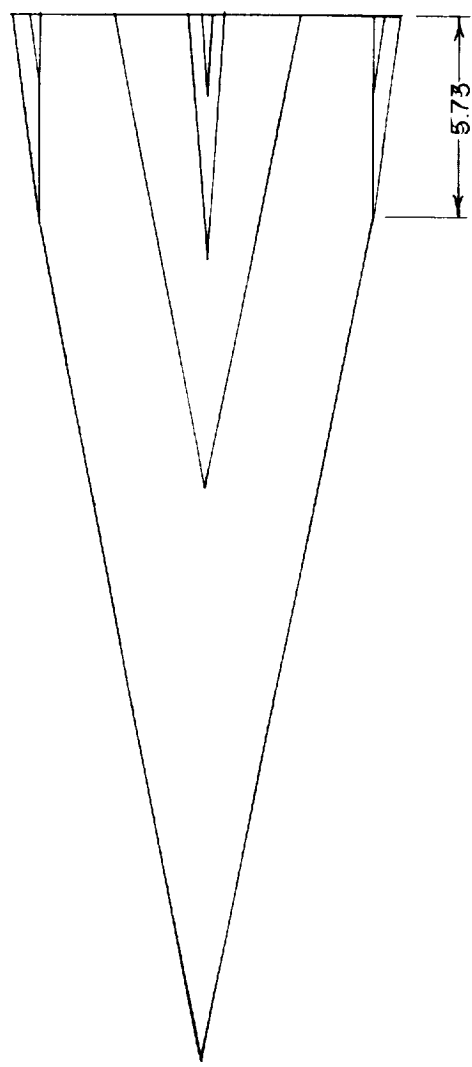
(e) Details of vertical fins on model 4.

Figure 2.- Continued.

Control hinge axis

13.11

11.72

10.33

7.50

2.10°

4.55°

5.53

Moment center

28.01

20.00

78°

Station 0

Angle of attack reference line

0.80

8.60°

3.58

12.75 (Theo.)

3.01

0.96

0.20

2.10°

1.22

30.00

0.18°

9.04°

14.50
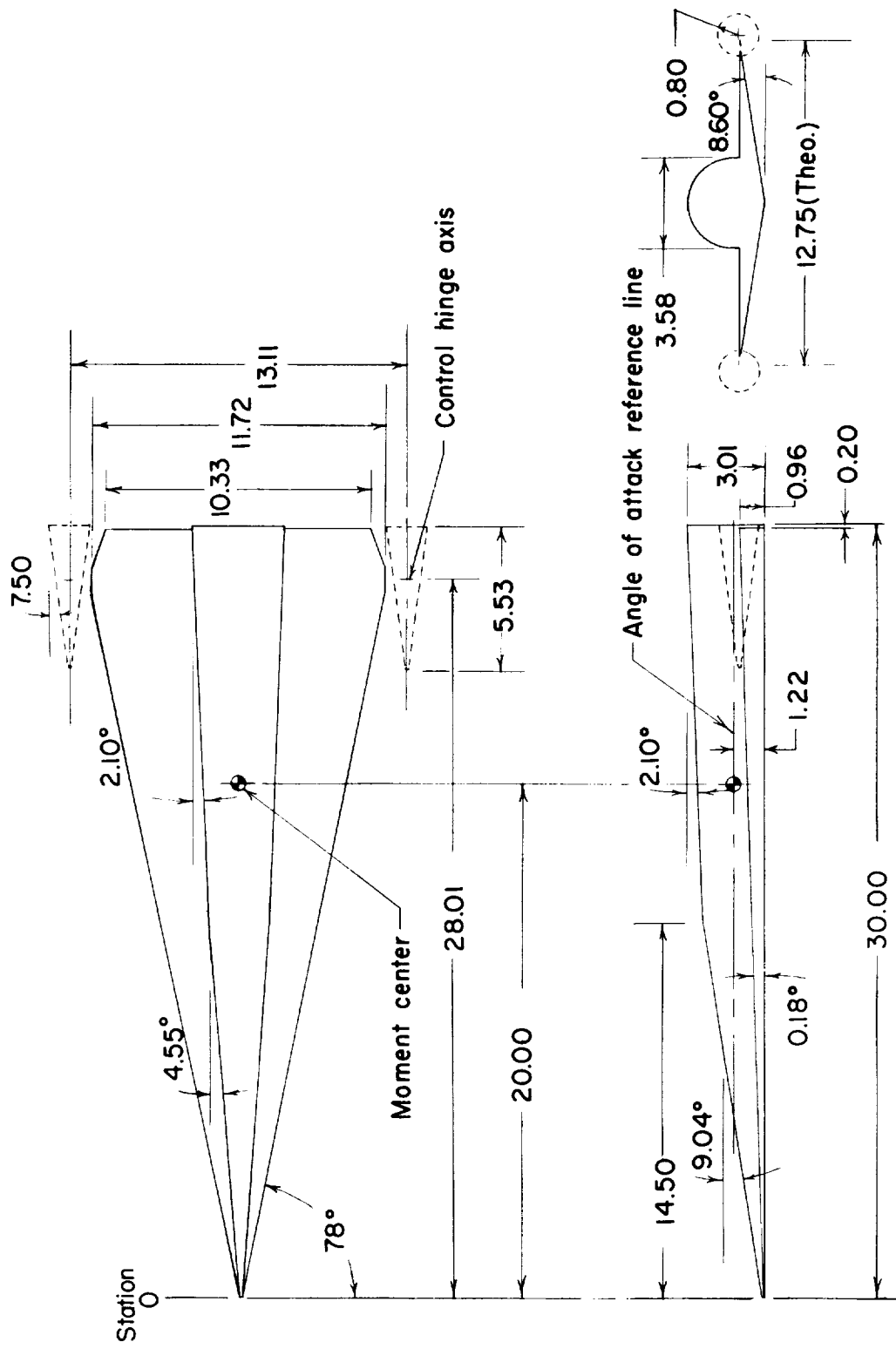
(f) Model 5.

Figure 2.- Continued.

Hinge line

2.00

0.75

1.26

Details of vertical flap

90°

4.90

10.00

3.57

Vertical and horizontal
flap hinge line

5.00°

3.00°

30.00

24.00

20.00

79.90°

73.43°

Moment center

6.00

28.00

5.00°

0.21

Station
O

(g) Model 6.

Figure 2.- Continued.

22
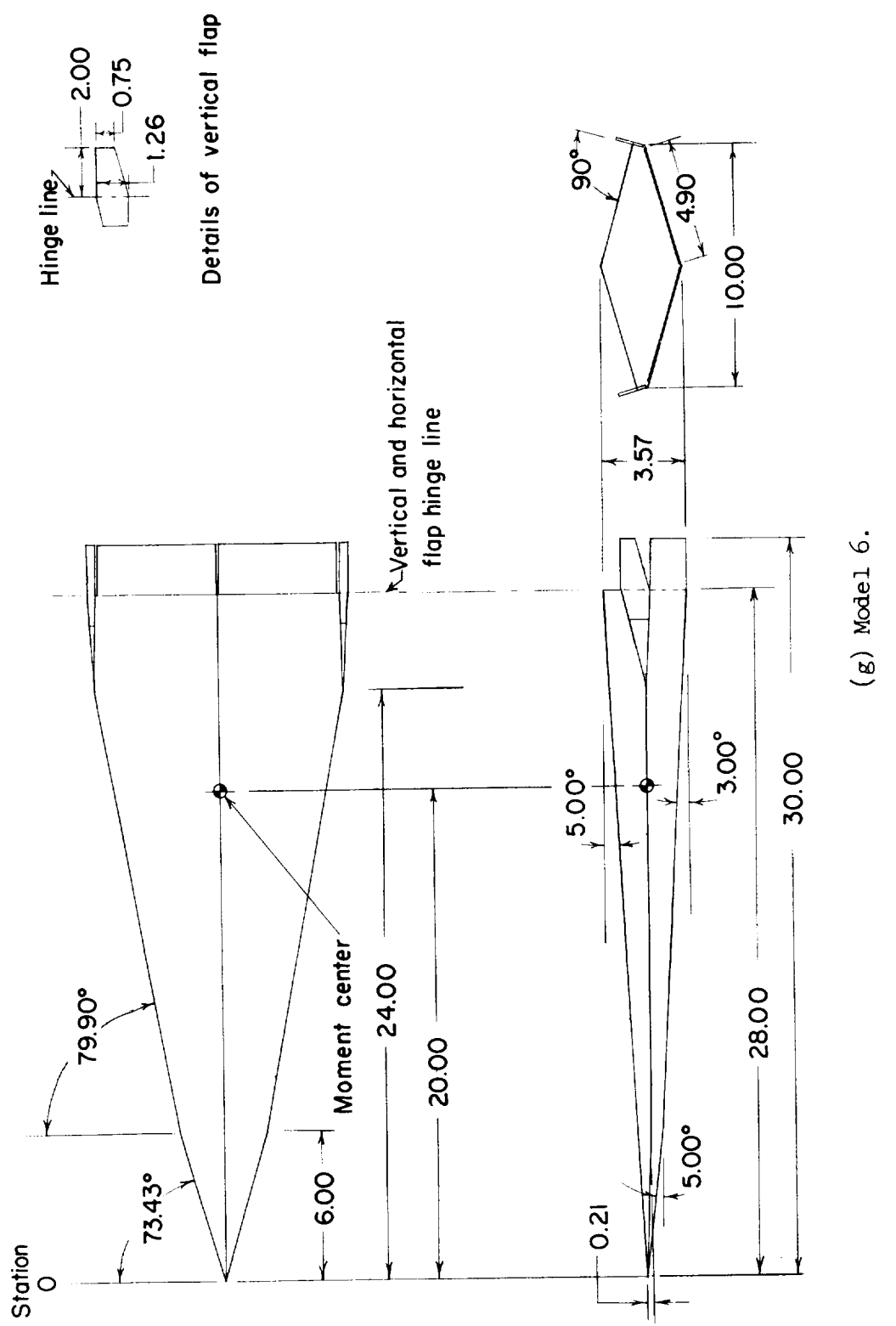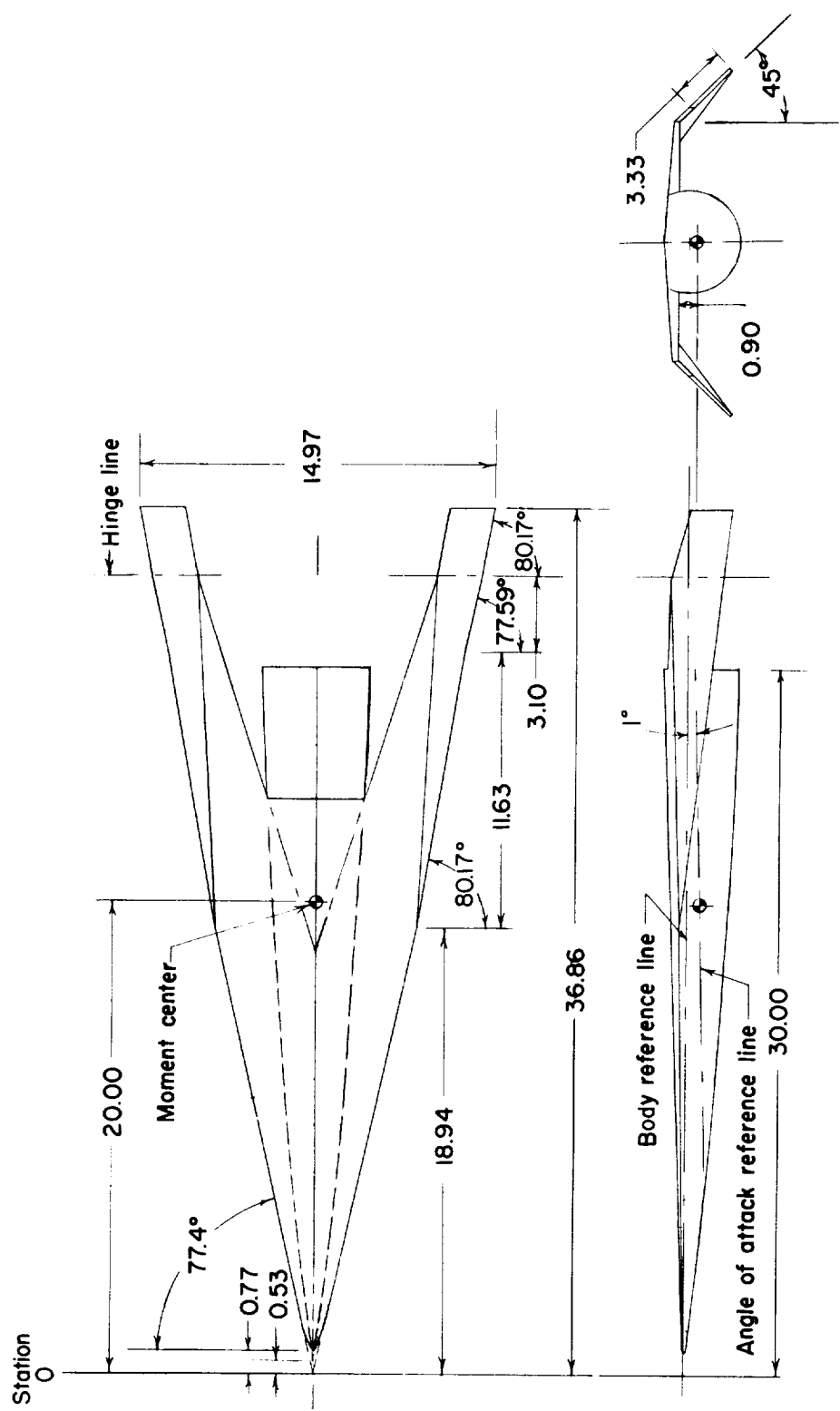
(h) Model 7.

Figure 2.- Concluded.

(a) Model 1.

L-58-2684

Figure 3.- Photographs of models.

L-58-2679
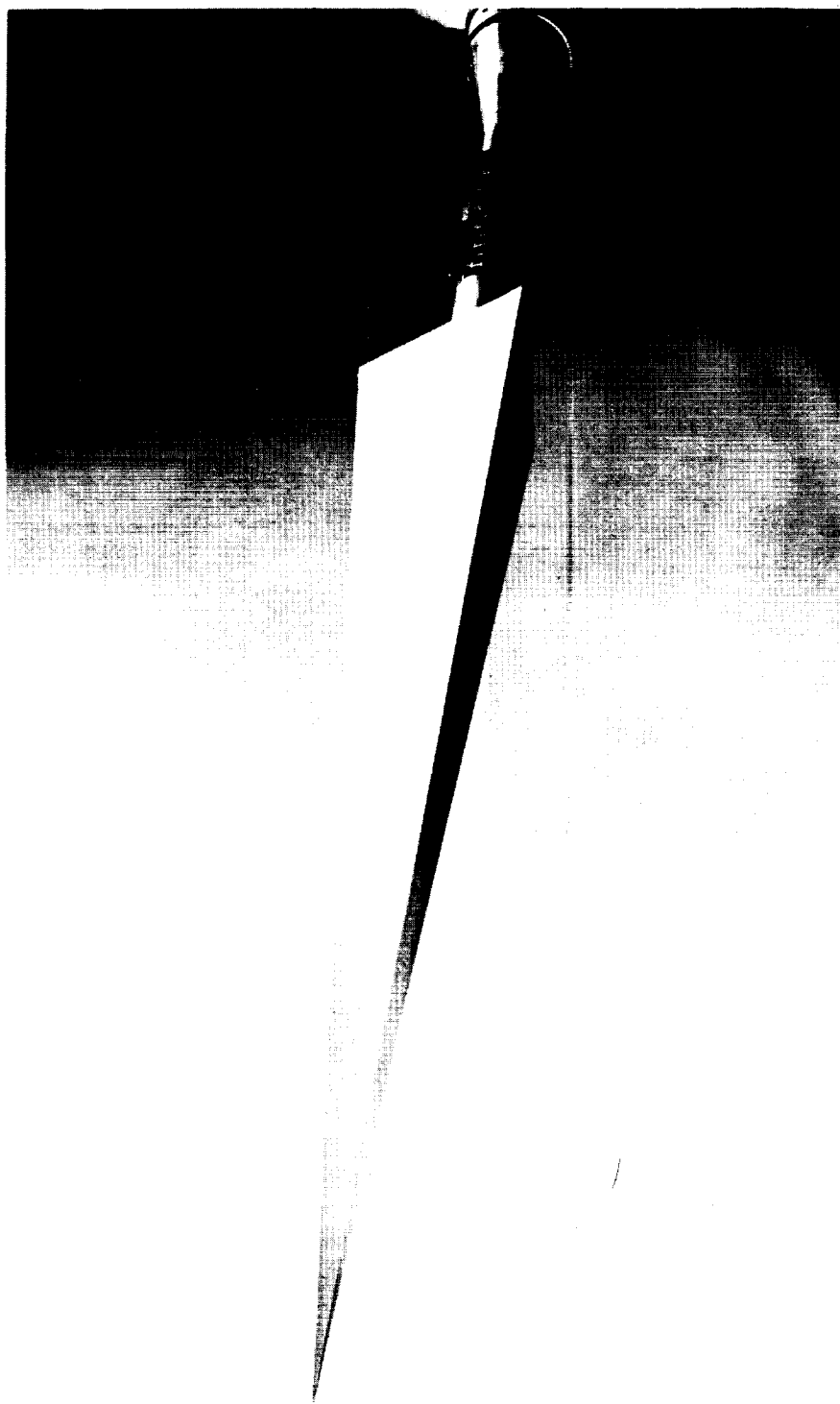
(b) Model 2.

Figure 3.- Continued.

L-58-2681

(c) Model 3.

Figure 3.- Continued.

(d) Model 4.

Figure 3.- Continued.

L-58-2682
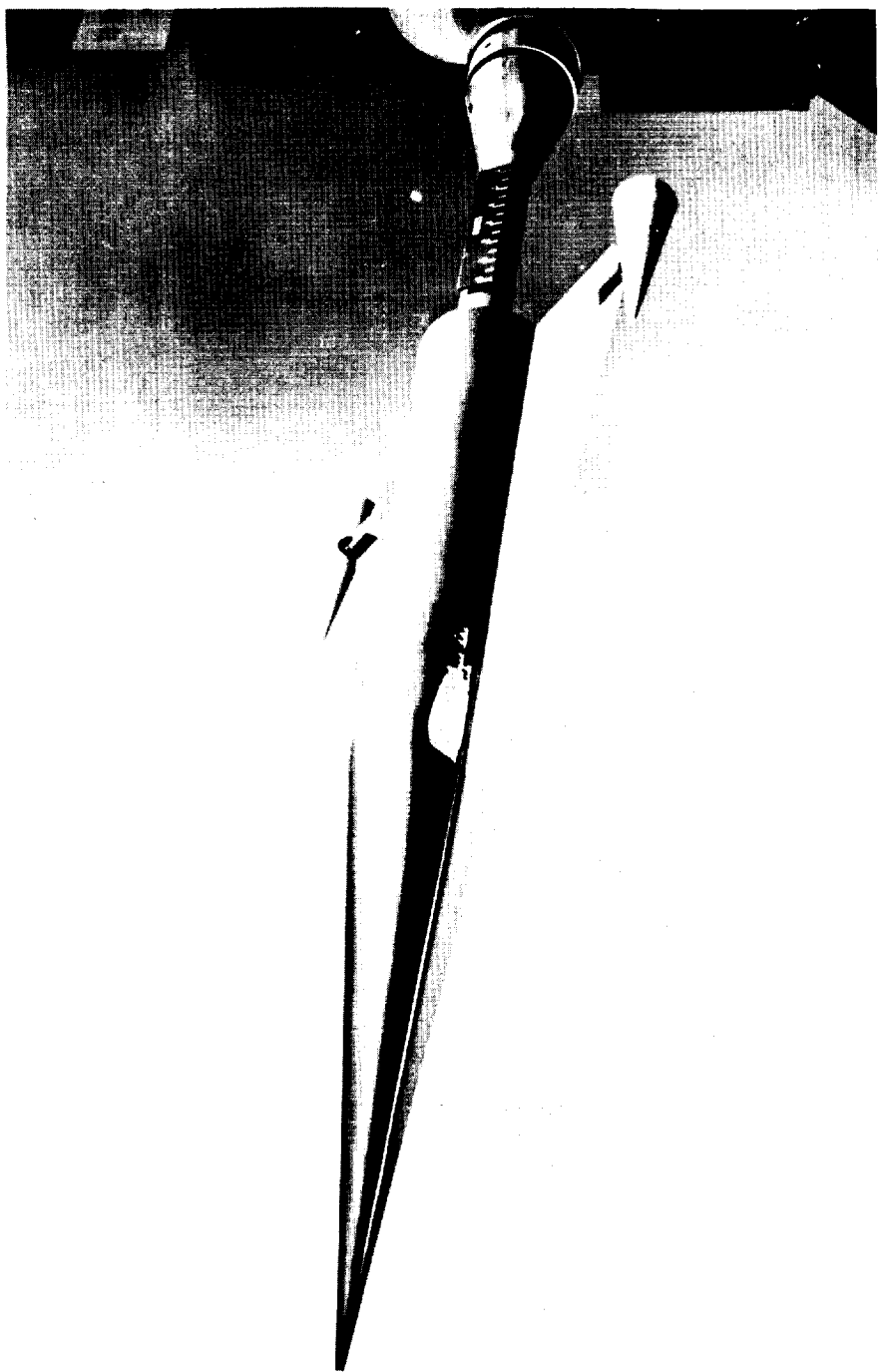
L-58-2676

(e) Model 5.

Figure 3.- Continued.
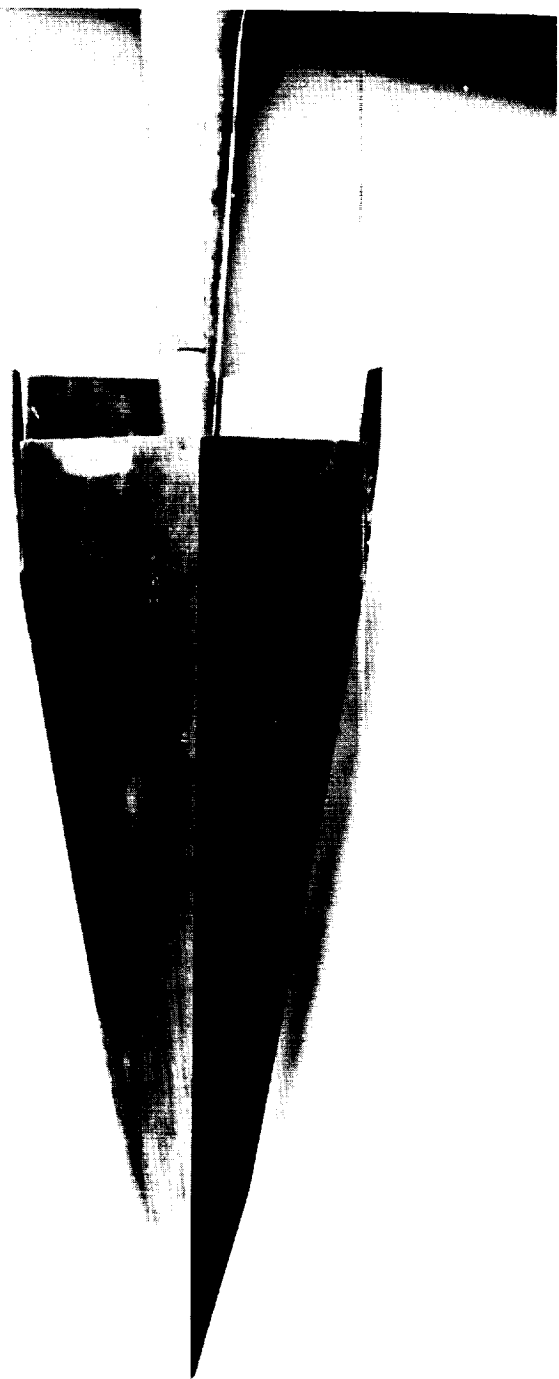
(f) Model 6.

Figure 3.- Continued.

L-58-3676
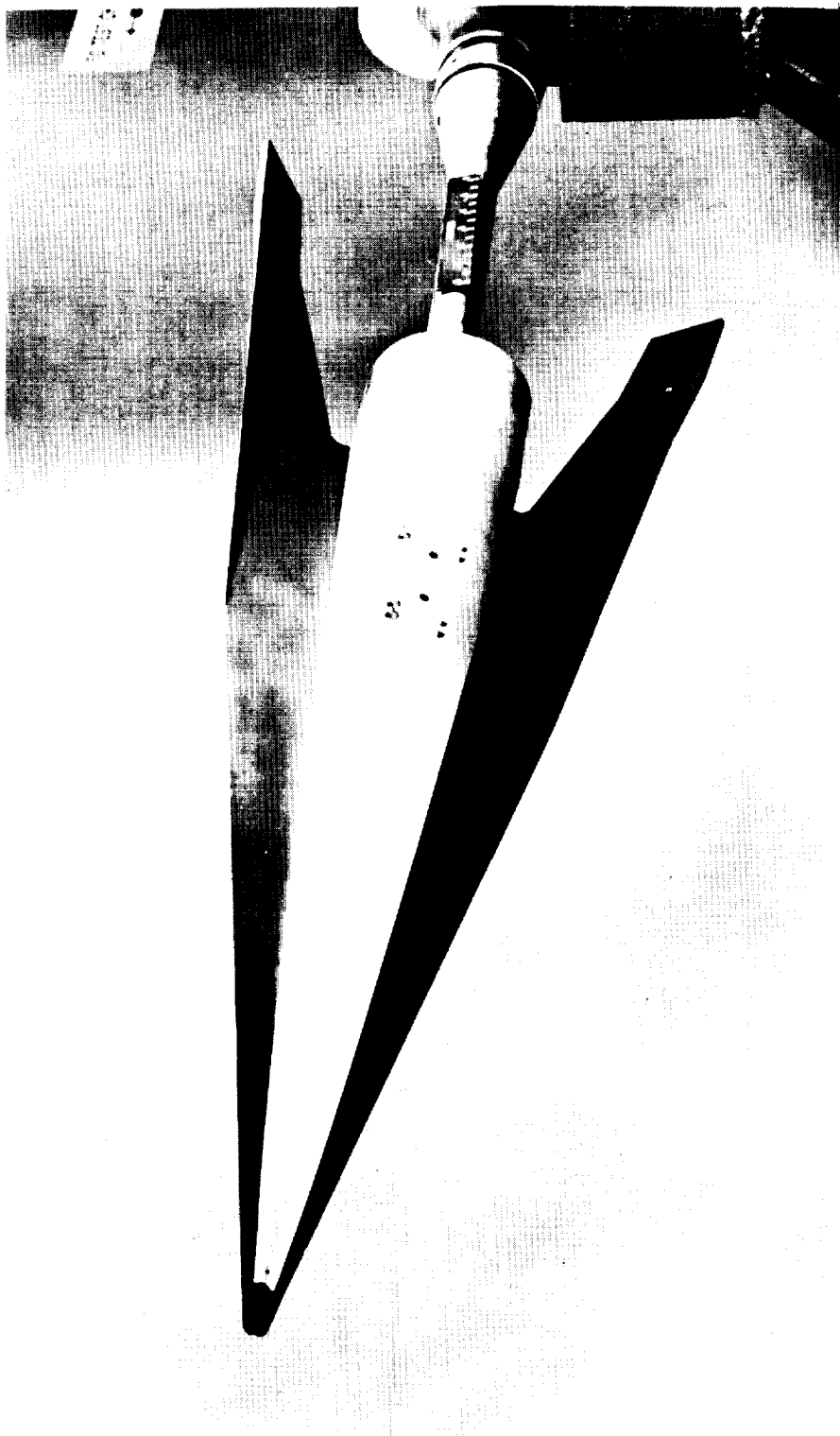
(g) Model 7.

Figure 3.- Concluded.

L-58-2677
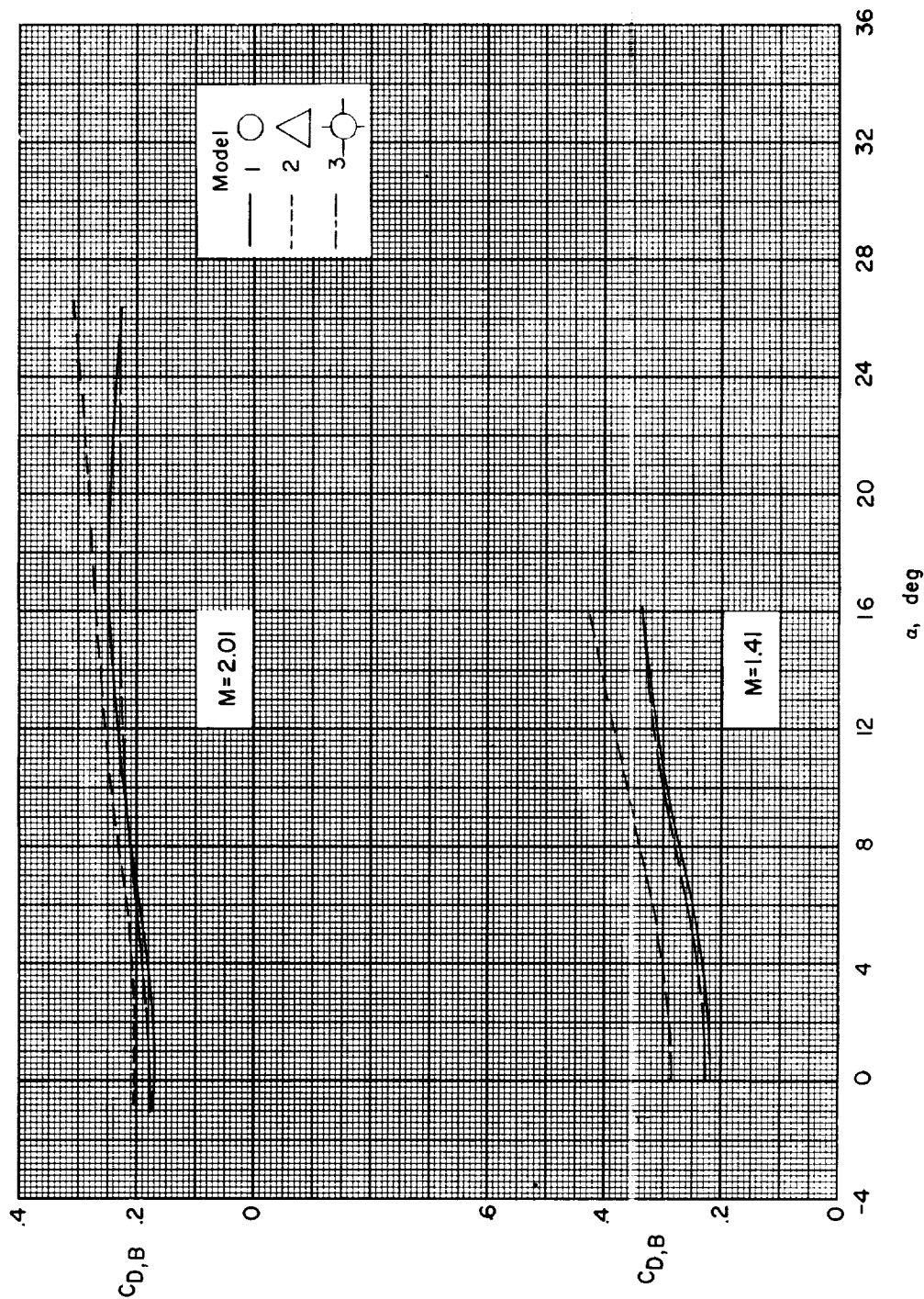
(a) Models 1 to 3.

Figure 4.- Variation of model base drag coefficient with angle of attack. $\beta \approx 0^\circ$.
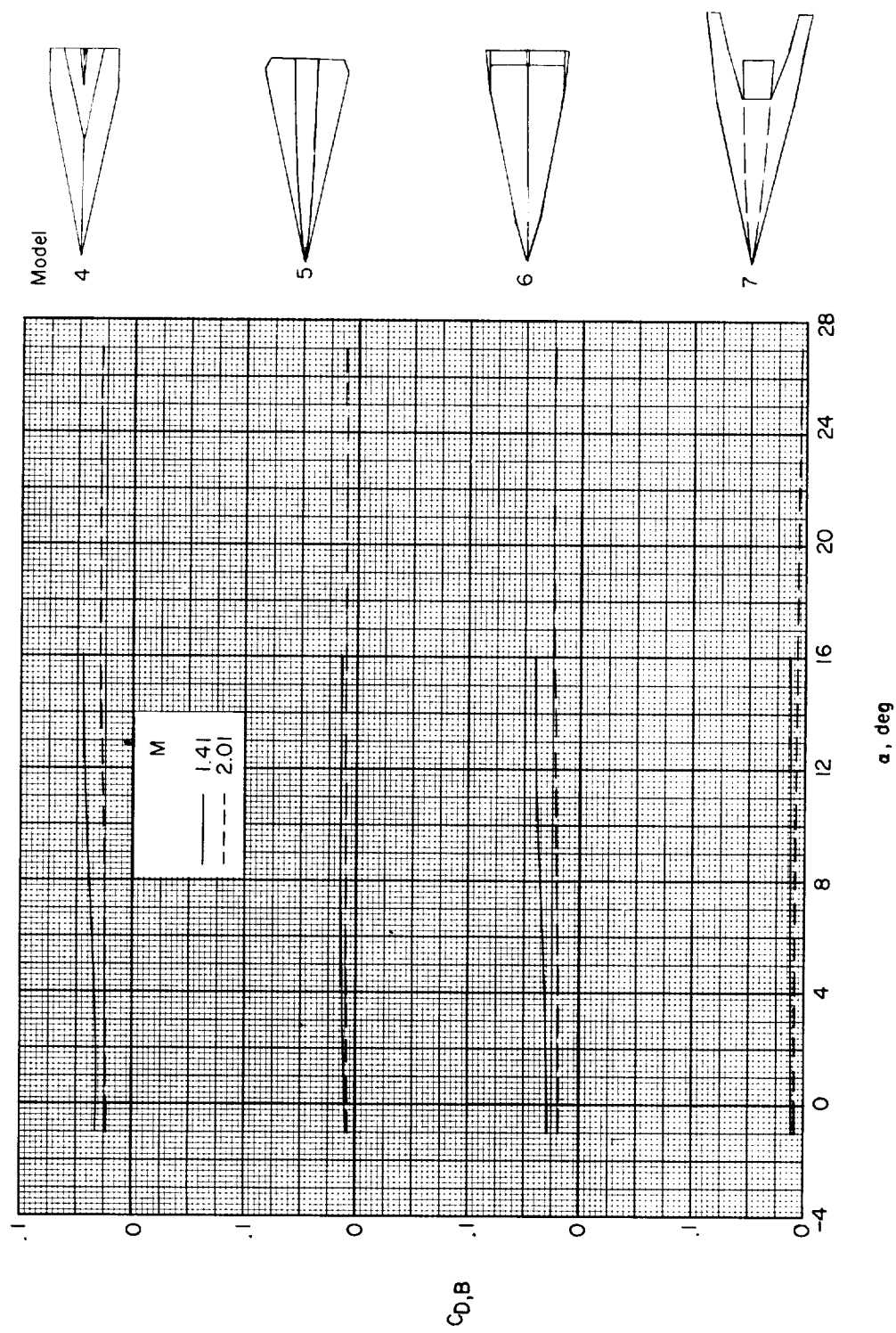
(b) Models 4 to 7.

Figure 4.- Concluded.
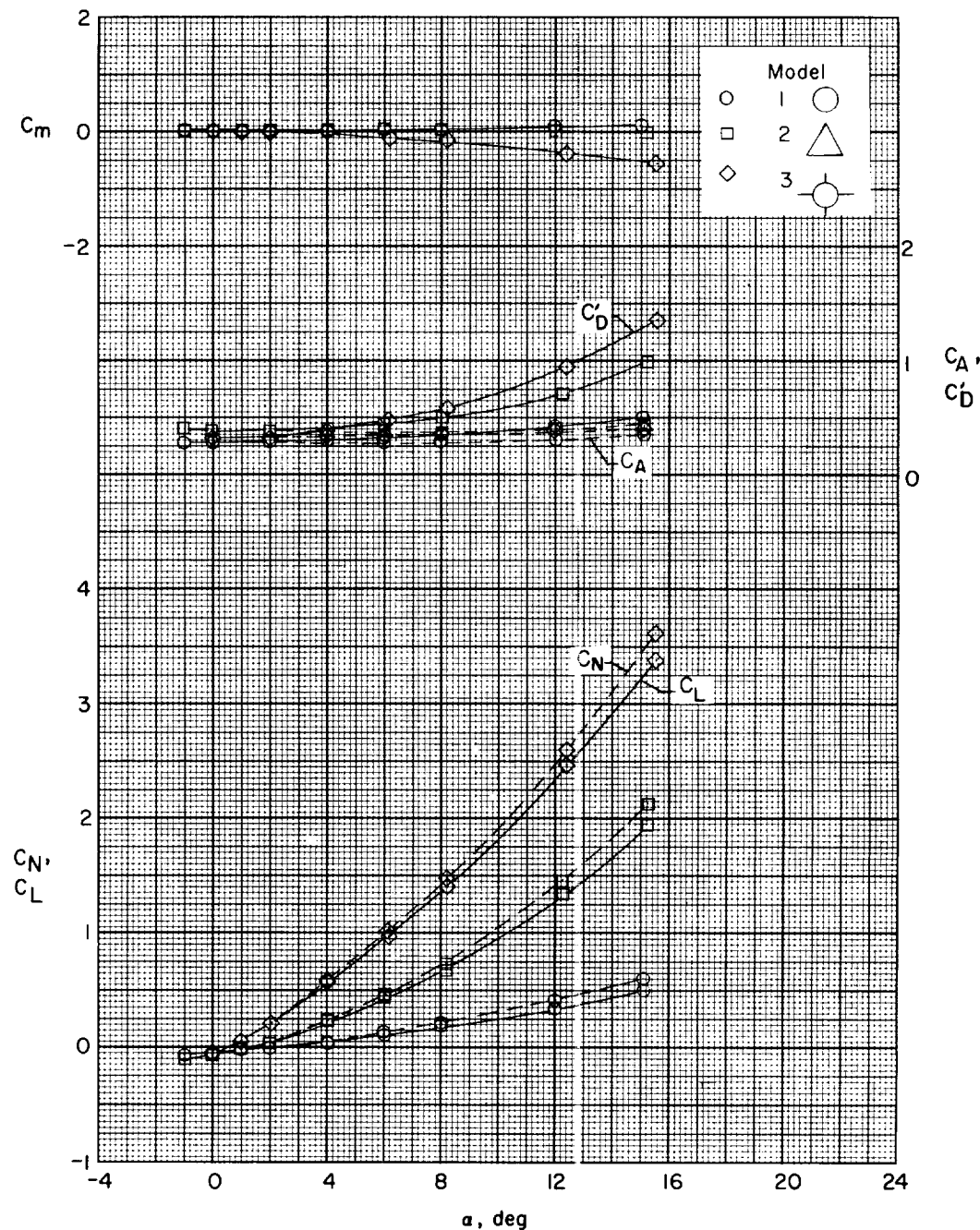
(a) M = 1.41.

Figure 5.- Variation of longitudinal aerodynamic characteristics of
models 1, 2, and 3 with angle of attack.
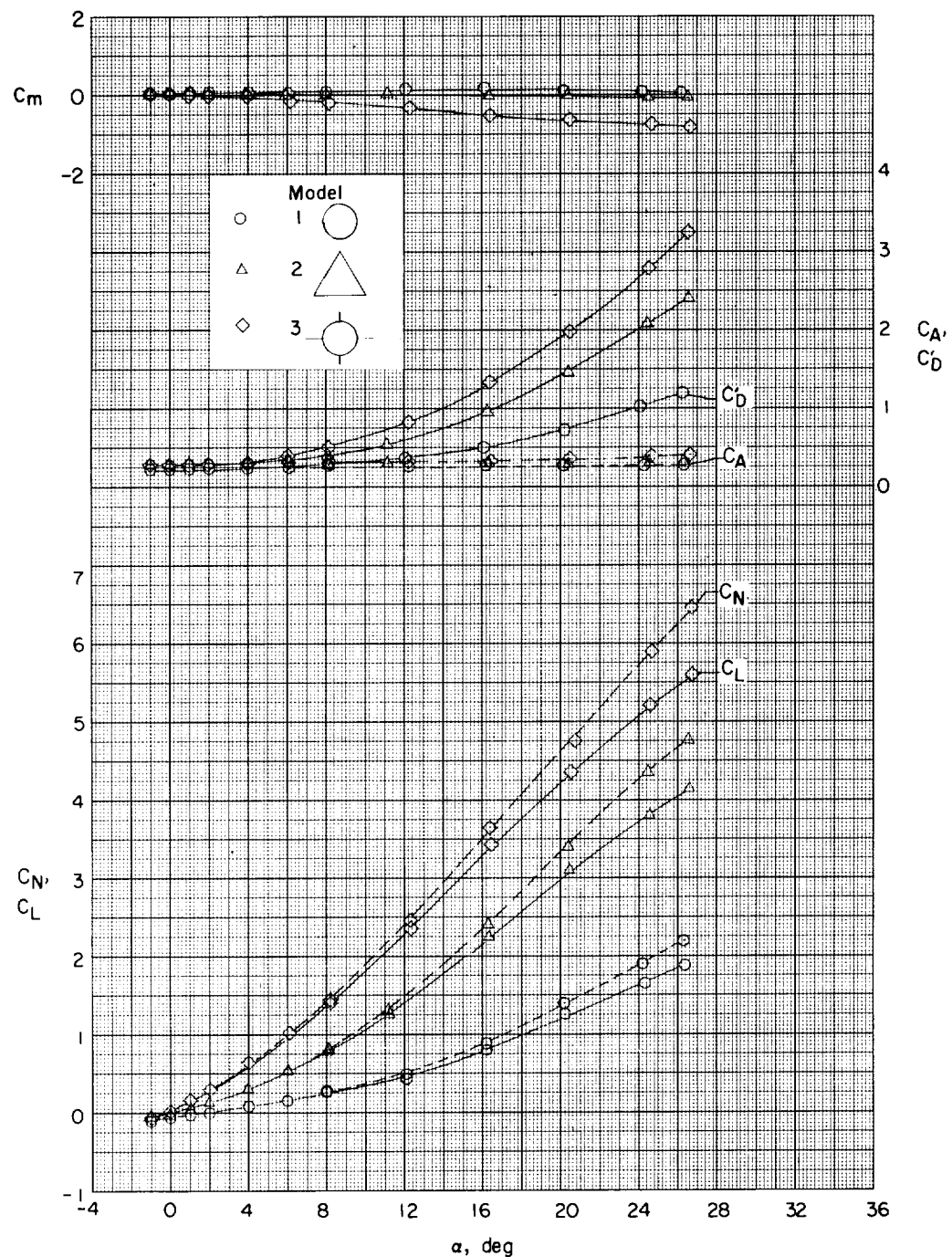
(b) M = 2.01.

Figure 5.- Concluded.
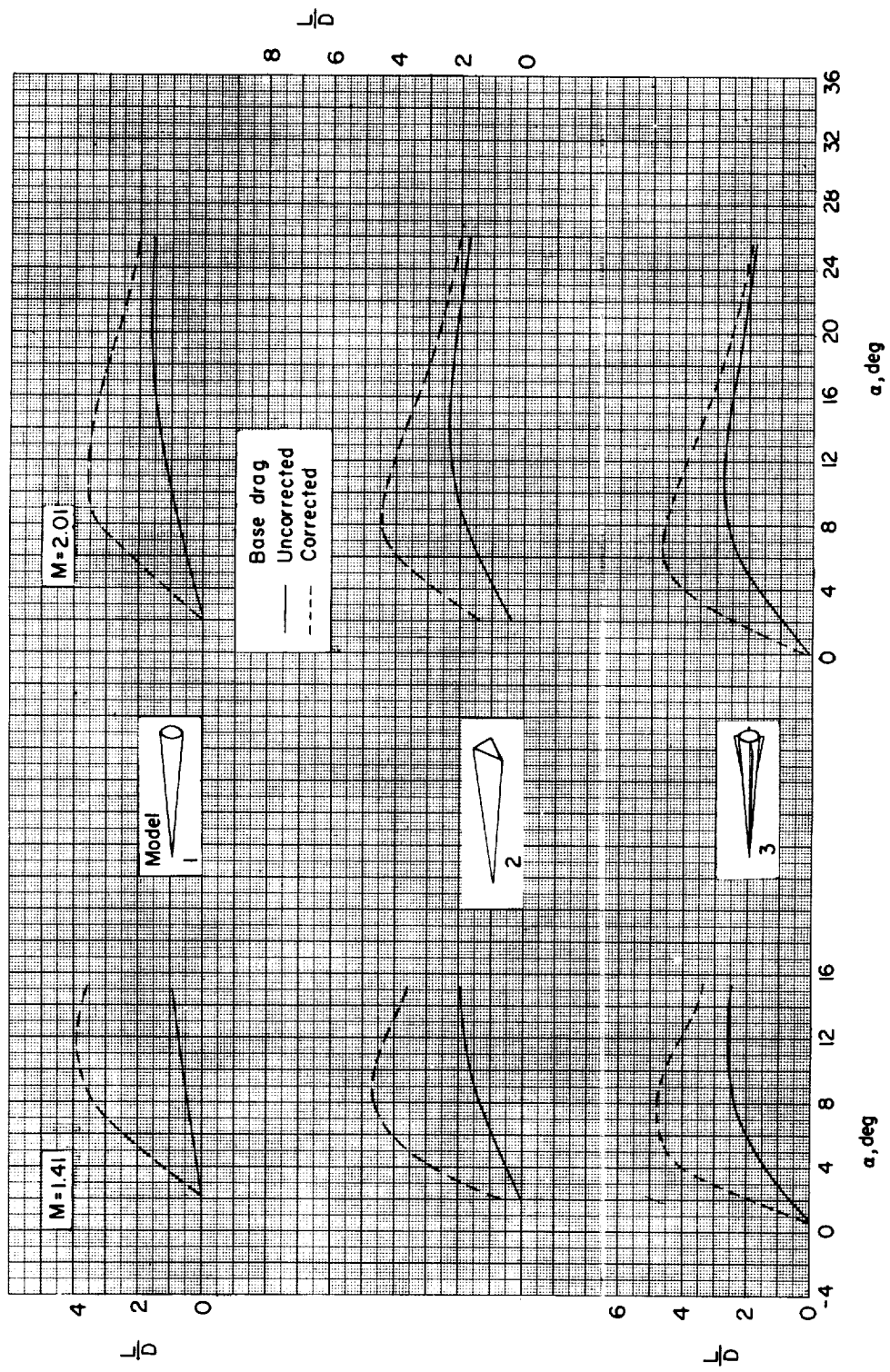
Figure 6.- Effect of model base drag on the variation of lift-drag ratio with angle of attack for models 1, 2, and 3. M = 1.41 and 2.01.
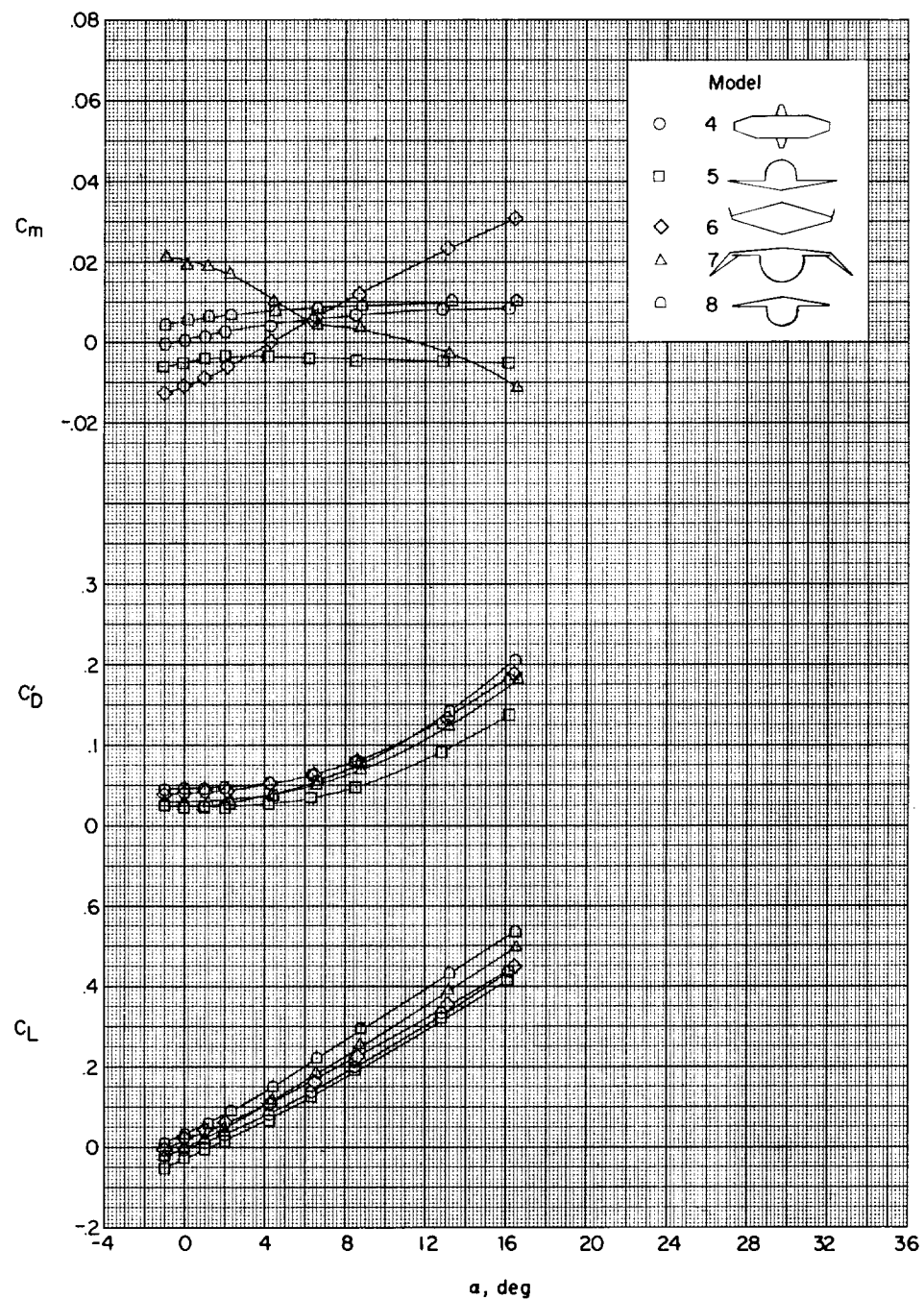
(a) M = 1.41.

Figure 7.- Variation of the longitudinal aerodynamic characteristics
with angle of attack for models 4, 5, 6, 7, and 8.

(b) M = 2.01.
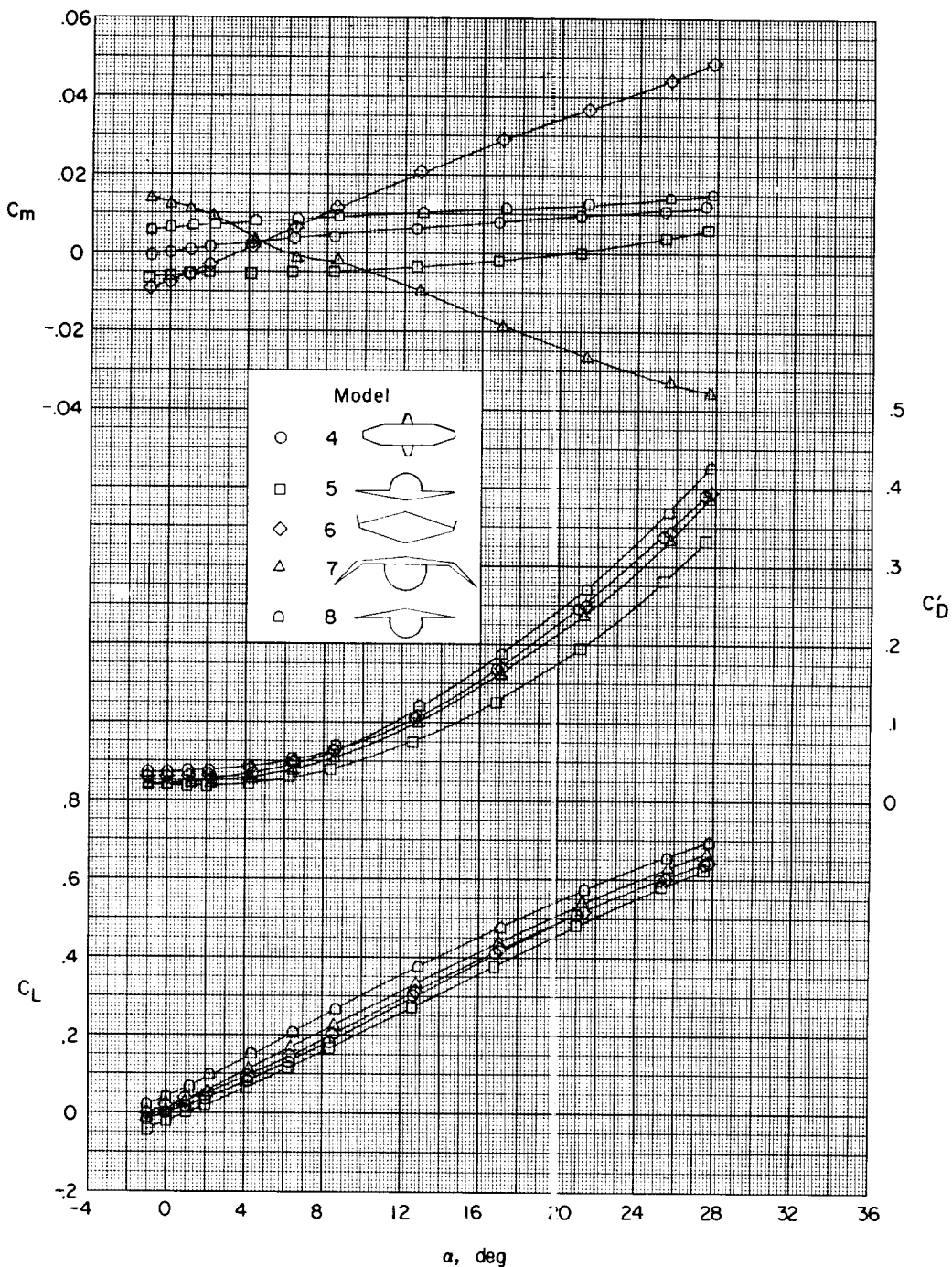
Figure 7.- Concluded.
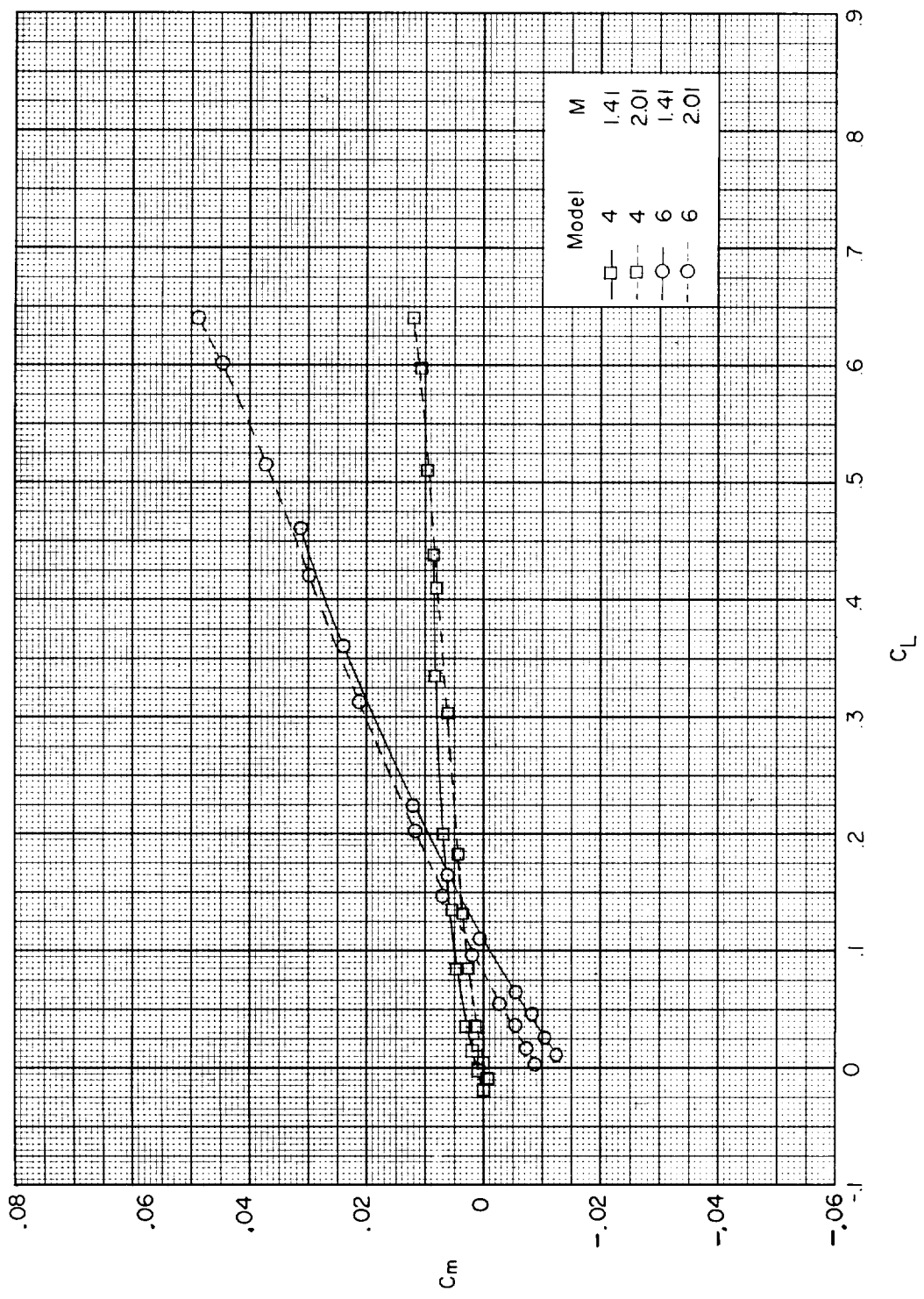
Figure 8.- Longitudinal stability characteristics of delta-wing configurations at M = 1.41 and 2.01.

38
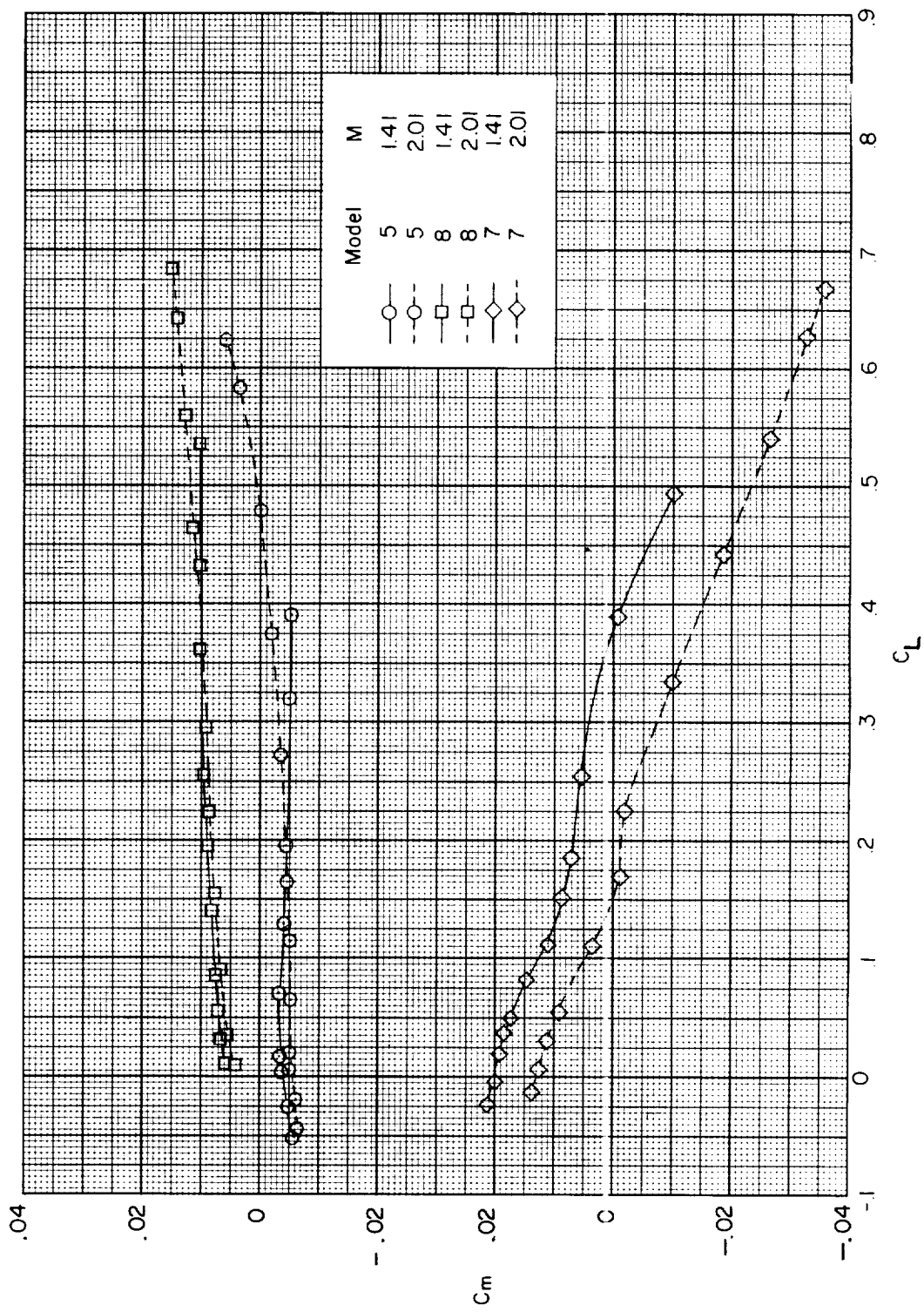
Figure 9.- Longitudinal stability characteristics of wing-body configurations at M = 1.41 and 2.01.
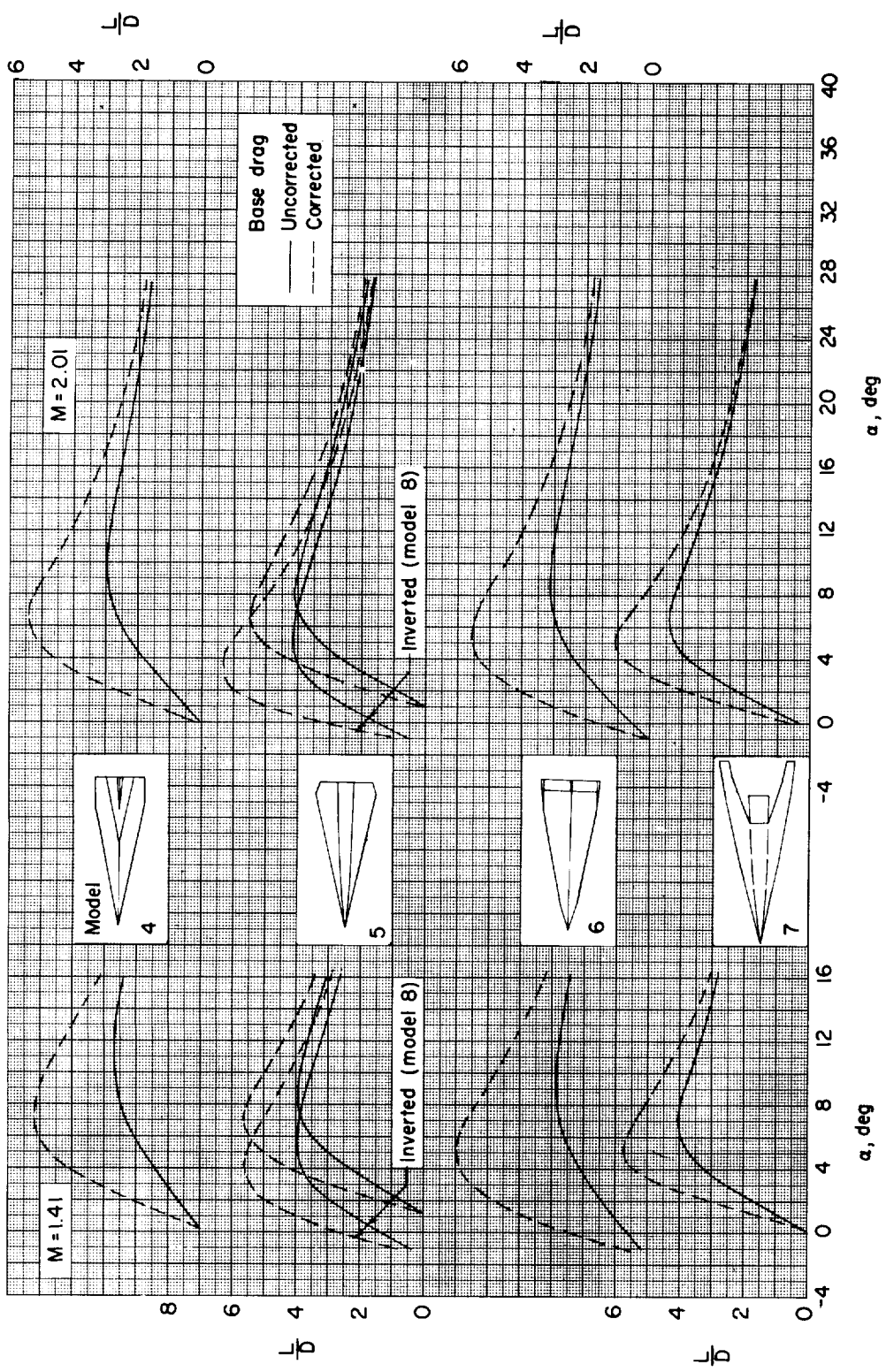
Figure 10.- Effect of model base drag on the lift-drag ratio with angle of attack for models 4, 5, 6, 7, and 8. M = 1.41 and 2.01.
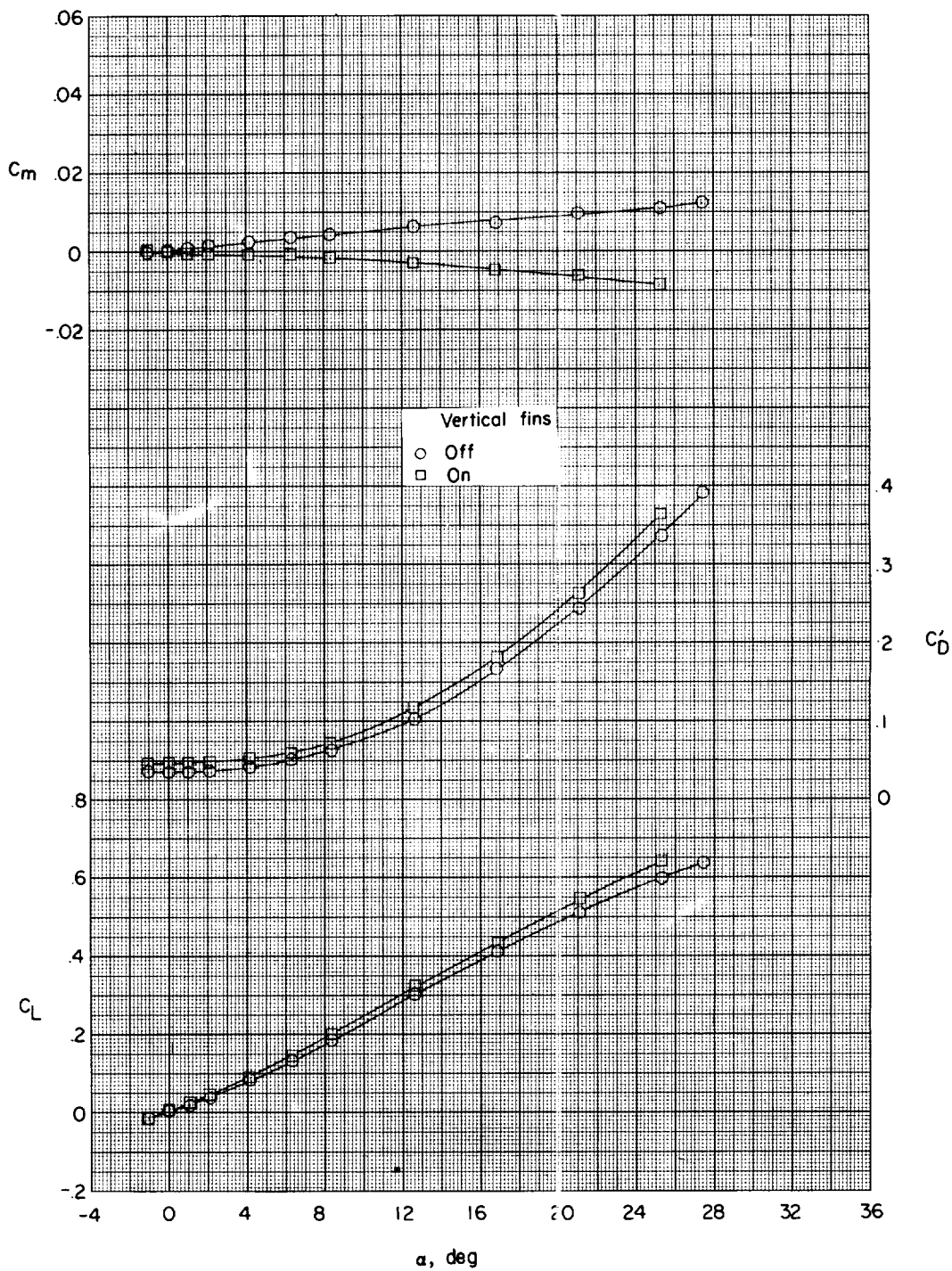
Figure 11.- Effects of vertical fins on the longitudinal aerodynamic characteristics of model 4. M = 2.01.
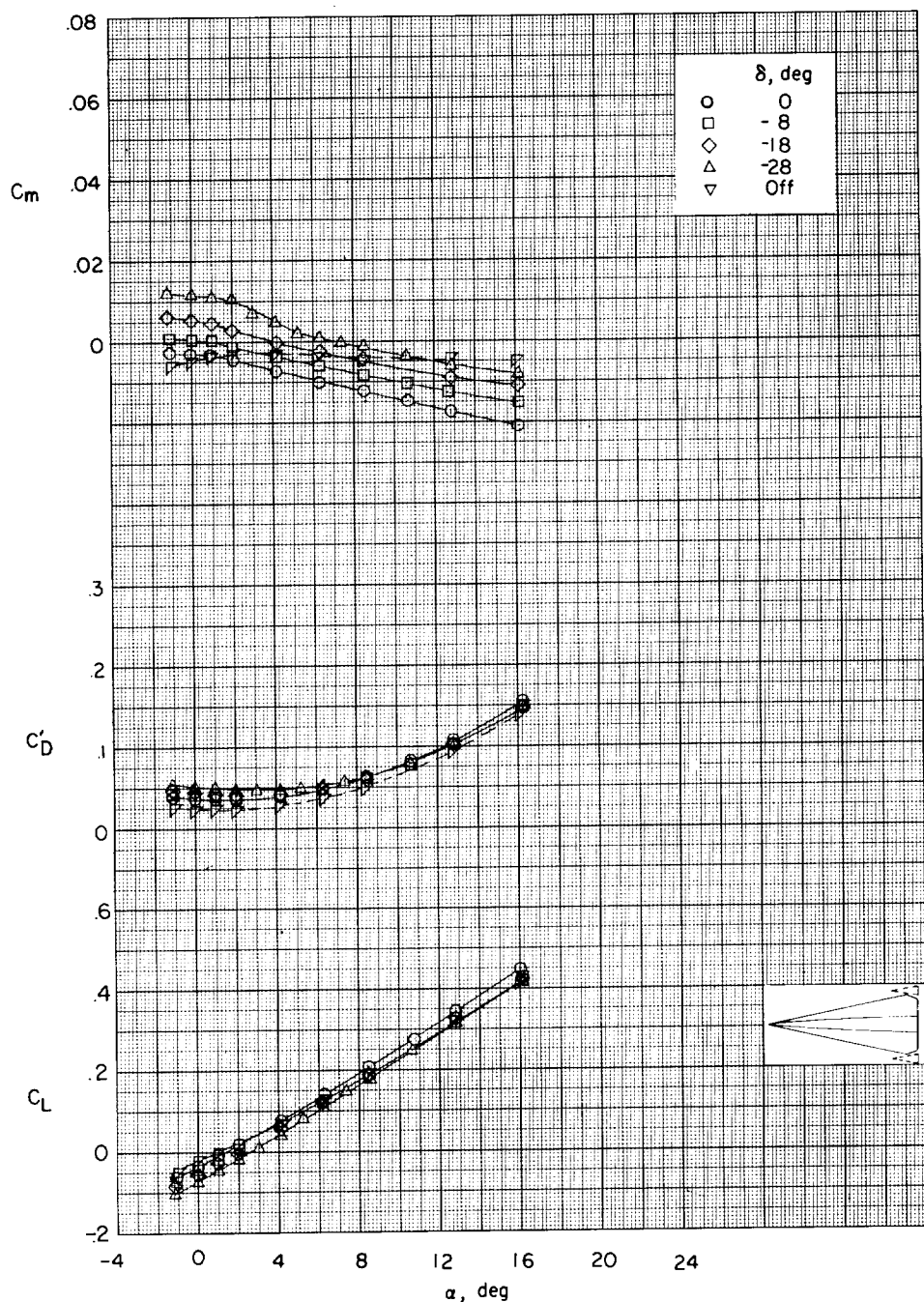
(a) M = 1.41.

Figure 12.- Effect of control deflection on the longitudinal aerodynamic characteristics of model 5.
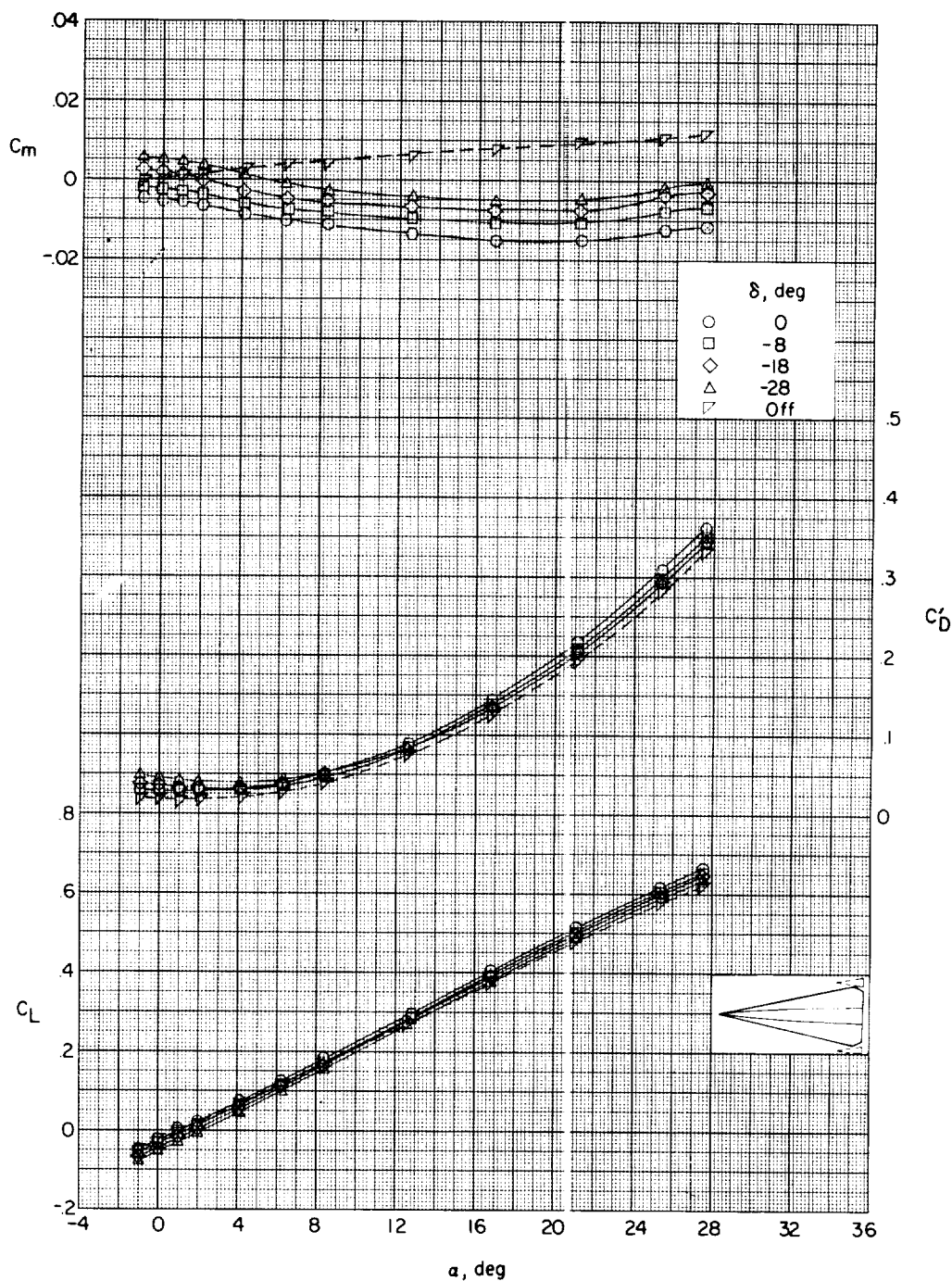
(b) M = 2.01.

Figure 12.- Concluded.
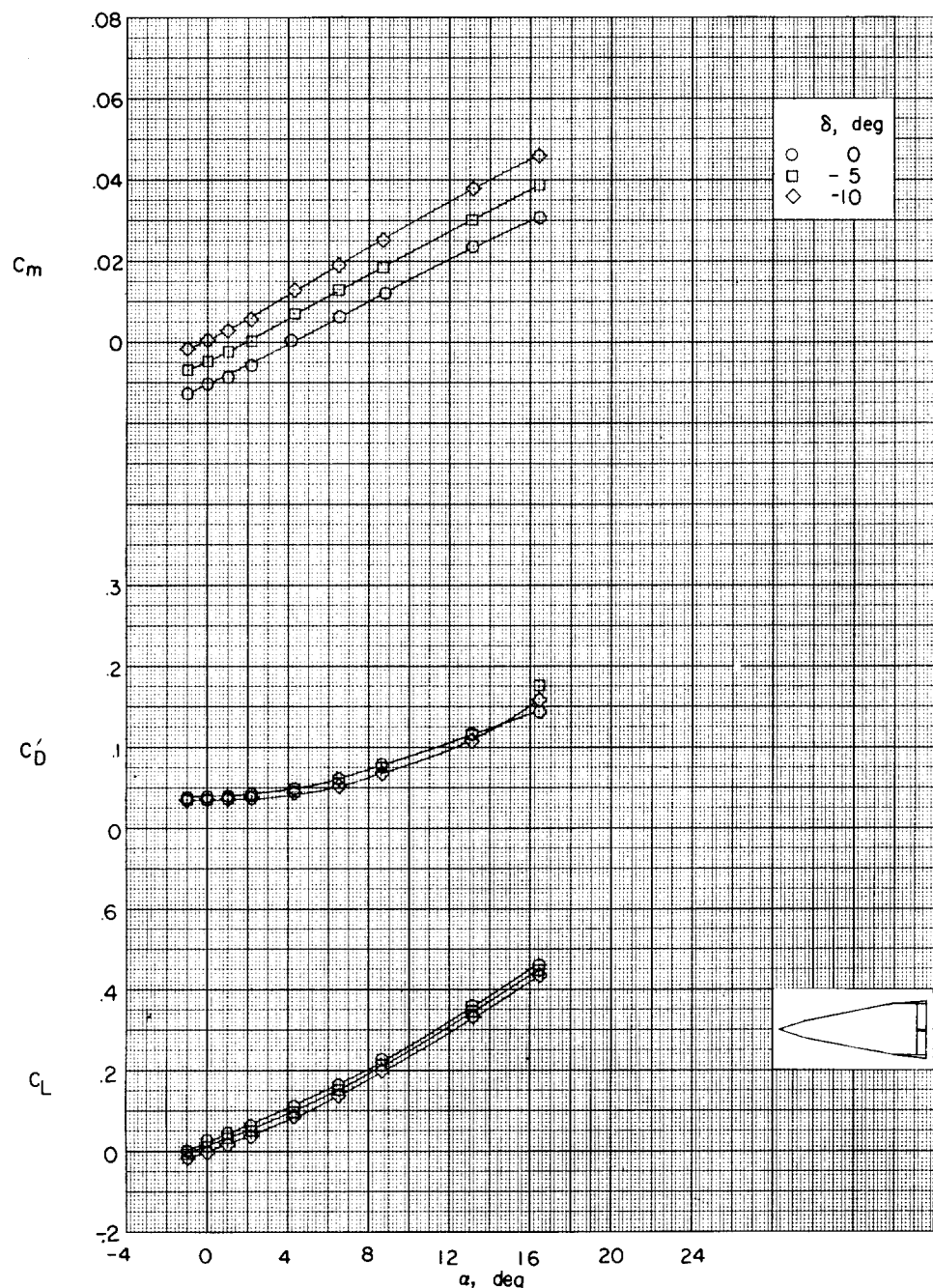
(a) M = 1.41.

Figure 13.- Effect of horizontal control deflection on the longitudinal
aerodynamic characteristics of model 6.
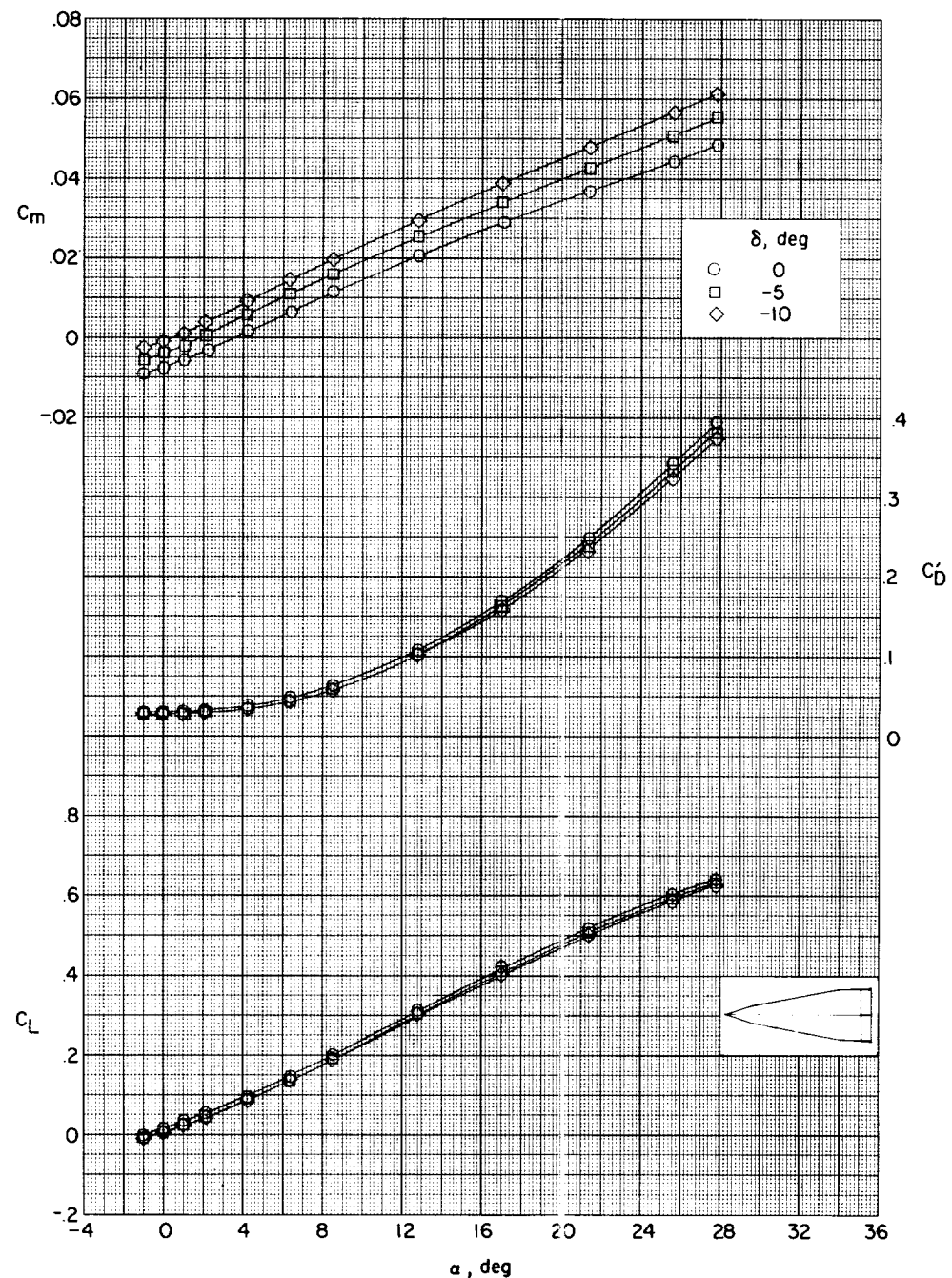
(b) M = 2.01.

Figure 13.- Concluded.
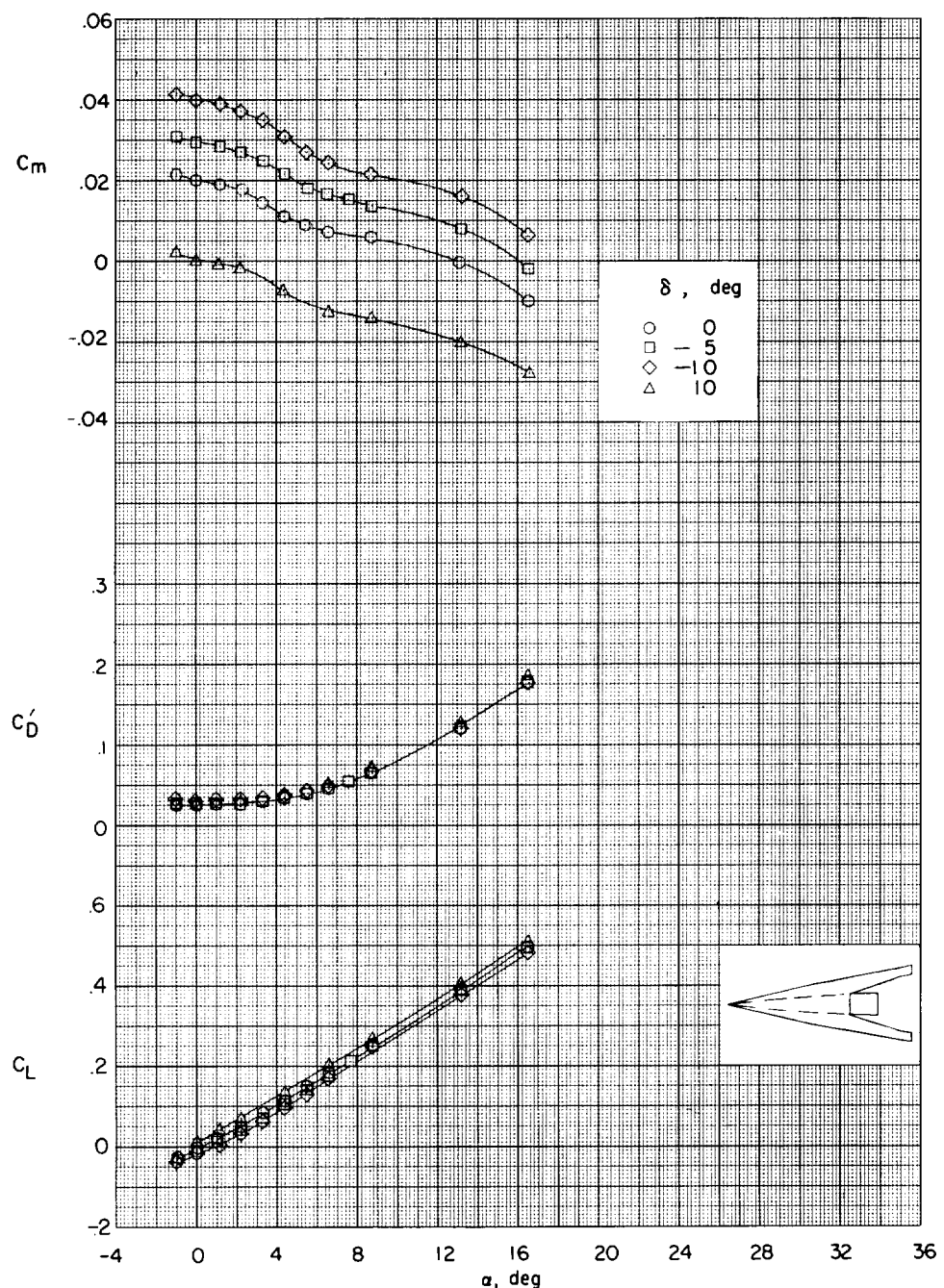
(a) M = 1.41.

Figure 14.- Effect of control deflection on the longitudinal aerodynamic characteristics of model 7.
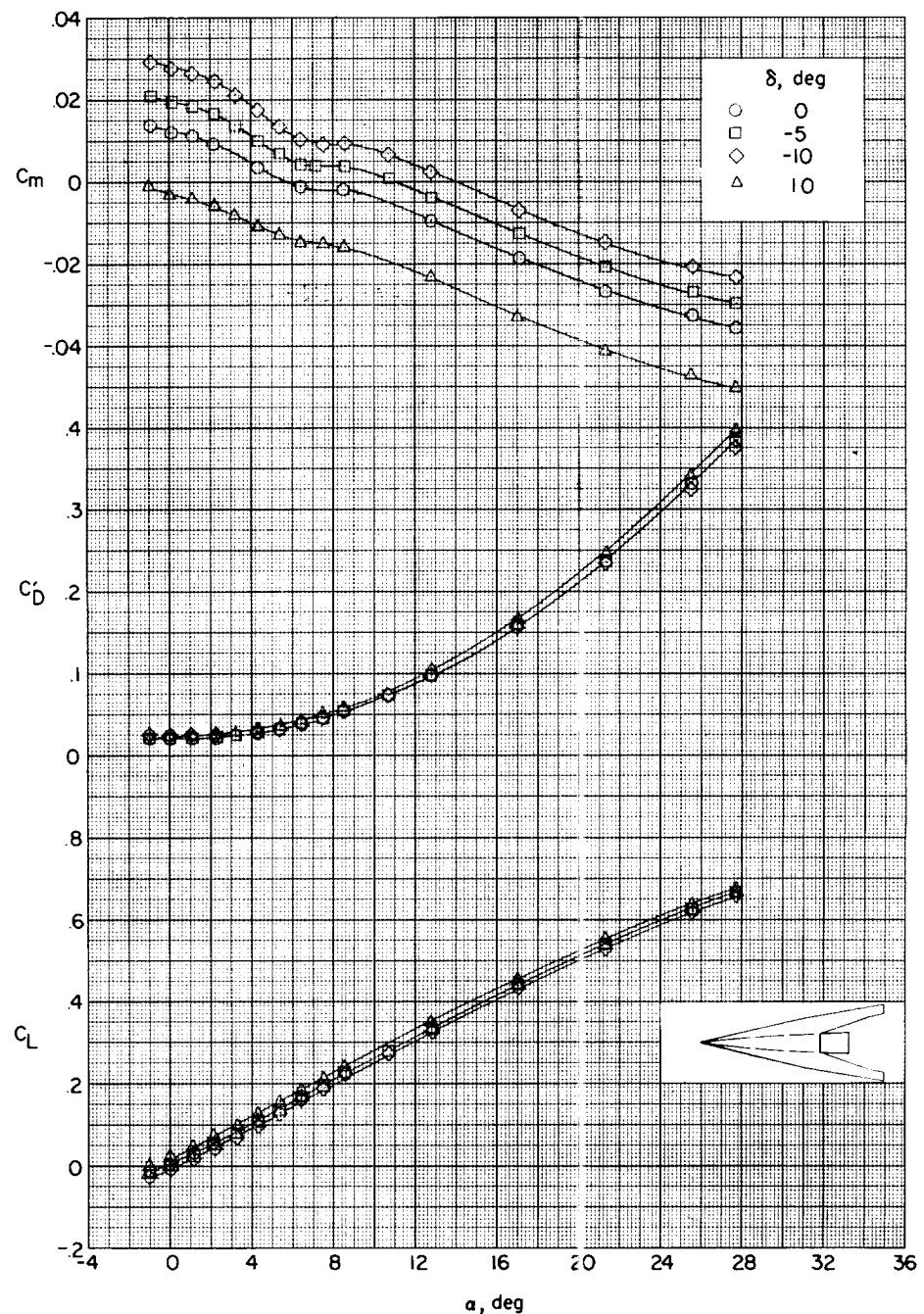
(b) M = 2.01.

Figure 14.- Concluded.
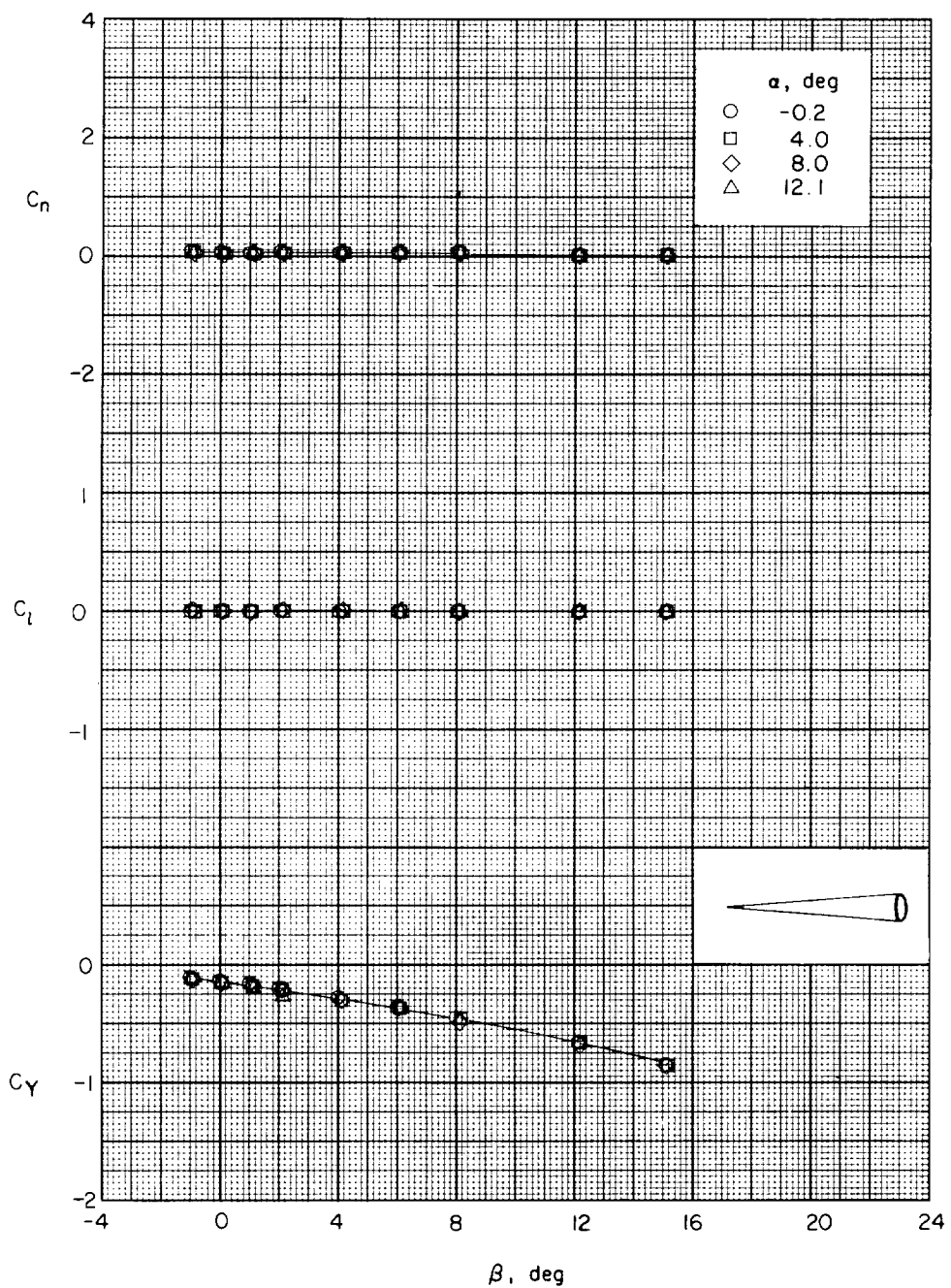
(a) M = 1.41.

Figure 15.- Variation of lateral aerodynamic characteristics of model 1
with sideslip angle.
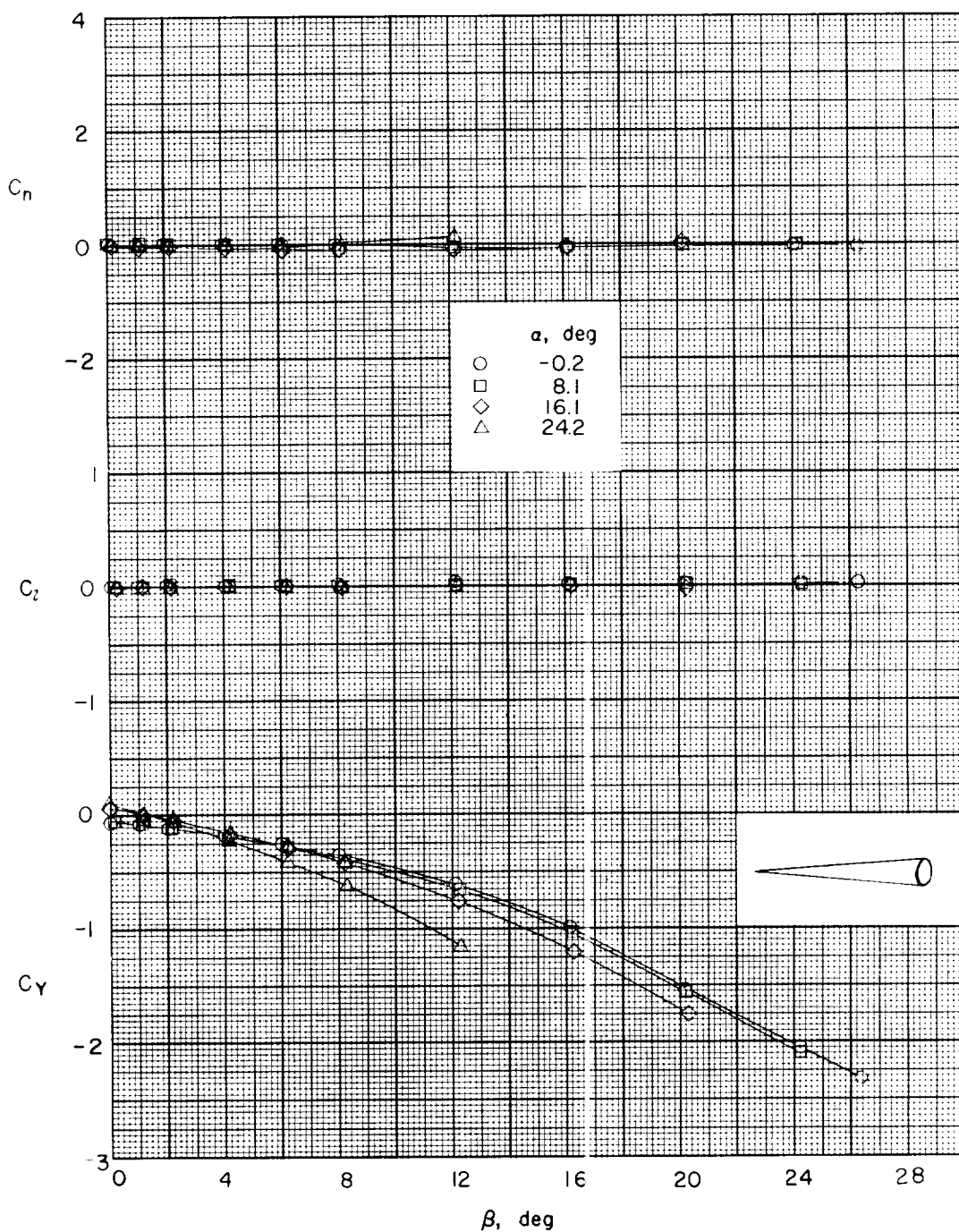
(b) M = 2.01.

Figure 15.- Concluded.
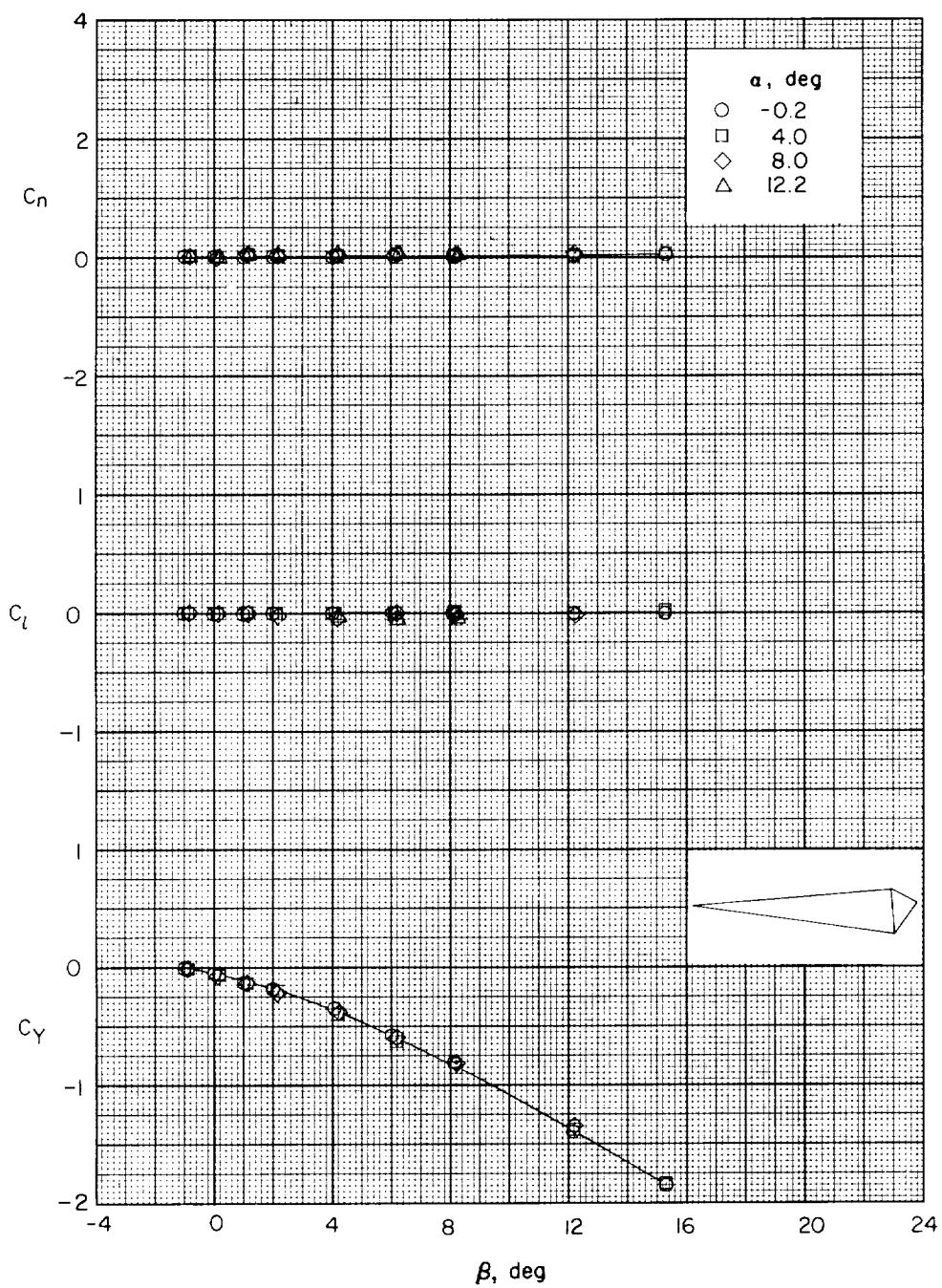
(a) M = 1.41.

Figure 16.- Variation of lateral aerodynamic characteristics of model 2
with sideslip angle.
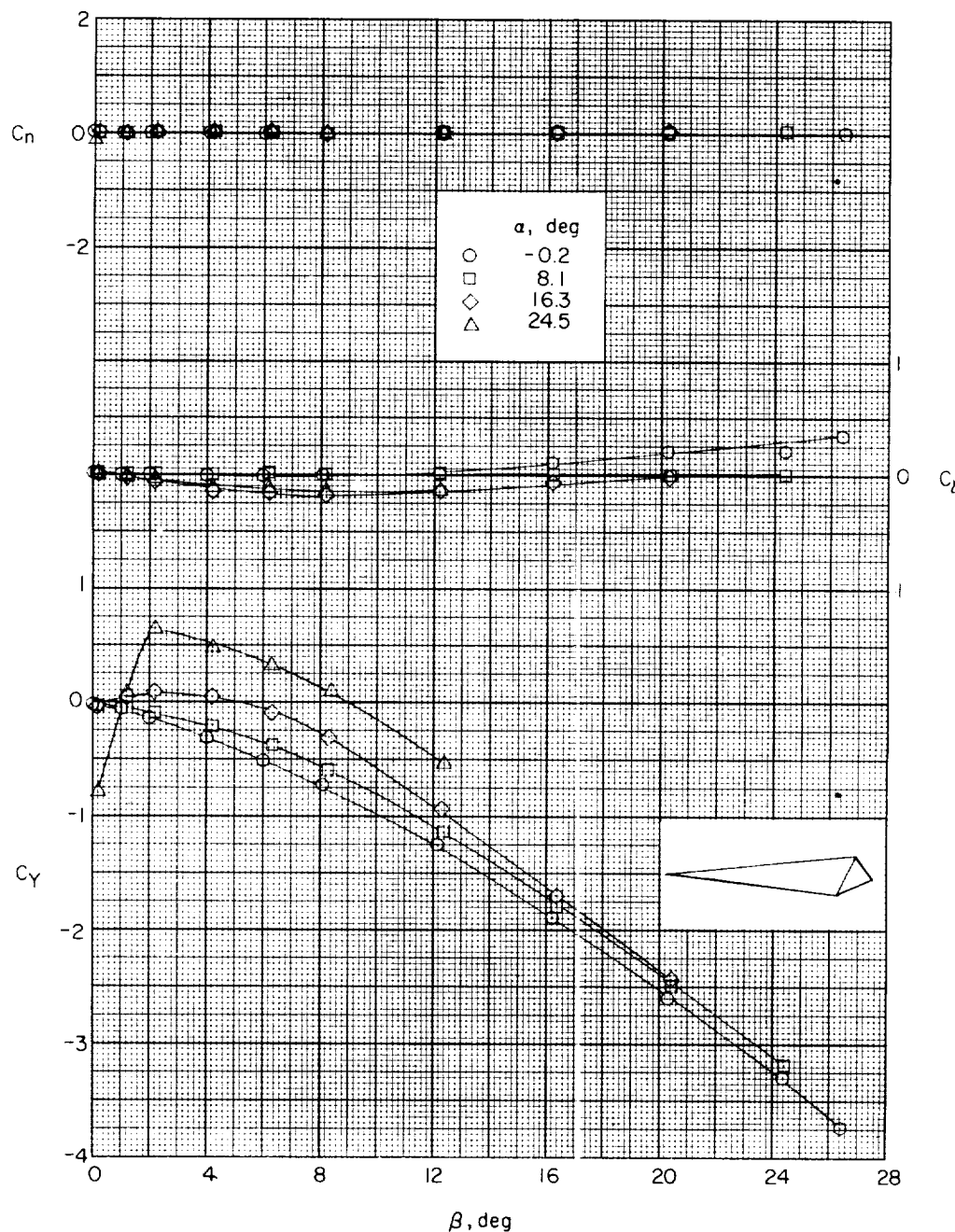
(b) M = 2.01.

Figure 16.- Concluded.
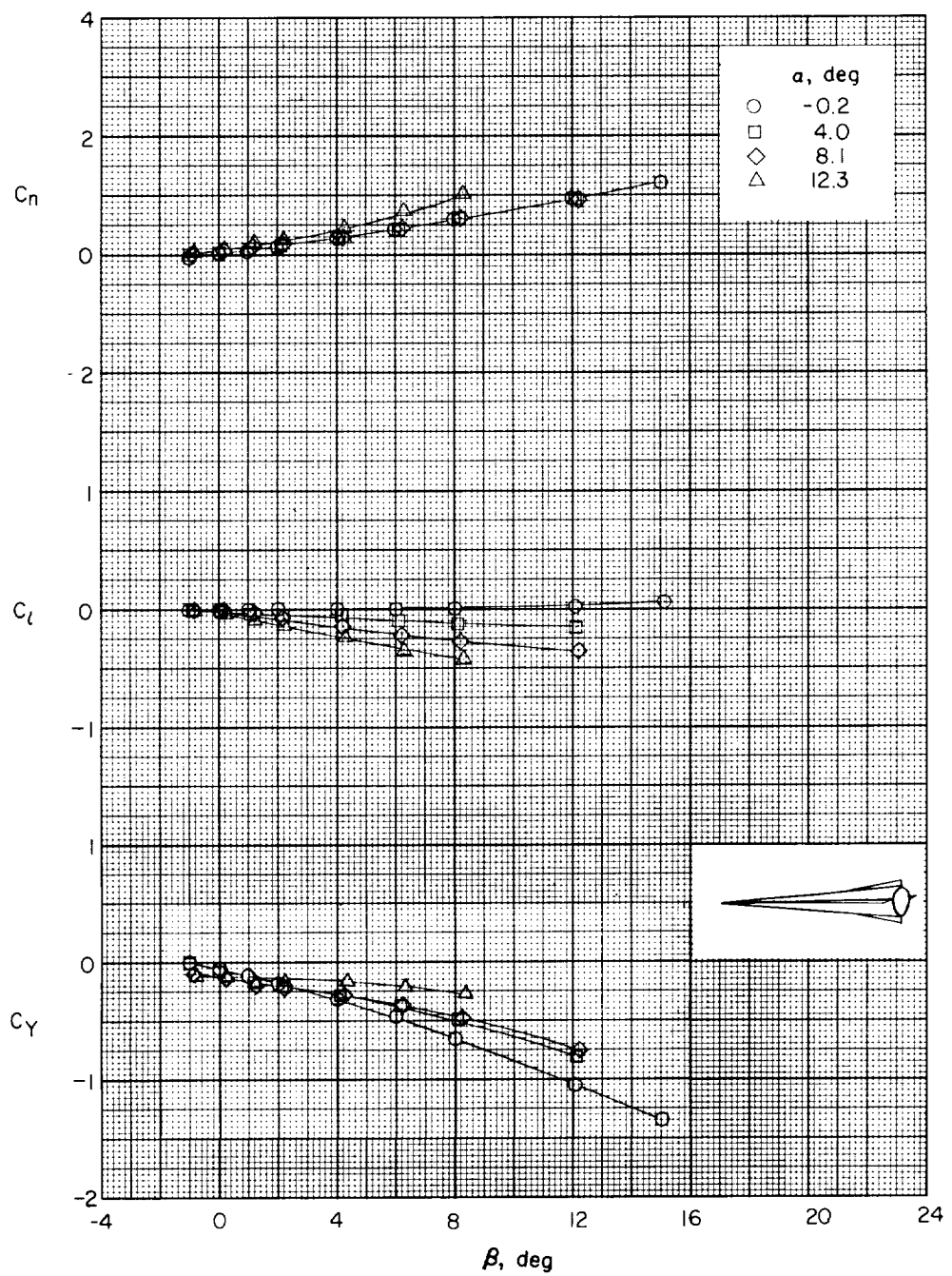
(a) M = 1.41.

Figure 17.- Variation of the lateral aerodynamic characteristics
of model 3 with sideslip angle.
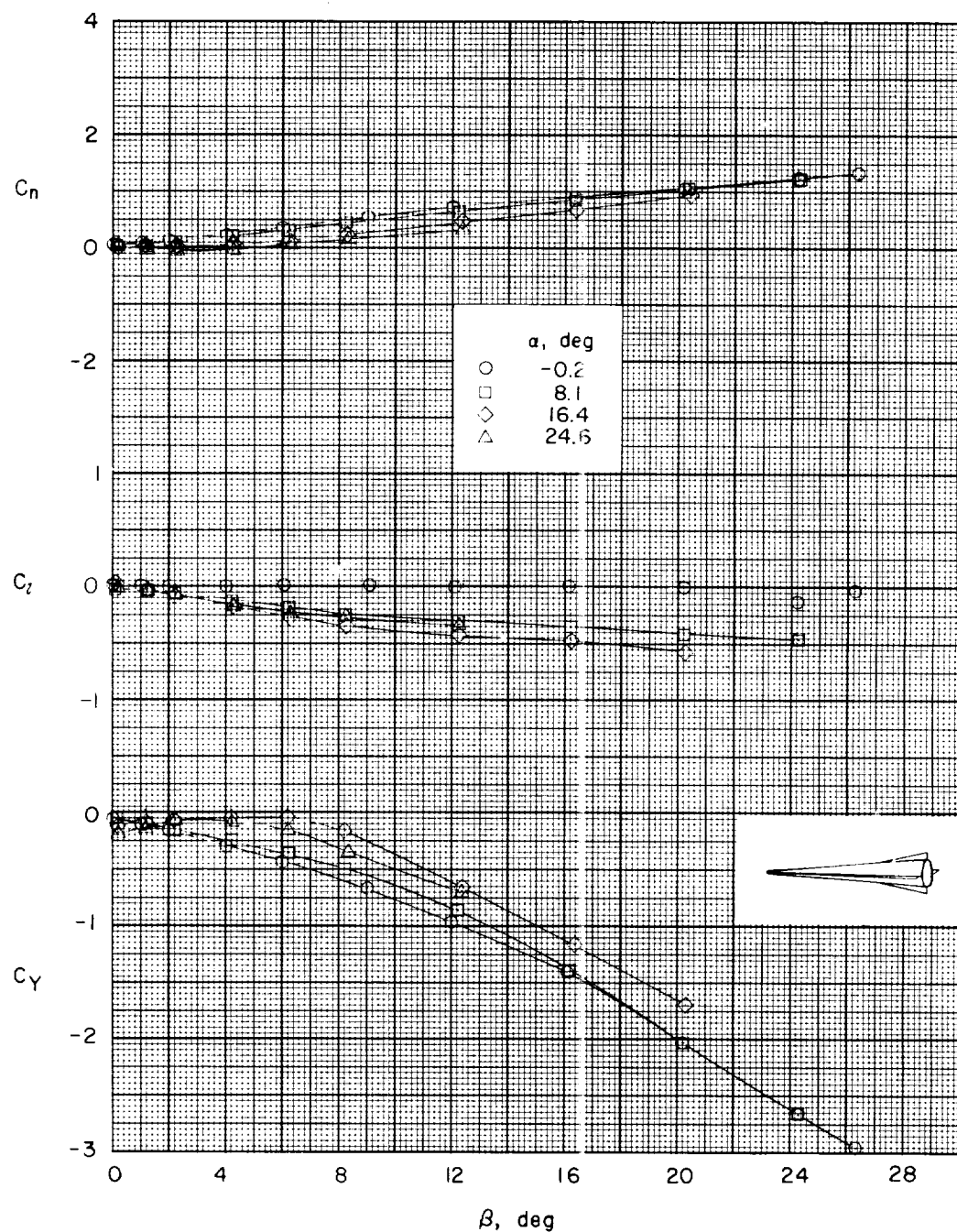
(b) M = 2.01.

Figure 17.- Concluded.
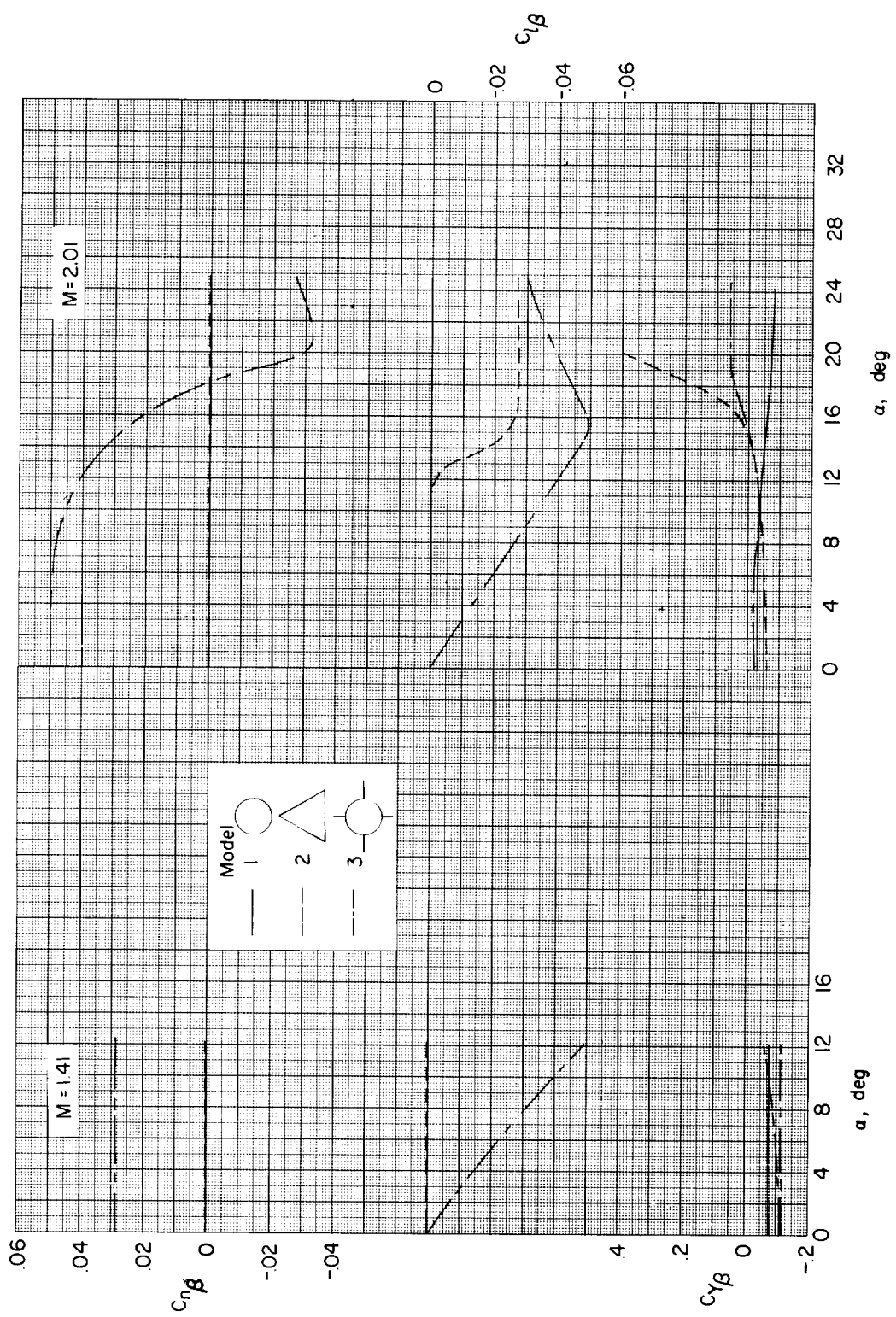
Figure 18.- Variation of the lateral stability parameters of models 1, 2, and 3 with angle of attack. M = 1.41 and 2.01.
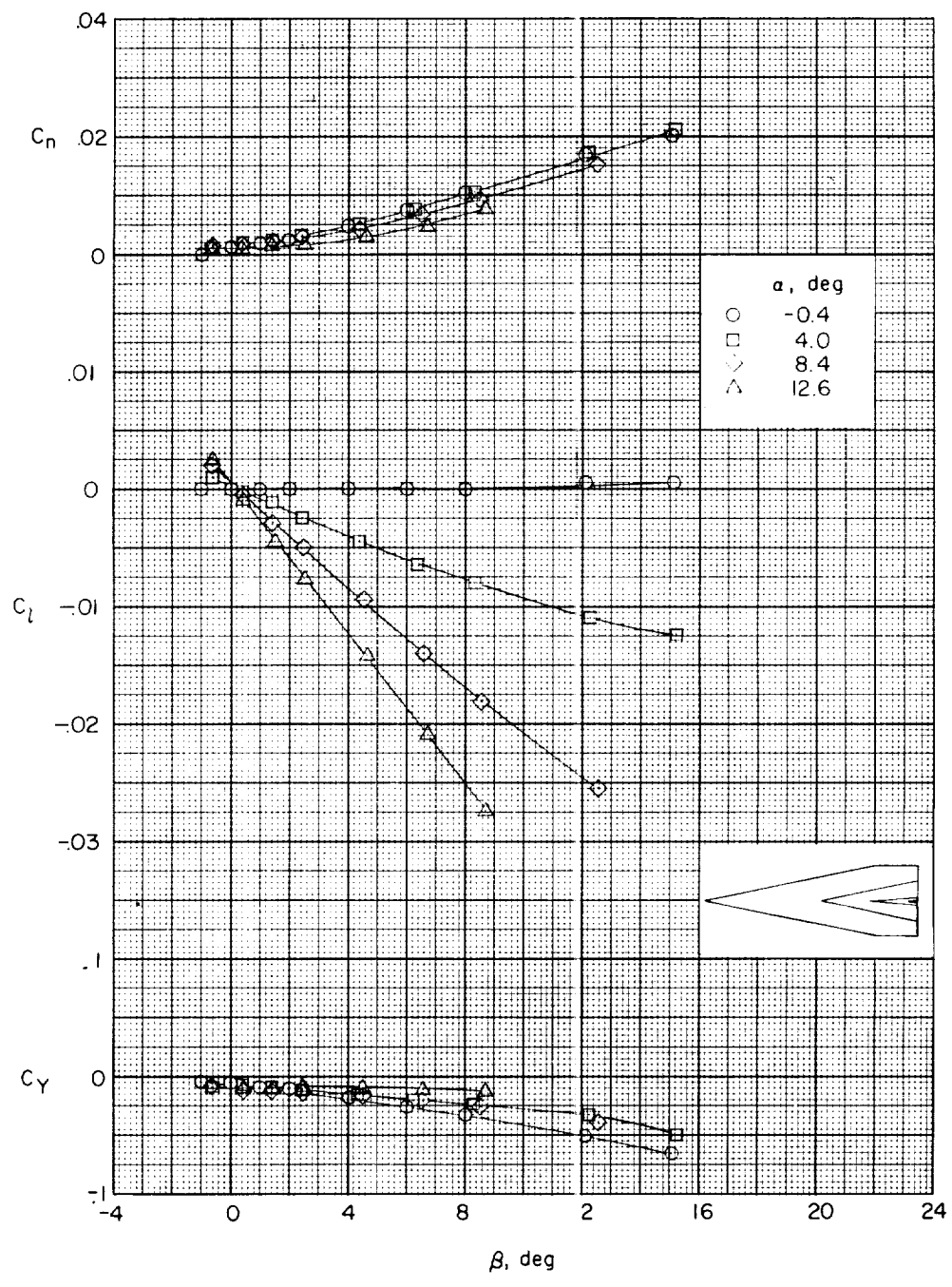
(a) M = 1.41.

Figure 19.- Variation of the lateral aerodynamic characteristics of model 4
with sideslip angle. Vertical fins off.
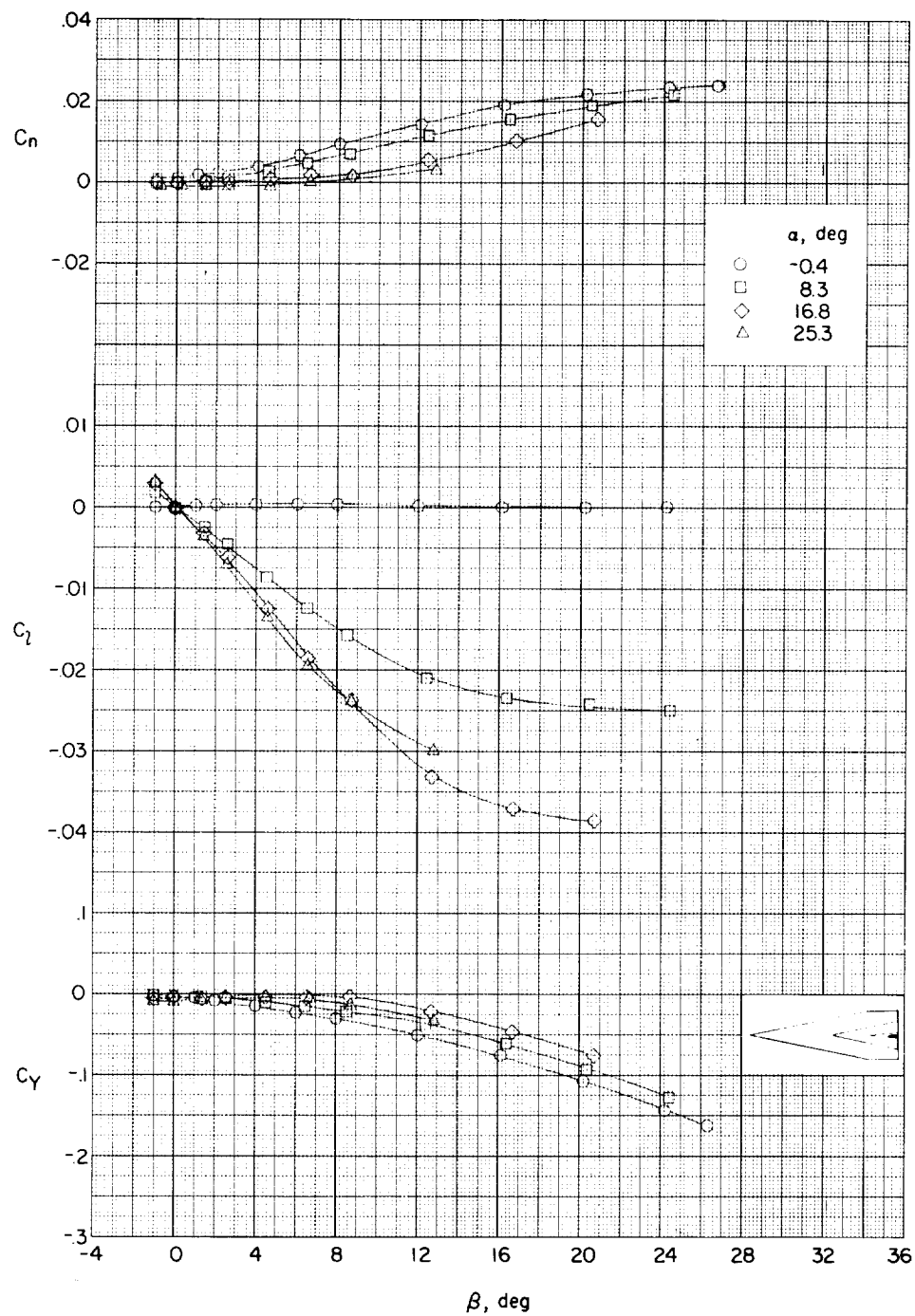
(b) M = 2.01.

Figure 19.- Concluded.
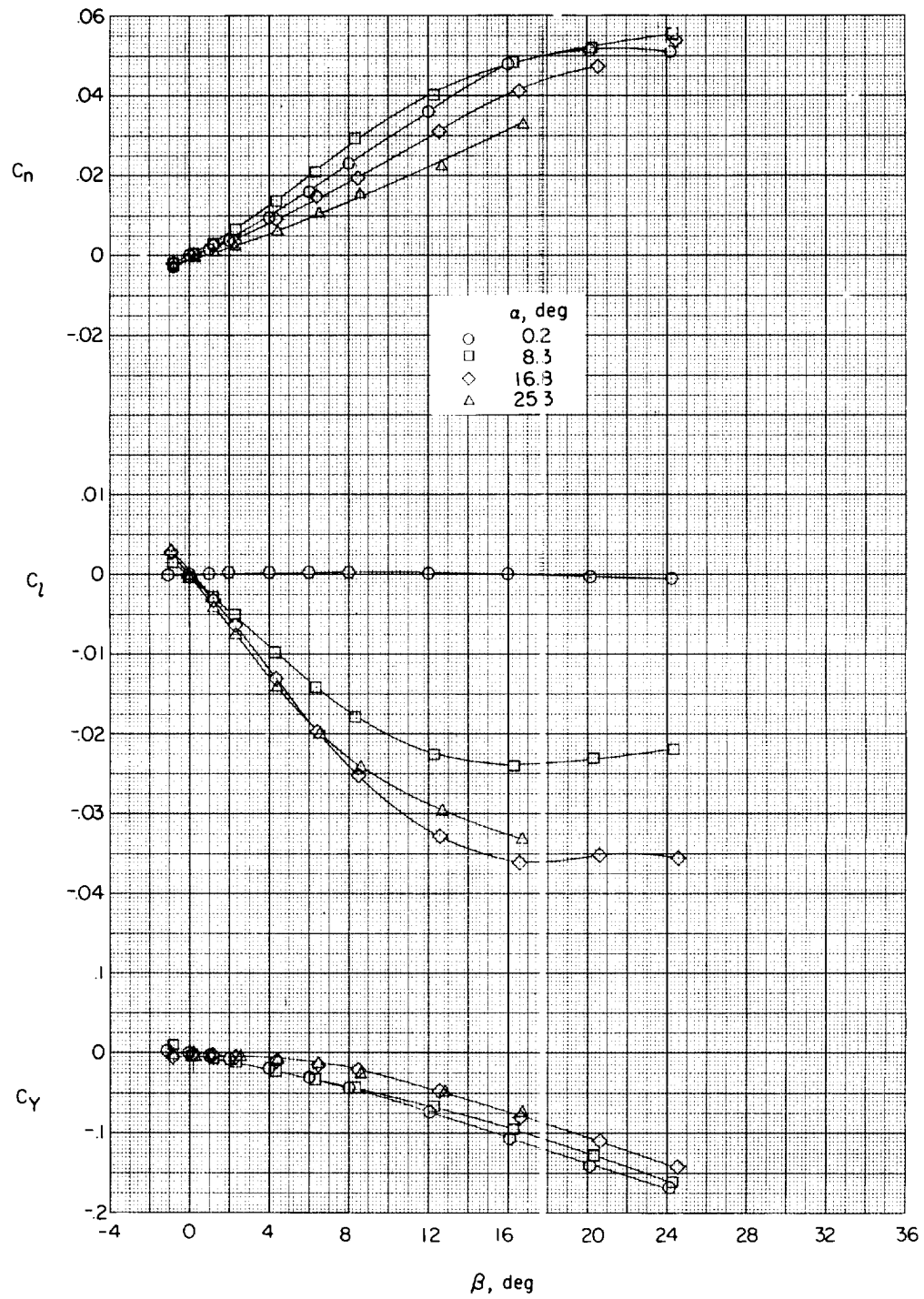
Figure 20.- Variation of the lateral aerodynamic characteristics of model 4 with sideslip angle. Vertical fins on; M = 2.01.
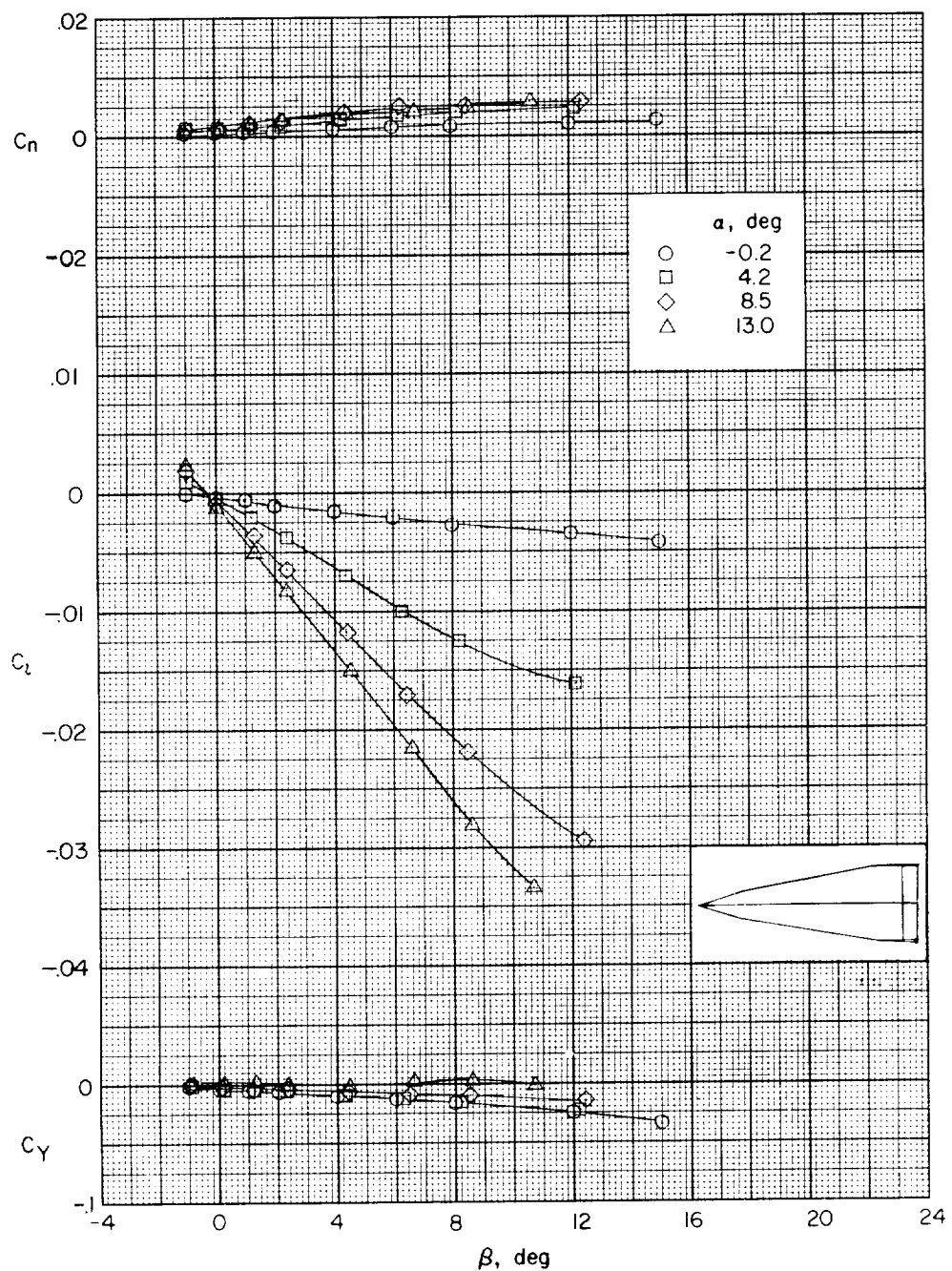
(a) M = 1.41.

Figure 21.- Variation of the lateral aerodynamic characteristics of model 6 with sideslip angle.
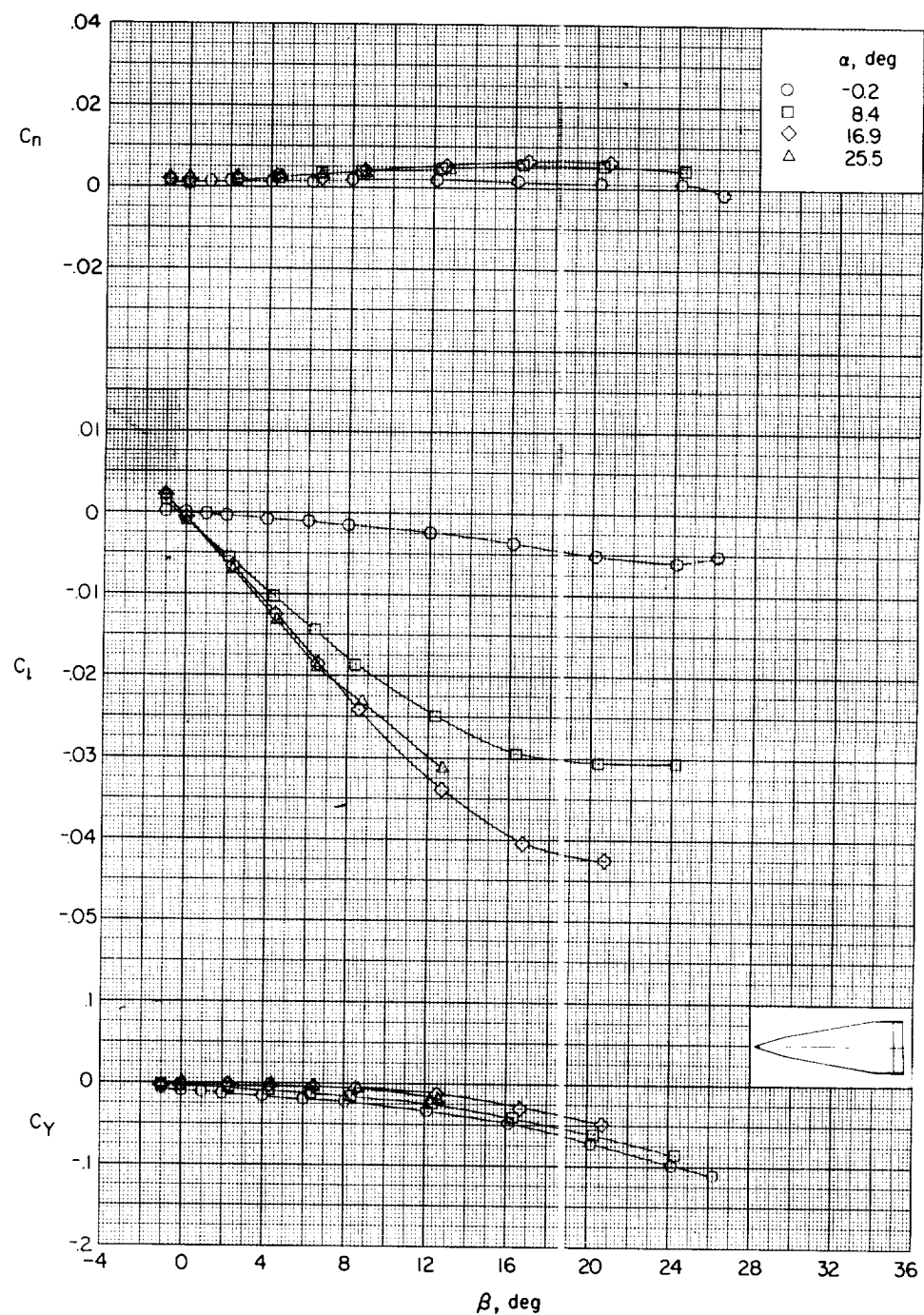
(b) M = 2.01.

Figure 21.- Concluded.
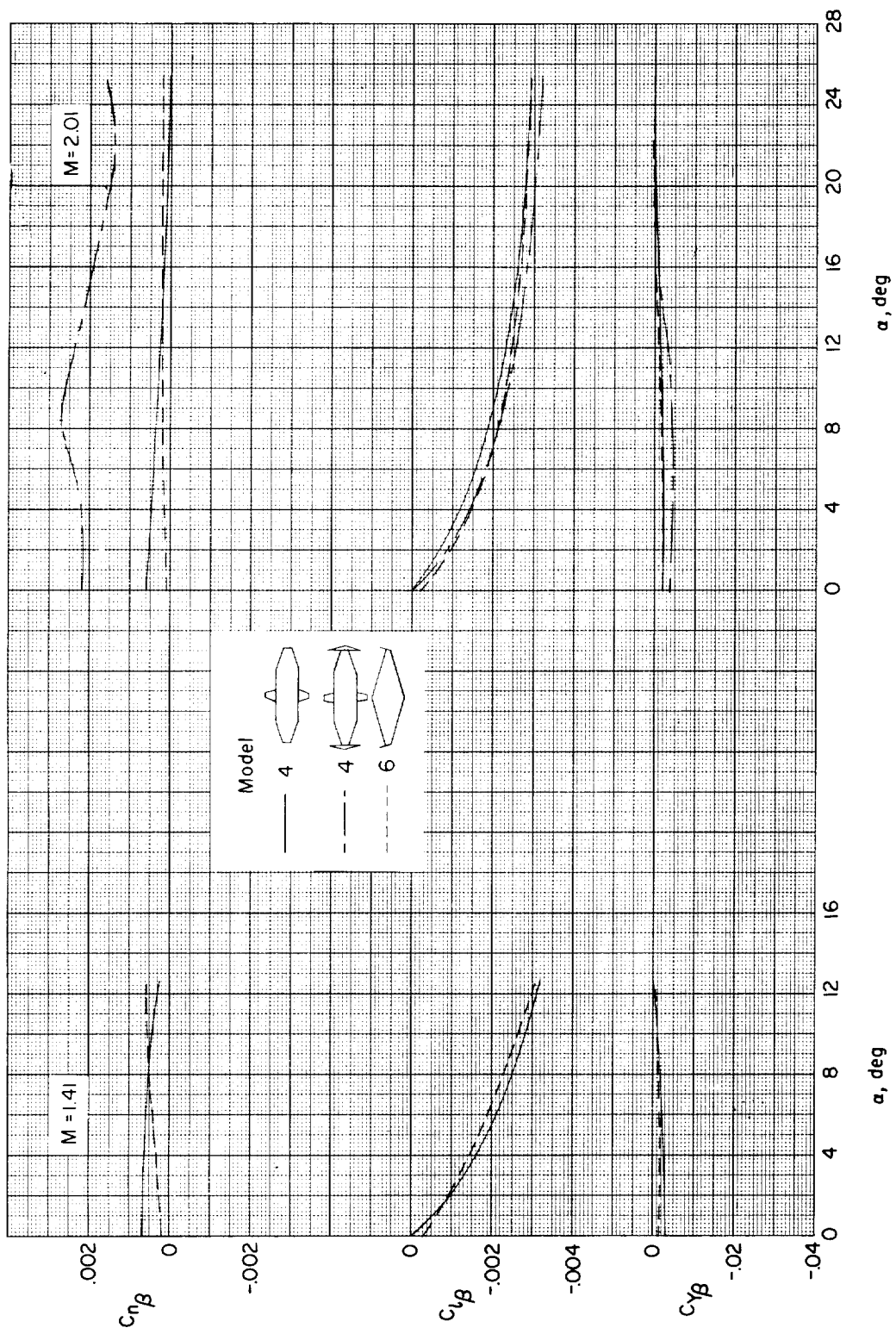
Figure 22.- Variation of the lateral stability parameter of models 4 and 6 with angle of attack. M = 1.41 and 2.01.
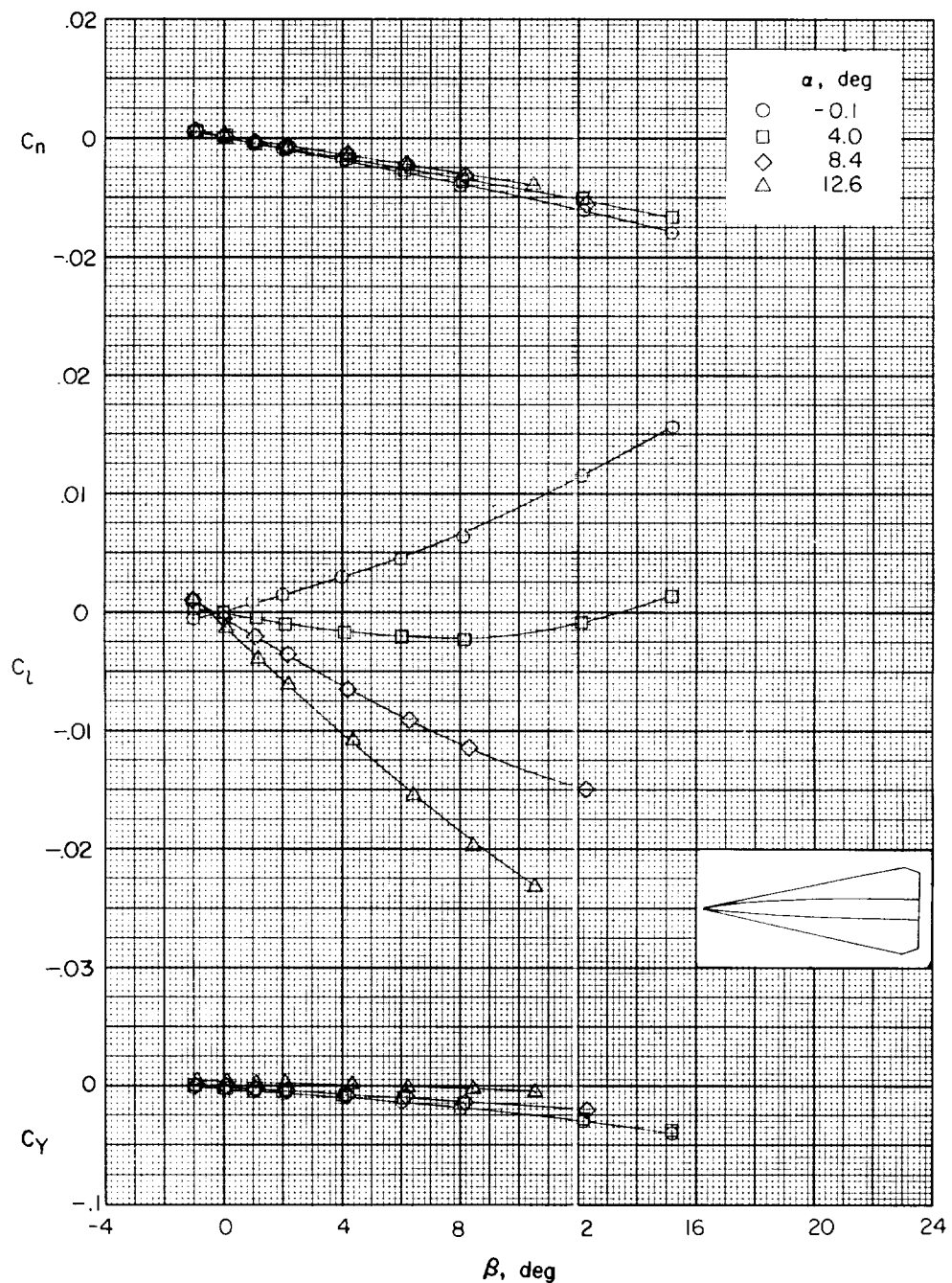
(a) M = 1.41.

Figure 23.- Variation of the lateral aerodynamic characteristics of model 5
with sideslip angle.
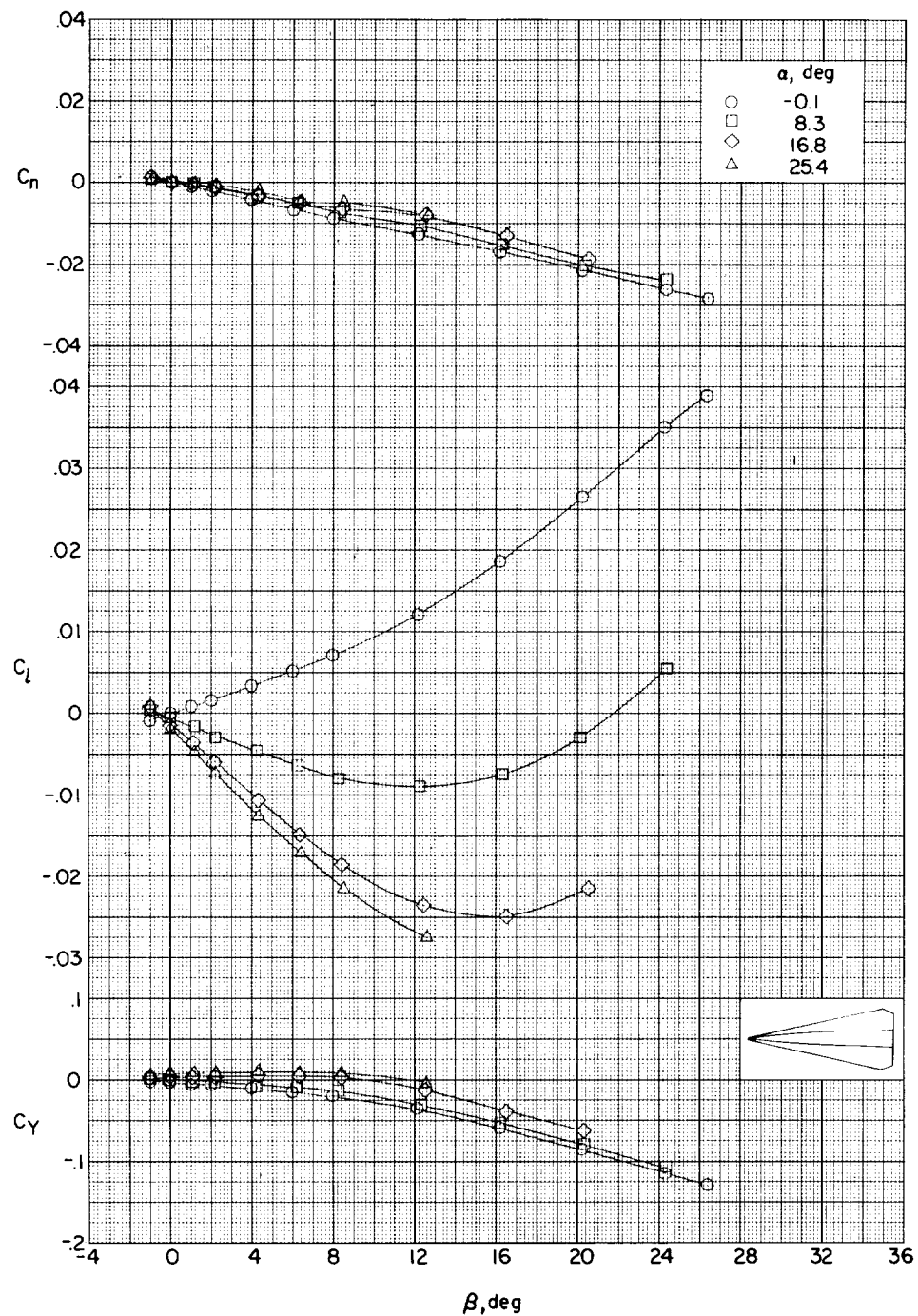
(b) M = 2.01.

Figure 23.- Concluded.
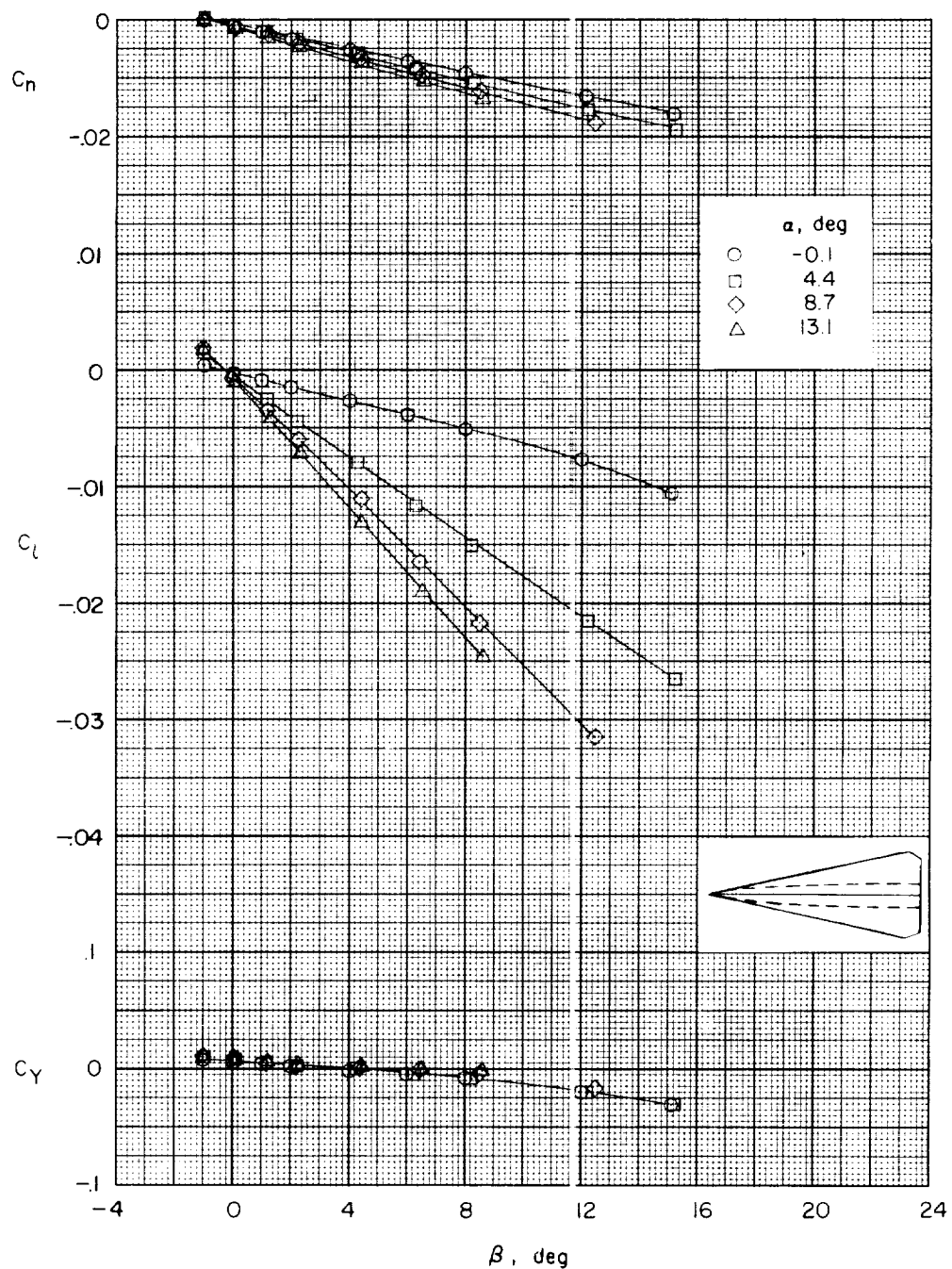
(a) M = 1.41.

Figure 24.- Variation of the lateral aerodynamic characteristics of model 8 with angle of attack.
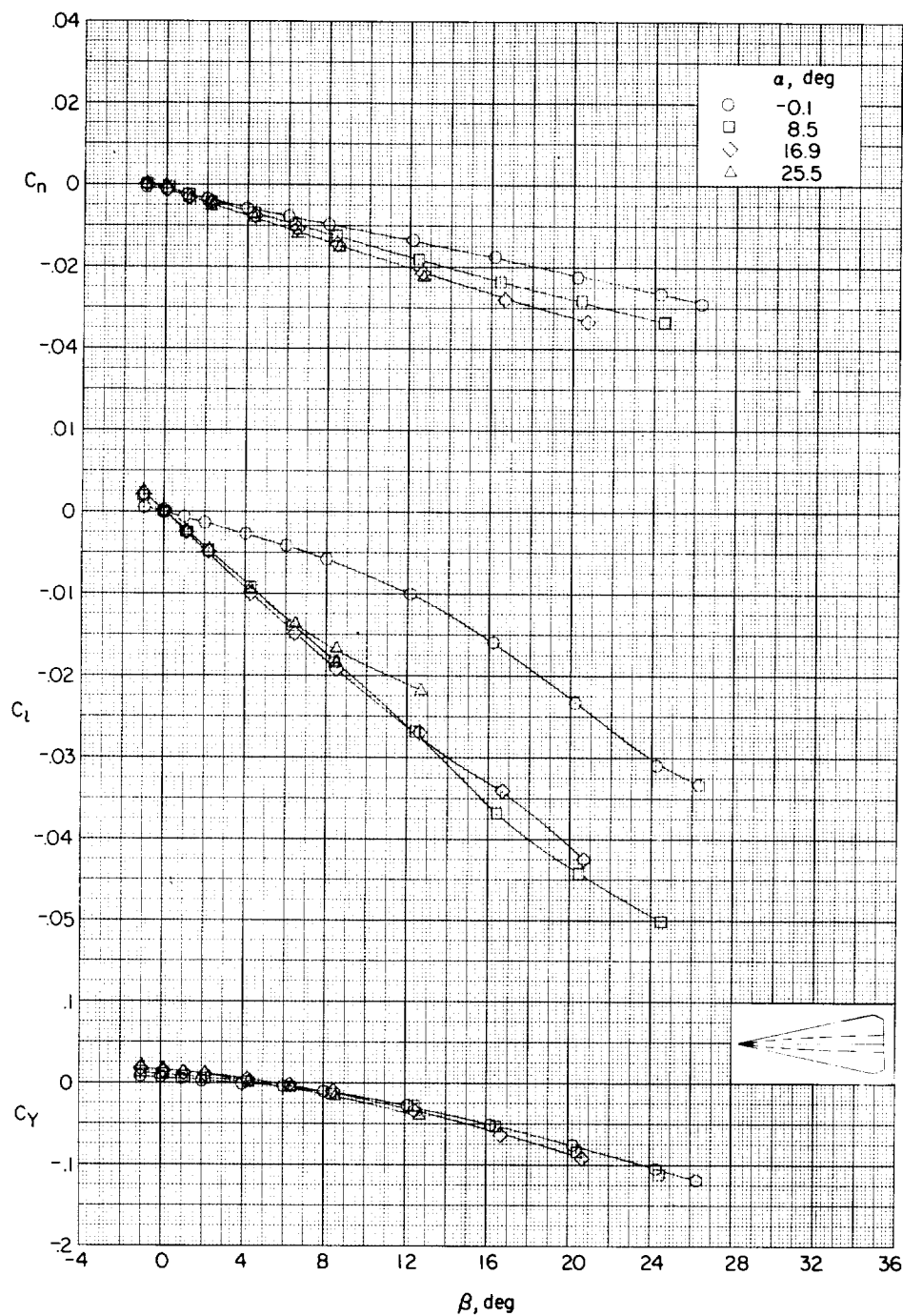
(b) M = 2.01.

Figure 24.- Concluded.
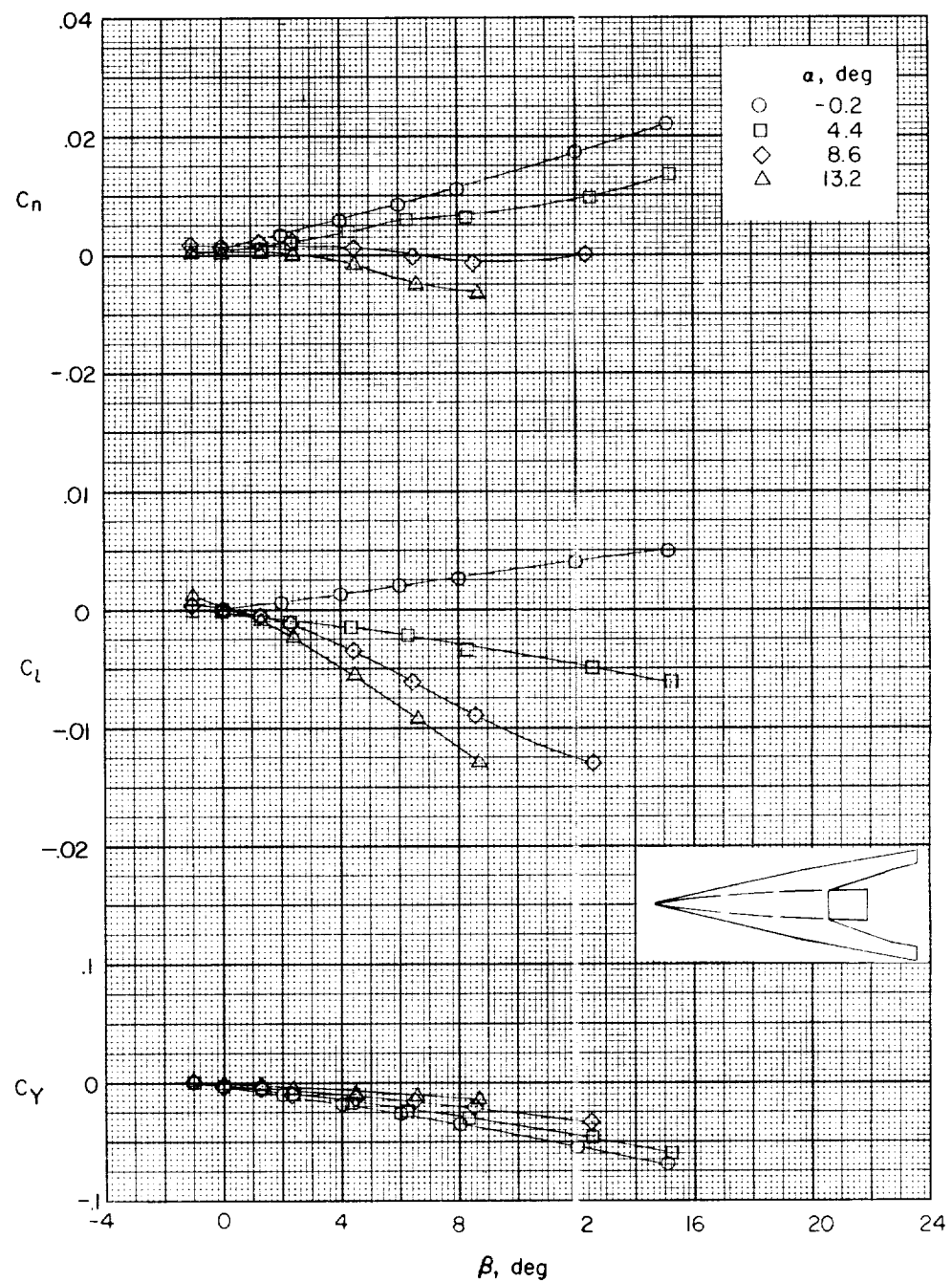
(a) M = 1.41.

Figure 25.- Variation of the lateral aerodynamic characteristics of model 7
with angle of attack.
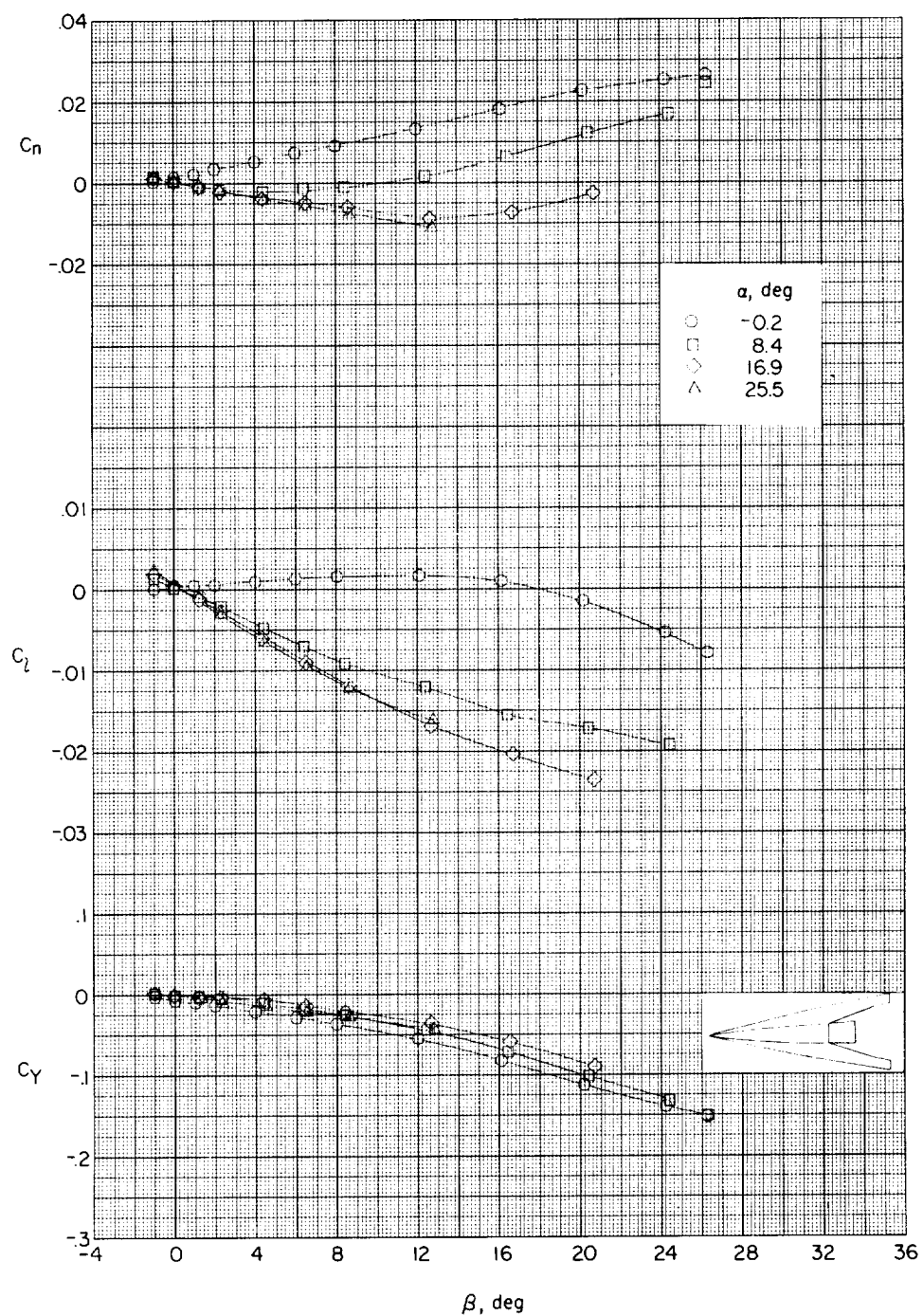
(b) M = 2.01.

Figure 25.- Concluded.
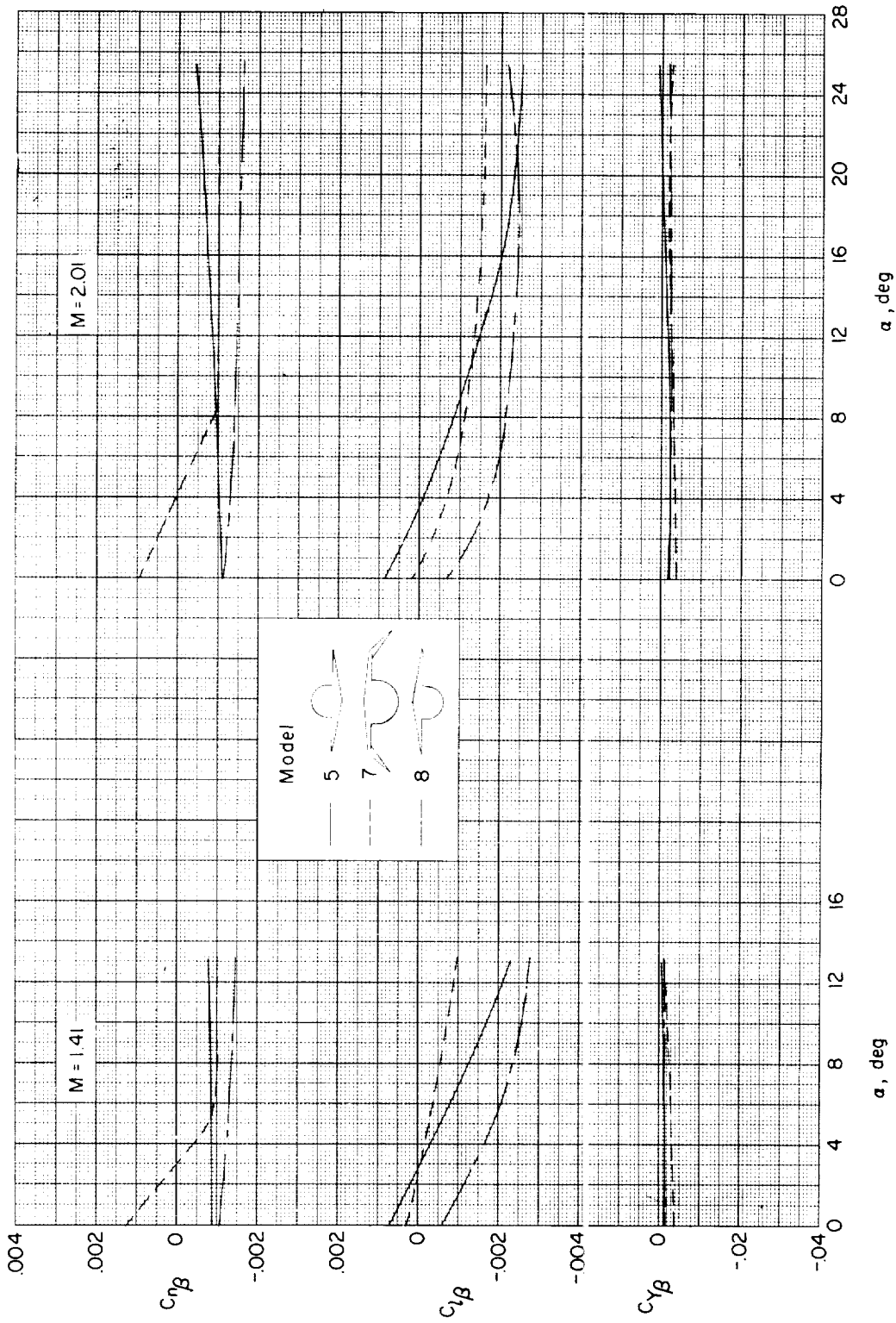
Figure 26.- Variation of the lateral stability parameters of models 5, 7, and 8 with angle of attack. M = 1.41 and 2.01.
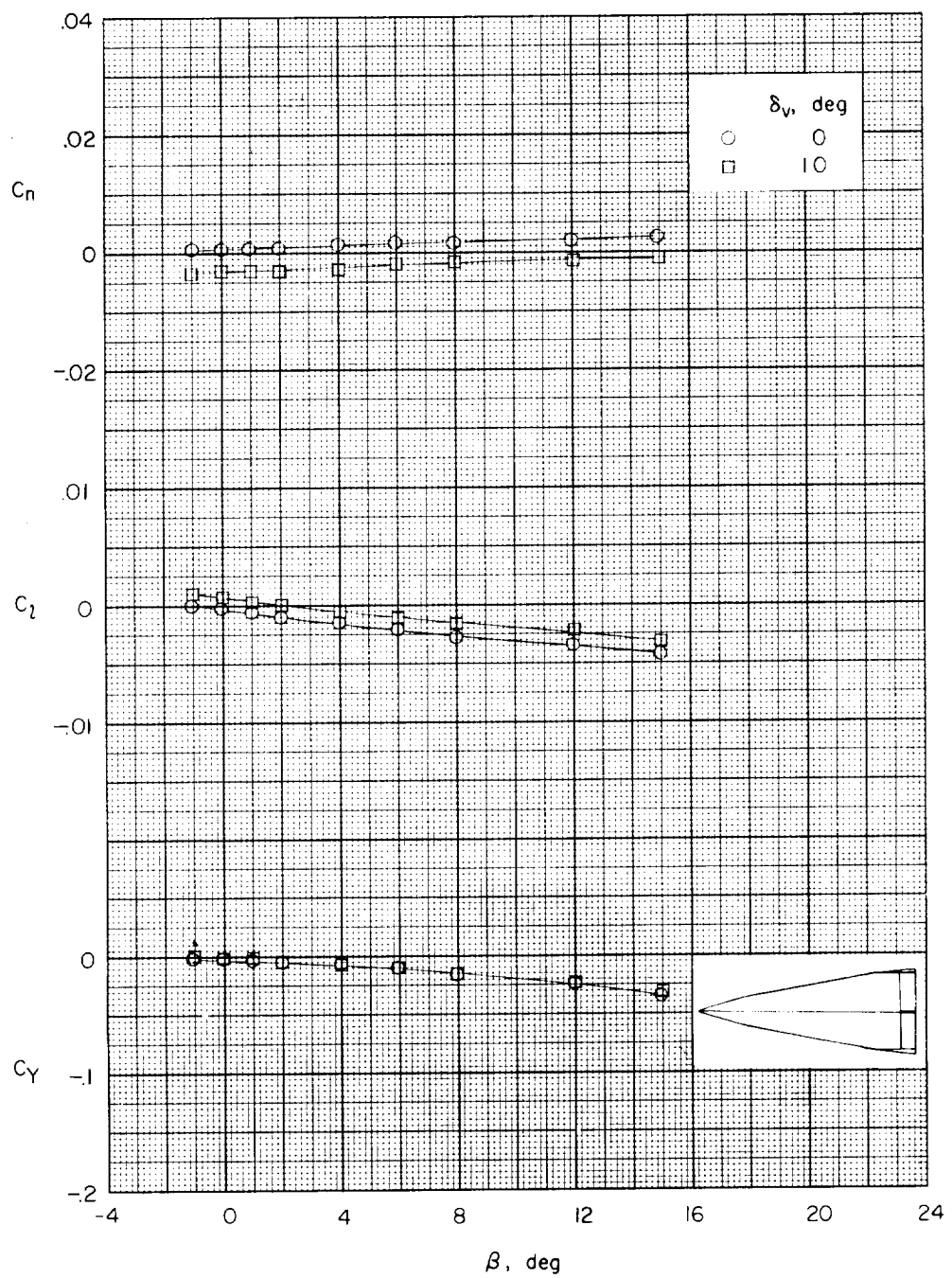
(a) α = -0.2.

Figure 27.- Effect of deflected yaw control of model 6 on the lateral
aerodynamic characteristics in sideslip. M = 1.41.
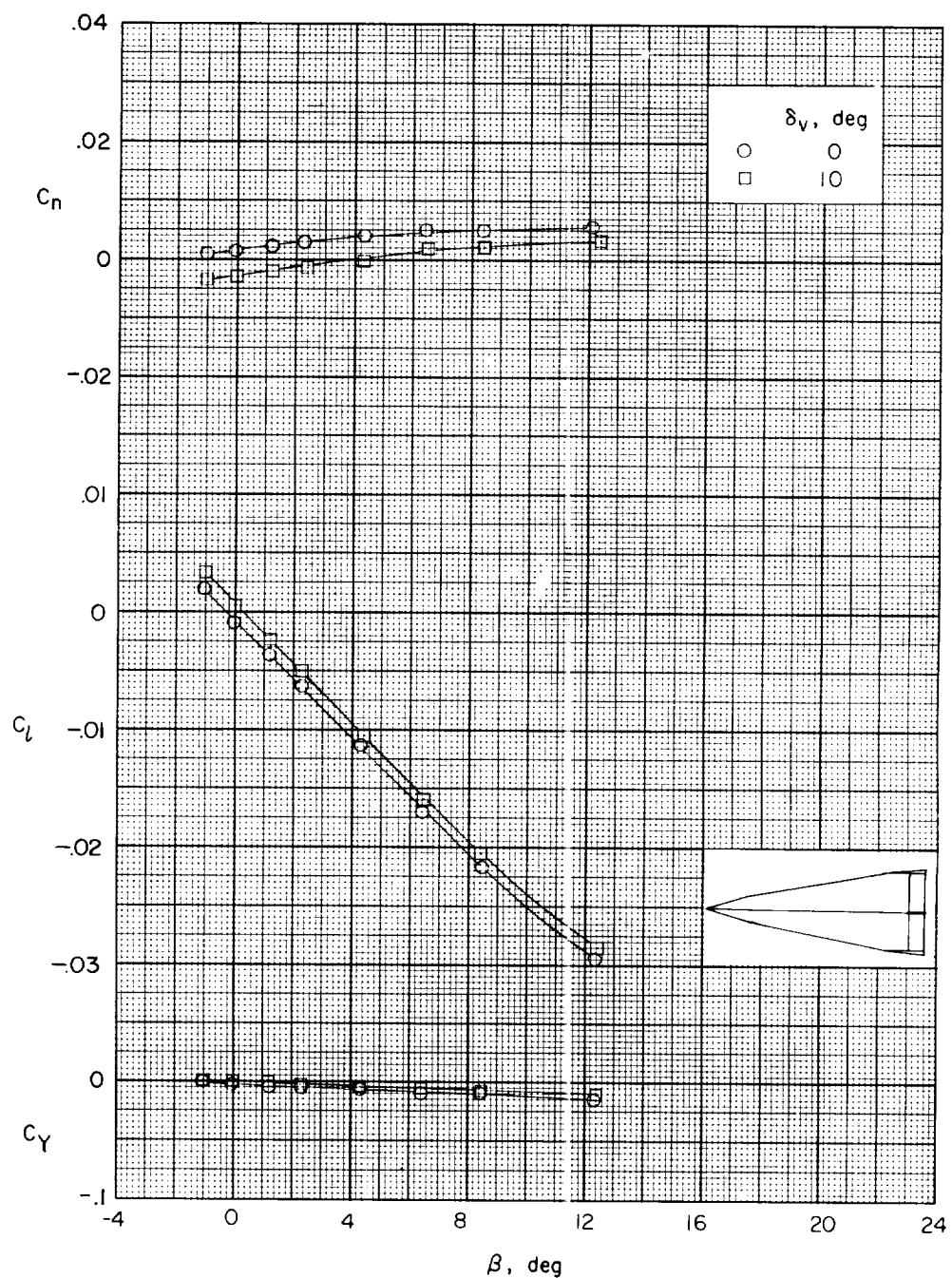
(b) $\alpha = 8.6^{\circ}$.

Figure 27.- Concluded.
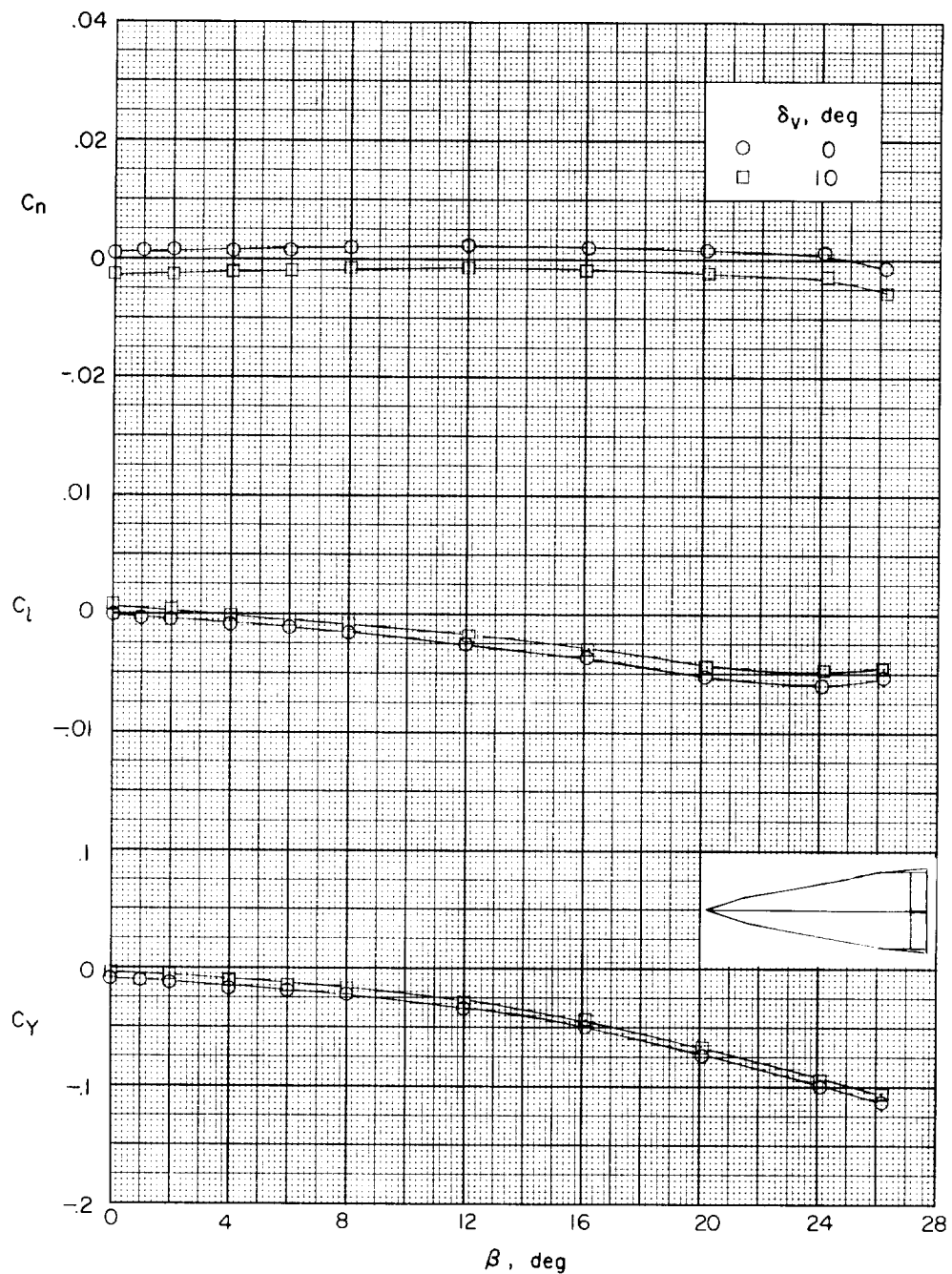
(a) $\alpha = -0.2^{\circ}$.

Figure 28.- Effect of deflected yaw control of model 6 on the lateral
aerodynamic characteristics in sideslip. M = 2.01.
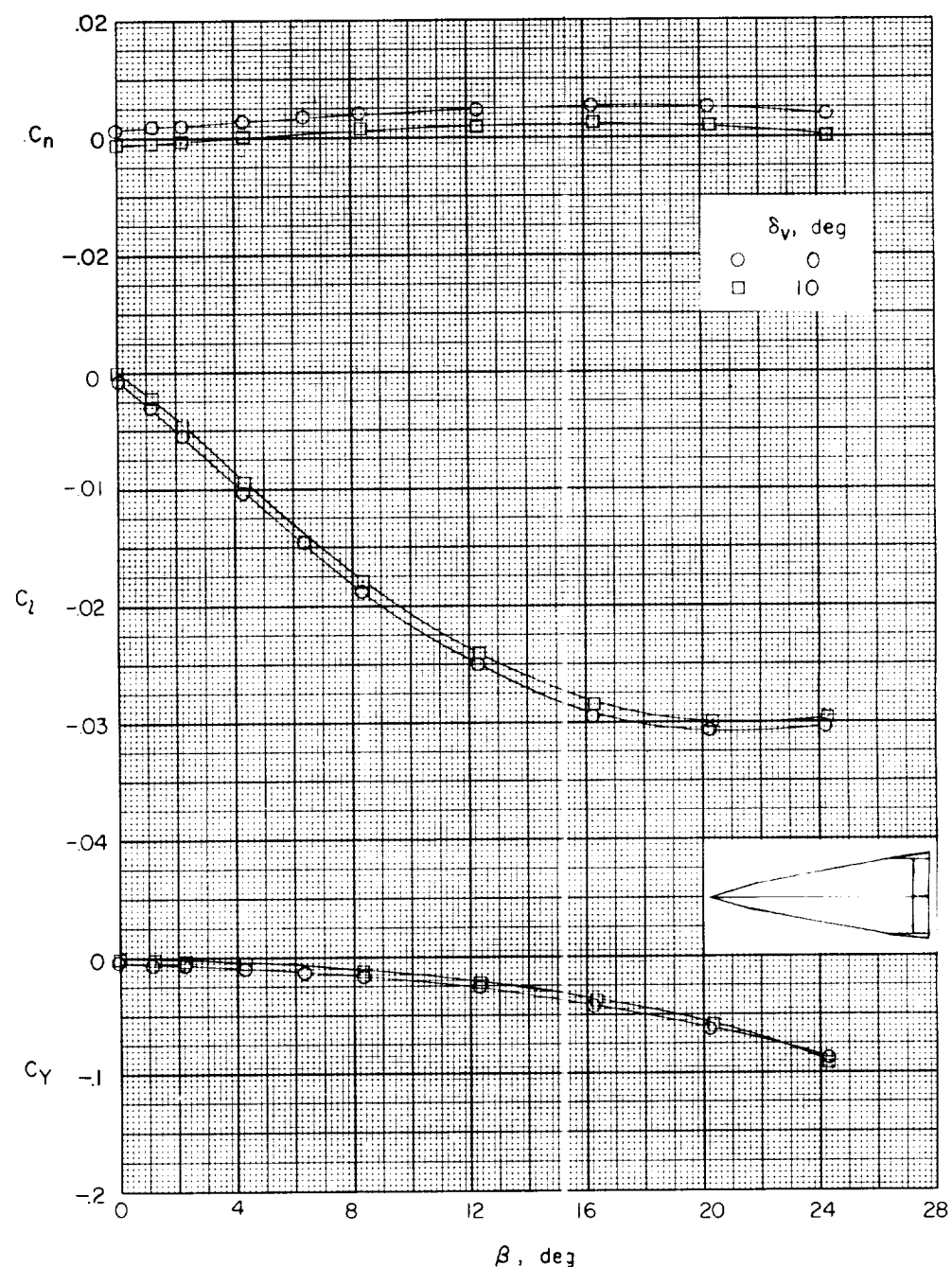
(b) $\alpha = 8.4°$.

Figure 28.- Concluded.
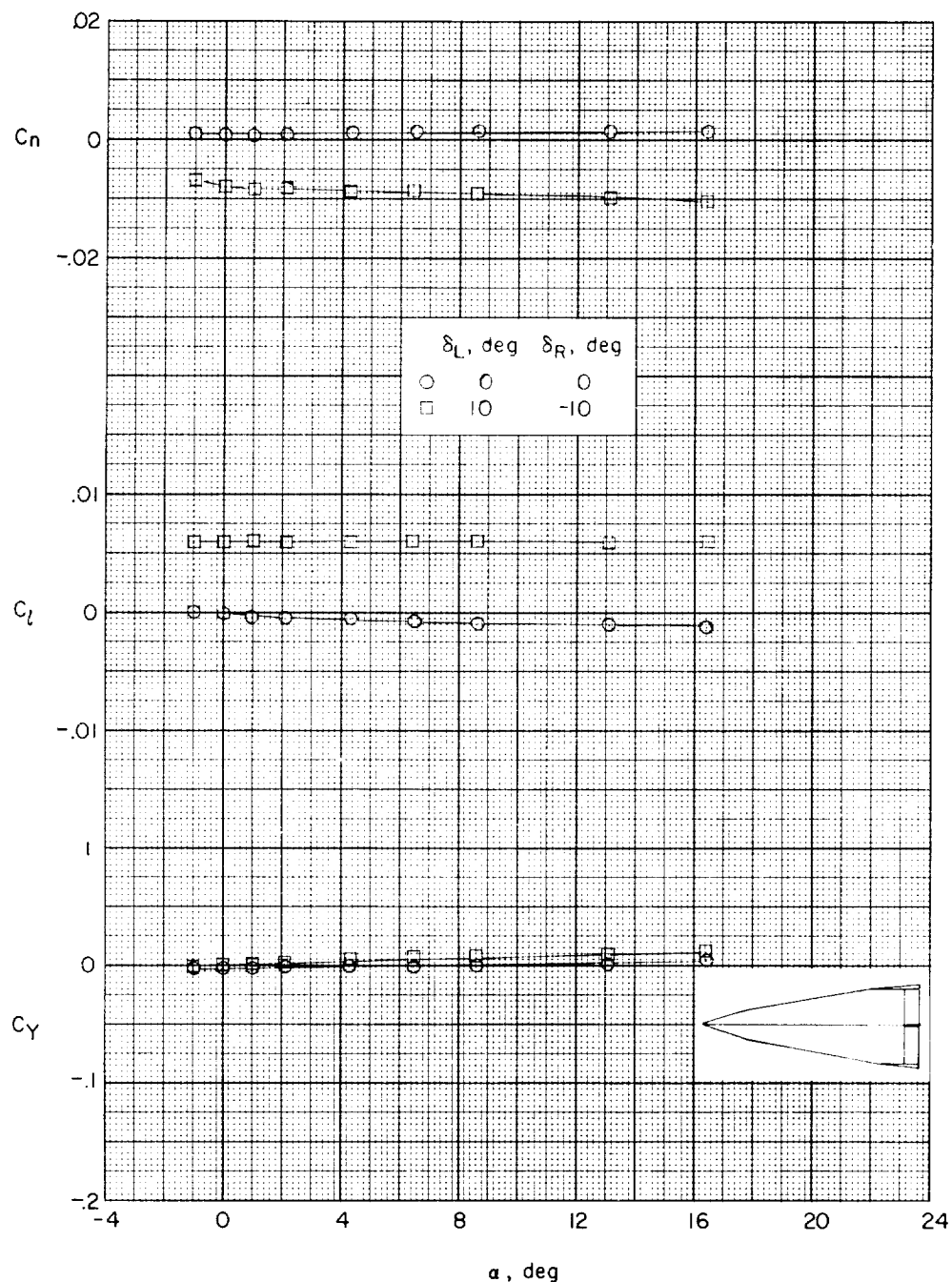
(a) Variation of C_n, C_l, and C_Y with α.

Figure 29.- Effect of deflected roll control of model 6 on the aerodynamic characteristics in pitch. $\beta = 0.2°$; $M = 1.41$.

(b) Variation of C_m, C_A, and C_N with α.

Figure 29.- Corcluded.
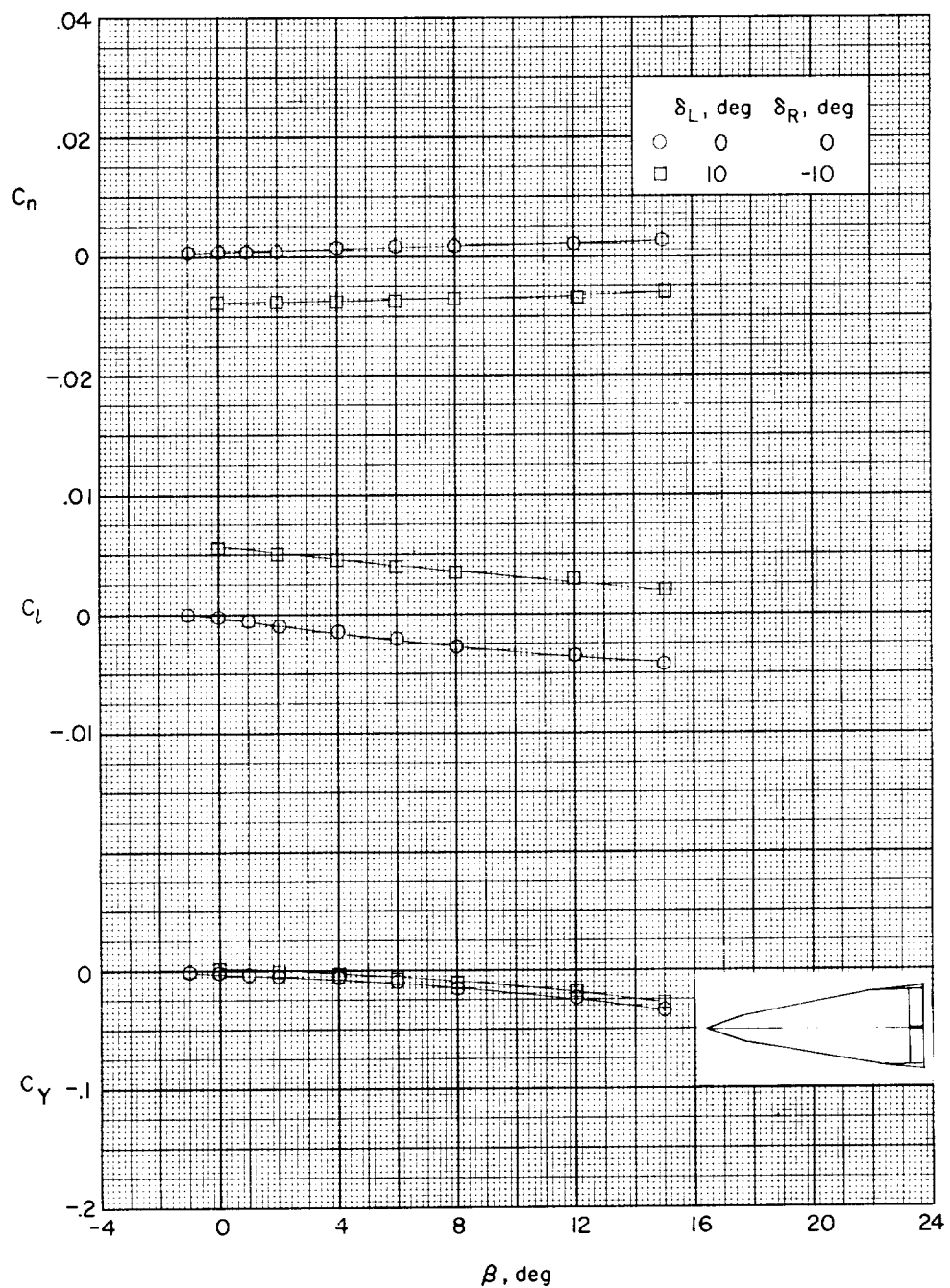
(a) α = -0.2°.

Figure 30.- Effect of deflected roll control of model 6 on the lateral
aerodynamic characteristics in sideslip. M = 1.41.

(b) a = 8.4°.
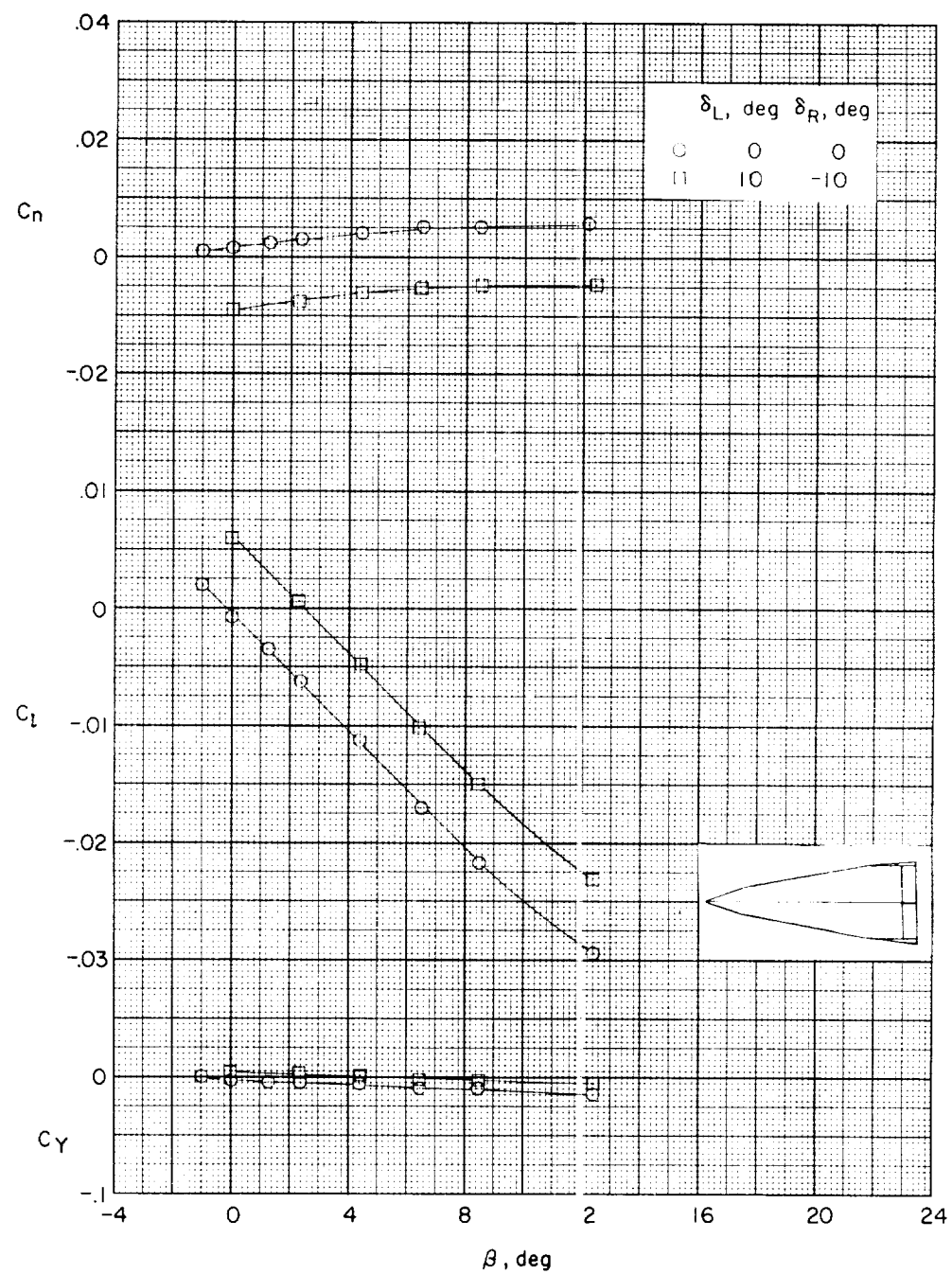
Figuer 30.- Concluded.

(a) Variation of C_n, C_l, and C_Y with α.

Figure 31.- Effect of deflected roll control of model 6 on the aerodynamic characteristics in pitch. $\beta = 0.2°$; $M = 2.01$.
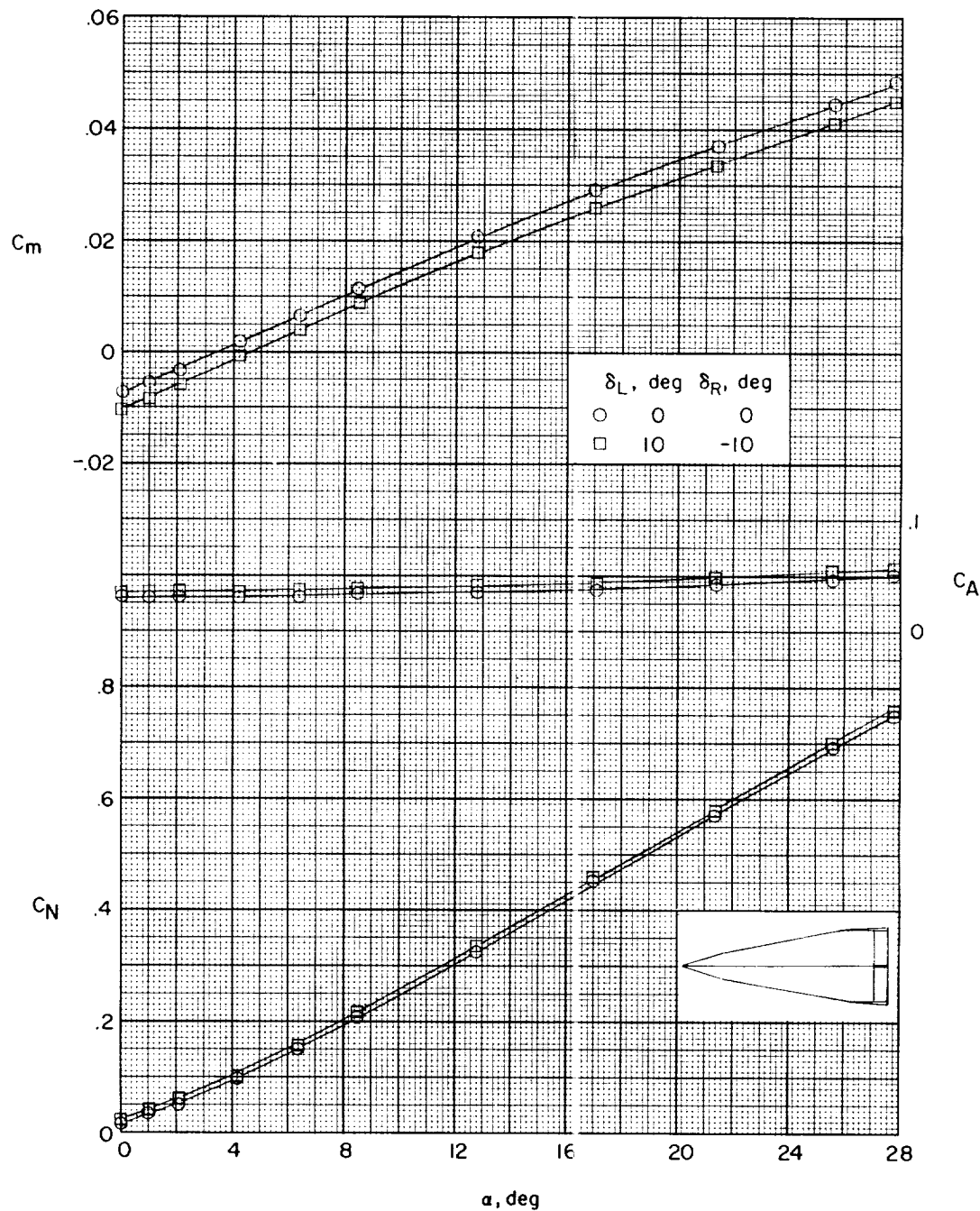
(b) Variation of C_m, C_A, and C_N with α.

Figure 31.- Concluded.
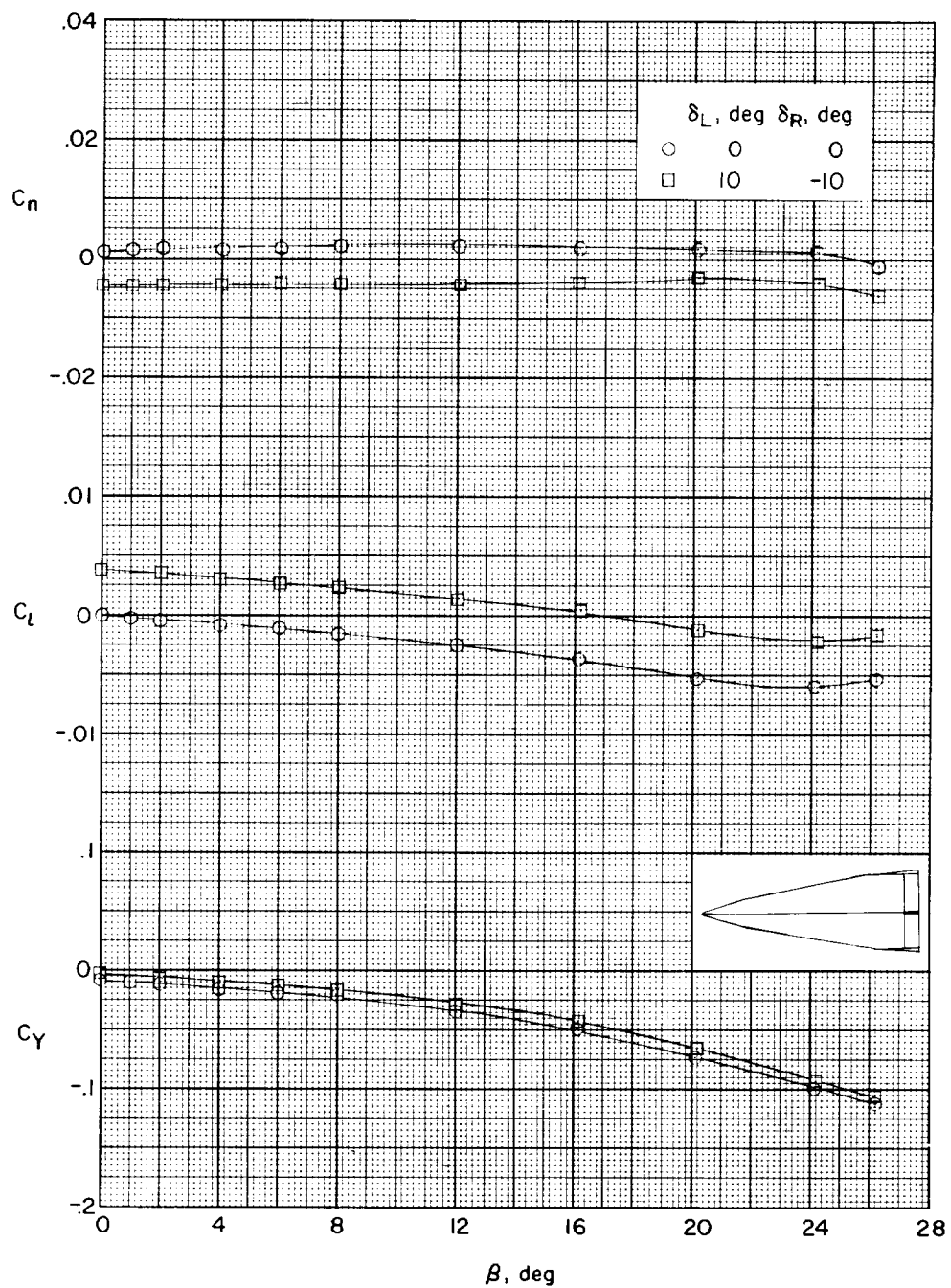
(a) α = -0.2°.

Figure 32.- Effect of deflected roll control of model 6 on the lateral
aerodynamic characteristics in sideslip. M = 2.01.
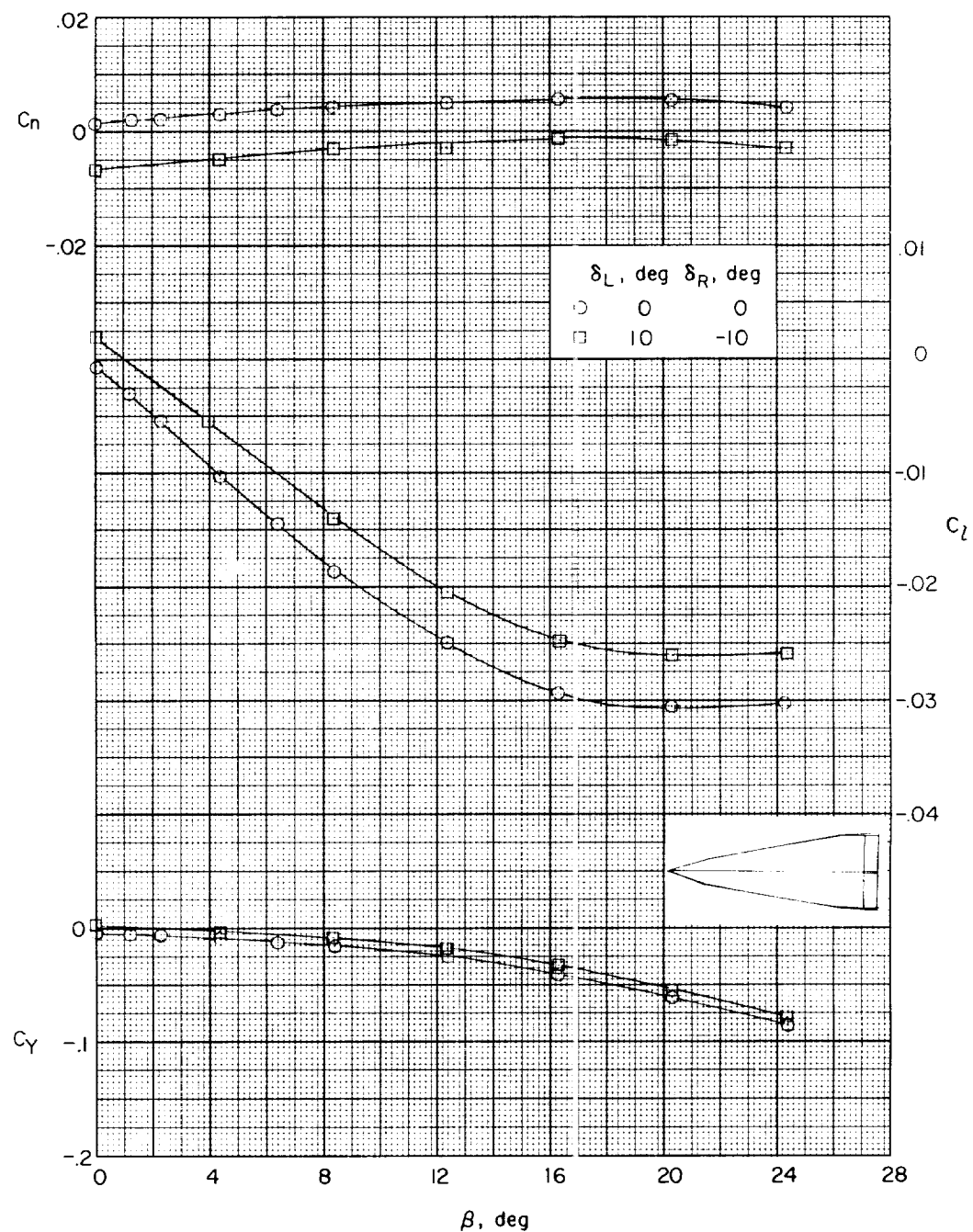
(b) $\alpha = 8.4^{\circ}$

Figure 32.- Concluded.
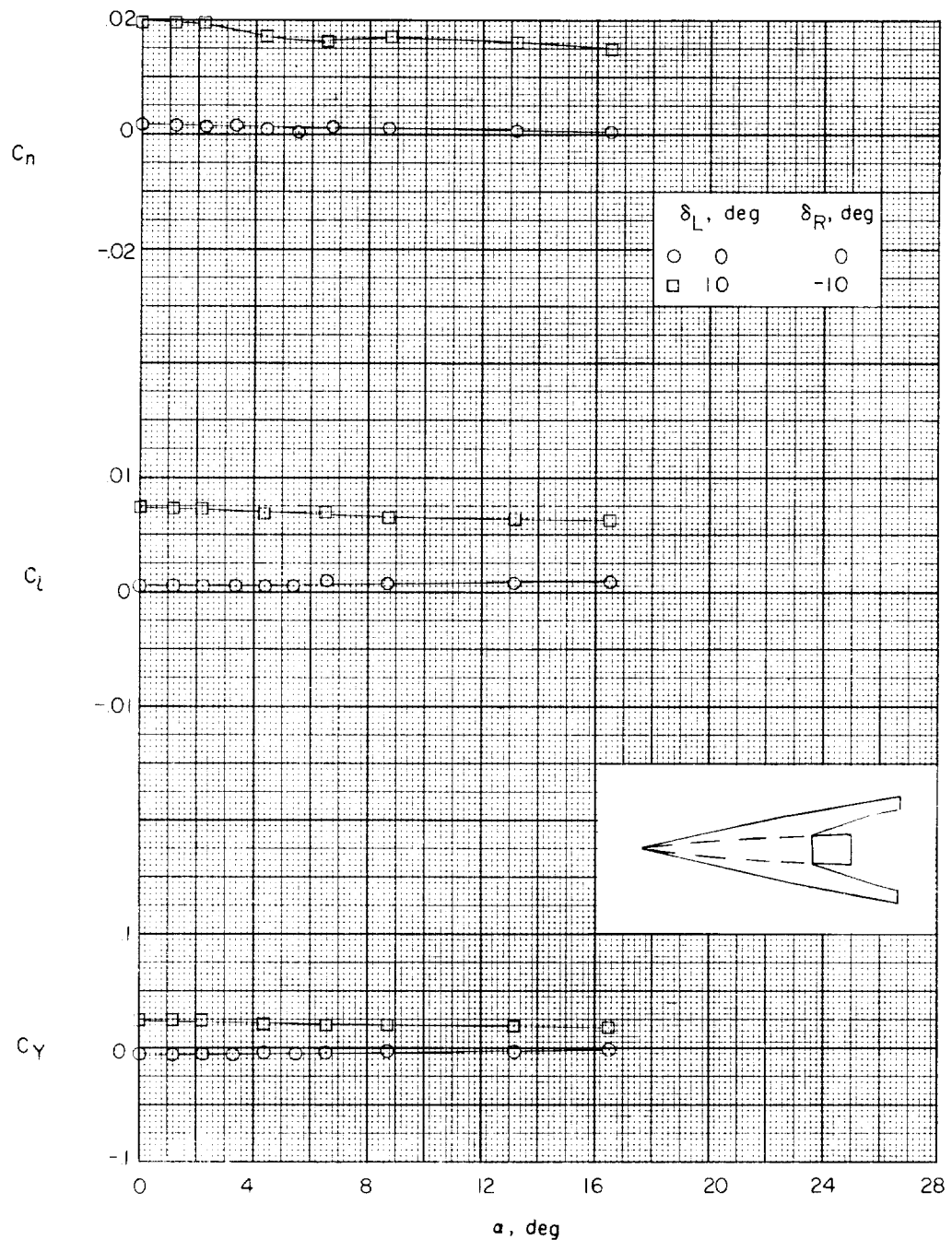
(a) Variation of C_n, C_l, and C_Y with α.

Figure 33.- Effect of deflected roll control of model 7 on the aerodynamic characteristics in pitch. M = 1.41.
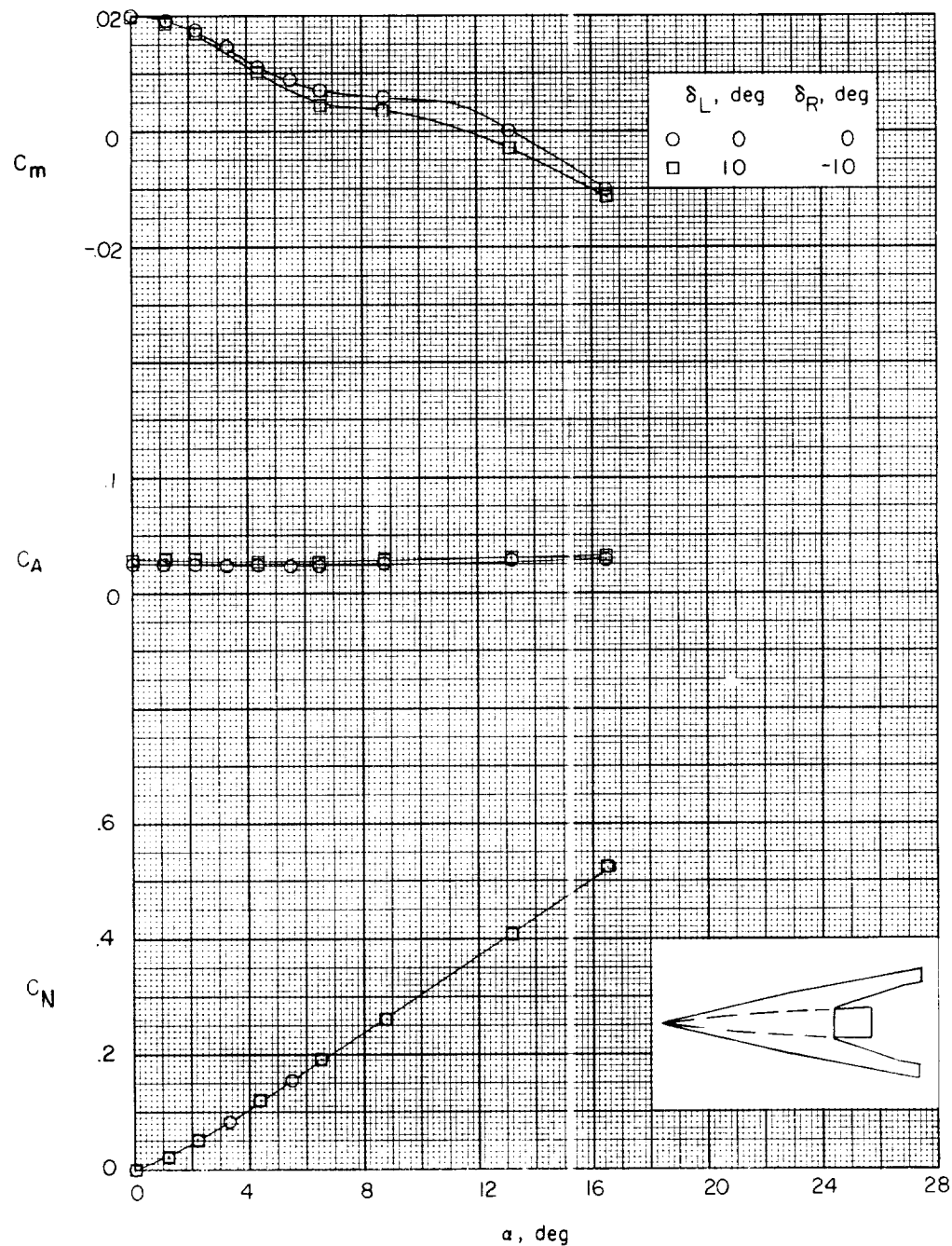
(b) Variation of C_m, C_A, and C_N with α.

Figure 33.- Concluded.
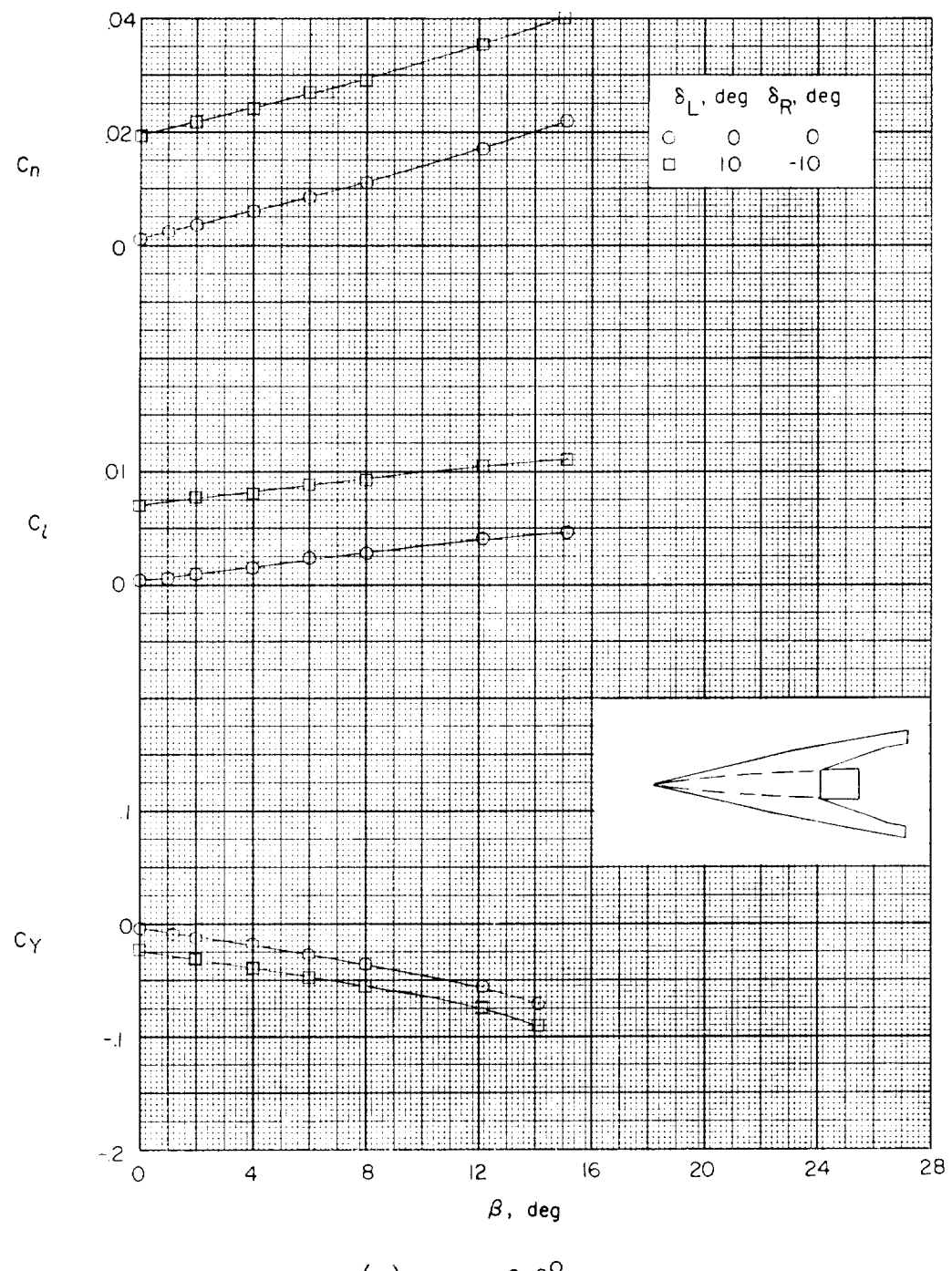
(a) $\alpha = -0.2^{\circ}$.

Figure 34.- Effect of deflected roll control of model 7 on the lateral
aerodynamic characteristics in sideslip. M = 1.41.
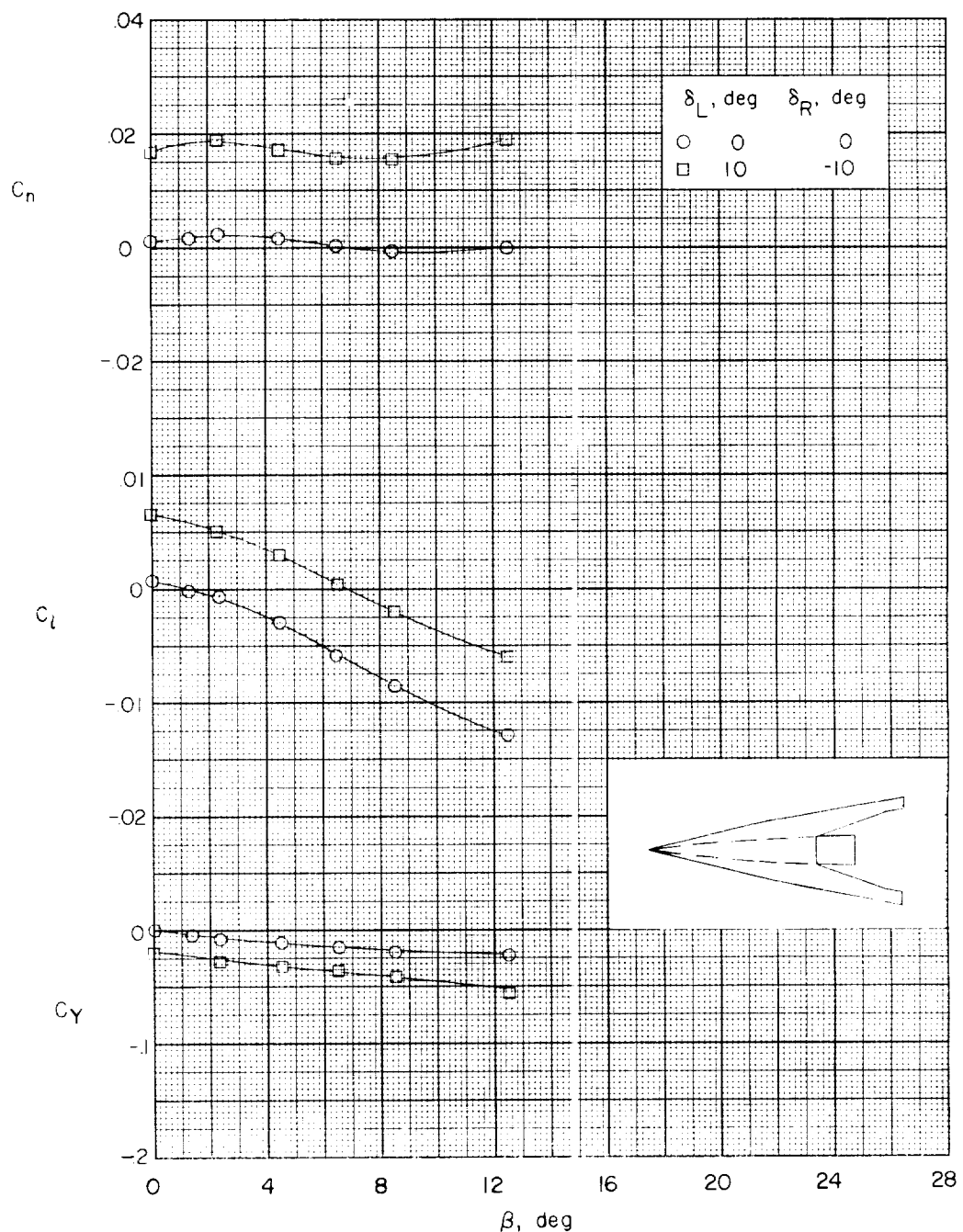
(b) $\alpha = 8.4°$.

Figure 34.- Concluded.
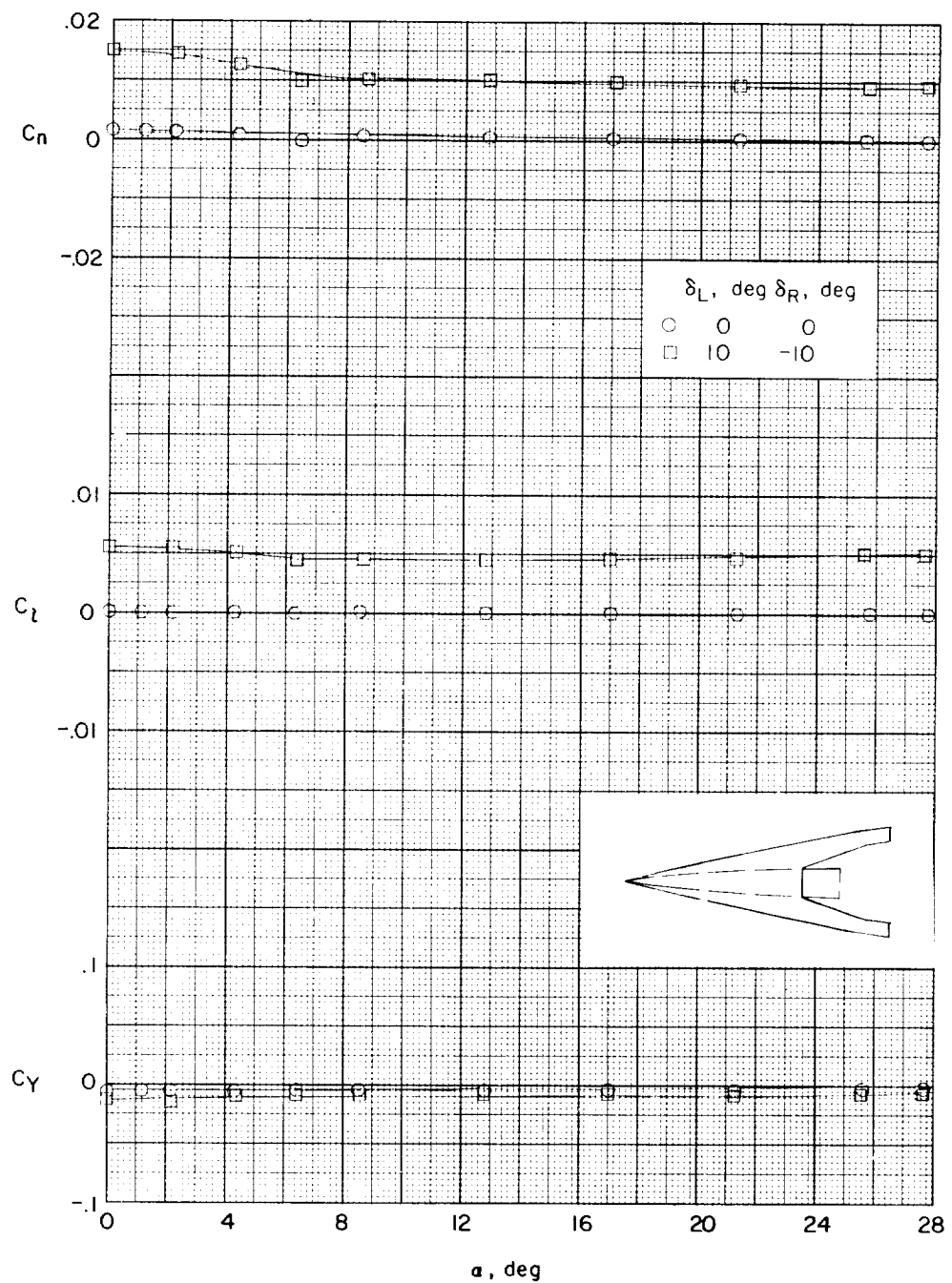
(a) Variation of C_n, C_l, and C_Y with α.

Figure 35.- Effects of deflected roll control of model 7 on the aerodynamic characteristics in pitch. $\beta = 0.2°$; $M = 2.01$.
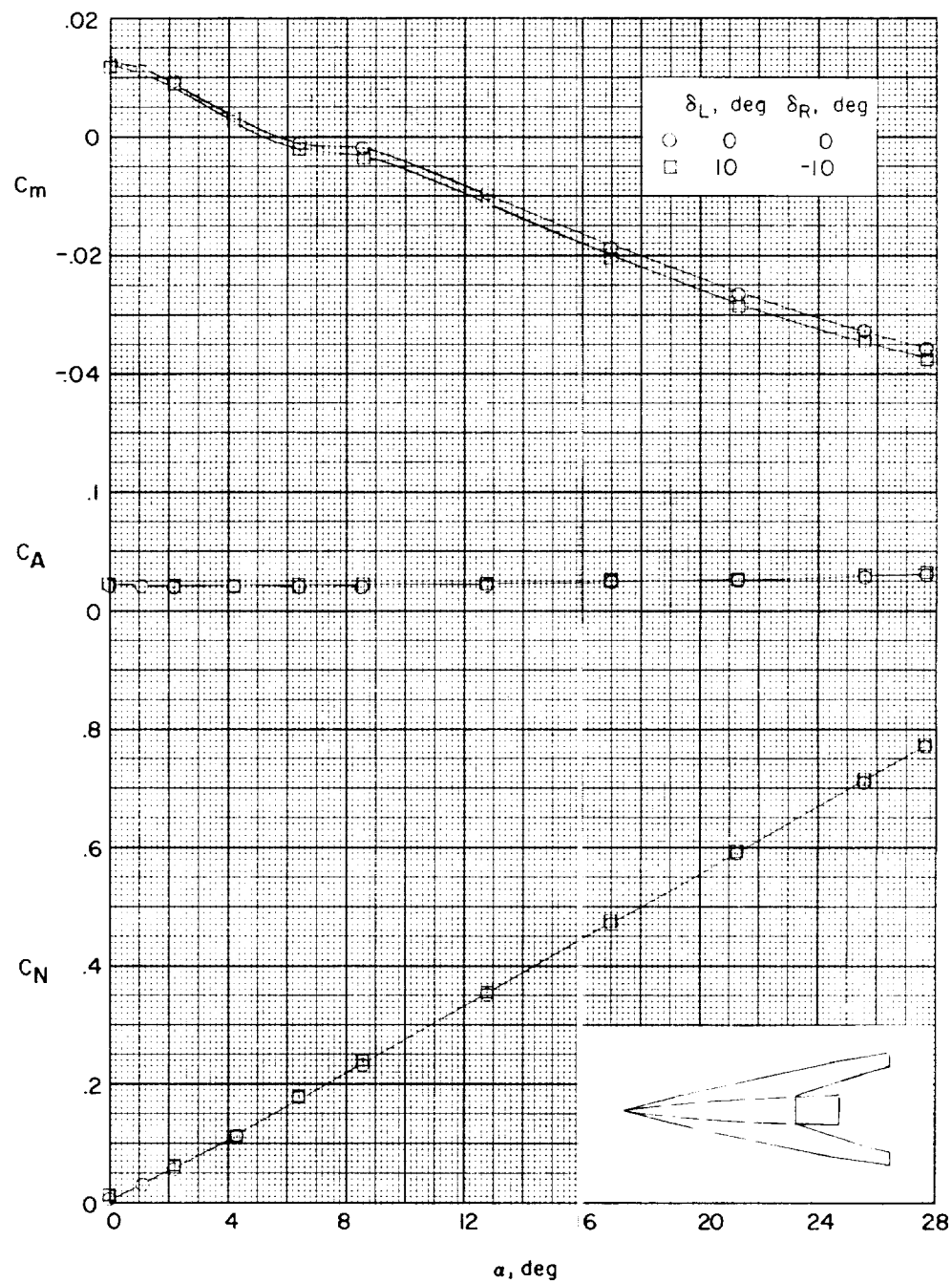
(b) Variation of C_m, C_A, and C_N with α.

Figure 35.- Concluded.
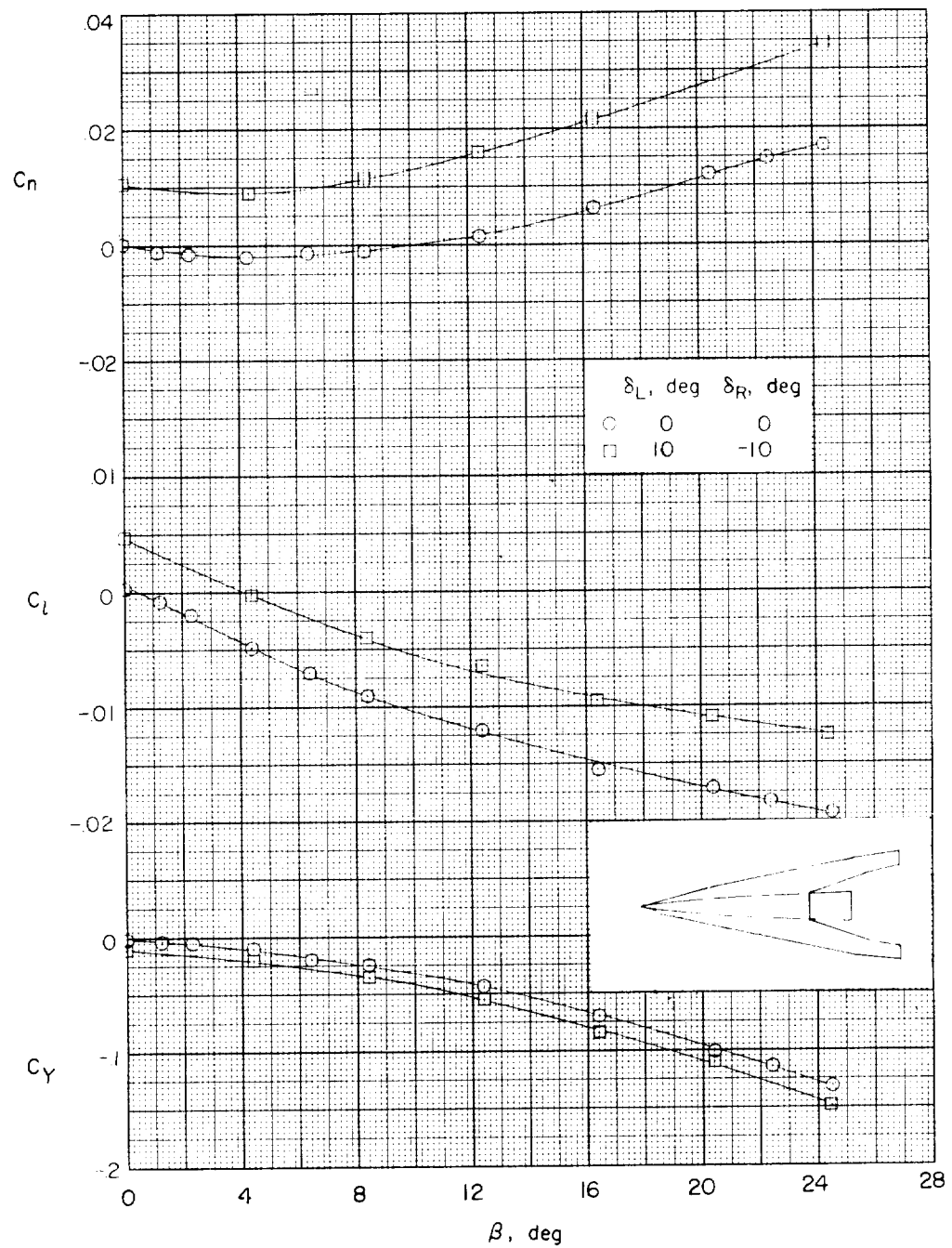
Figure 36.- Effects of deflected roll control of model 7 on the lateral
aerodynamic characteristics in sideslip. α = 8.4°; M = 2.01.